Idealised Models Of Sea Ice Thickness Dynamics

by

Daniel Godlovitch
B.Sc., University of Canterbury, 2003
M.Math., University of Waterloo, 2005

A Dissertation Submitted in Partial Fulfillment of the
Requirements for the Degree of

DOCTOR OF PHILOSOPHY

in the School Of Earth And Ocean Sciences

Idealised Models Of Sea Ice Thickness Dynamics

by

Daniel Godlovitch
B.Sc., University of Canterbury, 2003
M.Math., University of Waterloo, 2005

Supervisory Committee

Dr. G. Flato, Main Supervisor
(Canadian Centre For Climate Modelling And Analysis)

Dr. A. Monahan, Co-Supervisor
(School Of Earth And Ocean Sciences)

Dr. R. Illner, Outside Member
(Department Of Mathematics And Statistics)

Dr. H. Melling, Additional Member
(Institute Of Ocean Sciences)

Supervisory Committee

Dr. G. Flato, Main Supervisor
(Canadian Centre For Climate Modelling And Analysis)

Dr. A. Monahan, Co-Supervisor
(School Of Earth And Ocean Sciences)

Dr. R. Illner, Outside Member
(Department Of Mathematics And Statistics)

Dr. H. Melling, Additional Member
(Institute Of Ocean Sciences)

ABSTRACT

Thickness distributions of sea ice (g(h)) display a ubiquitous exponential decay ('tail') in ice above approximately 2 meters thick. This work uses idealised models to examine the root causes of the exponential tail of the sea ice thickness distribution. The ice of thickness greater than 2 meters is formed through the fracture and piling of ice caused by interactions between floes, driven by winds and currents. The material properties of sea ice are complex and mathematical descriptions of the relationship between force and deformation of a floe are still a topic of study. Smoluchowski Coagulation Models (SCMs) are used to develop an abstract representation of redistribution dynamics. SCMs describe populations whose members of fixed size combine at size-dependent rates. SCMs naturally produce exponential or quasi-exponential distributions. An SCM coupled with a thermodynamic component produces qualitatively realistic g(h) under a wide range of conditions. Using the abstract representation of redistribution dynamics from SCMs, a model developed from physical processes specific to sea ice is introduced. Redistribution events occur at rates dependent on the change in potential energy. This model is demonstrated to produce qualitatively

realistic g(h). Sensitivity analysis shows that primary model sensitivities are to the relative strengths of the dynamic and thermodynamic components of the model; and to the relative occurrence of ice ridging, shearing and rafting. The exact relationship between the rate of redistribution events and the energy they consume is shown to be of lesser importance. We conclude that the exponential tail of g(h) is a mathematical consequence of the coagulative nature of the ice thickness redistribution process, rather than the material properties of sea ice. These model results suggest the strongest controls on the form of the tail are the relative strengths of thermodynamic and dynamic action, and the relative occurrence of ice ridging, shearing and rafting.

Contents

List of Tables

List of Figures

ACKNOWLEDGEMENTS

I would like to thank my committee for all of their help during this degree: Greg for making all of this possible in the first place; Adam, for being a seemingly infinite font of encouragement, patience, and interesting ideas; Reinhard for taking the time to do some math with me and by doing so making this a deeper piece of work; and Humfrey for the data, and for showing me how it's done out in the real world. I am also grateful to everyone who has given me advice or encouragement over the last four and a half years, be it of the academic variety or the 'keep going' variety. I am equally grateful to the people who have provided me with distractions from my work, thus preventing total burn-out. Finally, I must thank Kristen, and assure her that I only need to do one of these.

Chapter 1

Introduction

The sea ice found in the polar oceans plays a major role in the Earth's climate. Its high albedo influences the global radiation budget, and its presence at the air-sea interface influences fluxes of energy, momentum and matter between the atmosphere and ocean. Inclusion of a dynamic sea ice component in General Circulation Models (GCMs) is essential for accurate modelling of the Earth's climate, and the sensitivity of climate simulations by GCMs to the representation of sea ice has been well studied, *e.g.*, [7], [22]. Among the most difficult aspects of modelling sea ice is the inclusion of the processes which create thick ice through the compressive fracture and piling of floes. The complex material properties of sea ice hinder mathematical representation of the interactions between ice floes, which is a requisite component of a dynamic sea ice model. This complexity, coupled with the many spatial scales over which the interactions occur, makes the modelling of sea ice dynamics a challenging task.

Sea ice has one of the highest albedos of any surface feature on Earth. The surface of sea ice can reflect between 15 and 87 percent of incident solar insolation, depending on the state of the ice [5], [50]. Due to this high albedo, the extent of the sea ice cover has a considerable effect on the amount of solar radiation the Earth receives. It is well known that the relationship between temperature and planetary albedo exhibits a positive feedback, which is due in part to the presence of sea ice: decreasing temperatures enhance ice formation, which increases the surface albedo, which leads to a further decrease in temperature, and *vice versa*. The formation and melting of sea ice also affects the density profile of the polar waters. As the water at the base of the ice freezes, much of the salt is not incorporated into the ice mass, producing a body of cold, highly saline water. This can cause an unstable stratification in the water column, and the dense water at the base of the ice floe sinks. This

process has been identified as the primary source of the Arctic and Antarctic Deep Water, which is a primary agent in feeding the thermohaline circulation.

The evolution of sea ice displays a strong seasonality, due to the ice's response to the annual cycle in the thermodynamic forcing. Every summer ice below a certain thickness is unable to survive the melt season. At any time during the year, the population of sea ice is heterogeneous, consisting of ice less than one year old, which formed in the most recent winter period, and ice which is over one year old, having survived at least one summer's melt. Under typical conditions, sea ice can grow via thermodynamic processes to a maximum thickness of between 1.5 and 3m through the conductive transfer of heat from the water below it to the atmosphere above [18],[39],[61]. Despite this limit, ice thicker than 2.5 meters is commonplace, and observations of floes with thicknesses in the tens of meters are not uncommon. Any ice thicker than the maximum to which it can grow through thermodynamic processes is created through the process of ridging or rafting. Ridging occurs when two ice floes are driven together with sufficient force to cause the ice to break into smaller pieces. Additional forcing can drive these fragments both above and below the two parent floes, substantially increasing the thickness of the ice at the point where the two parent floes meet. If the displaced fragments are left undisturbed for a sufficiently long time, they will consolidate by freezing together. Rafting is a similar process which has been observed in ice up to a 3.3m thick[4], although it is more typically seen in ice under 1m thick. This thinner ice may bend without fracturing, and a sheet of thin may be ice forced over a neighbouring floe without having to fragment.

Ridge features comprise all sea ice above approximately 2.5 meters, and their added thickness imparts an increased ability to survive a melting season. Because these features are common, and account for much of the ice able to survive a summer, it is essential to include a description of the effects of ridging in sea ice models. Without a representation of this process, a model would produce sea ice that was the result of purely thermodynamic processes, which would be unrealistic. Due to the importance of the redistribution process, a central issue in sea ice modelling concerns the most appropriate and accurate way to represent the process of dynamic interaction between floes in sea ice models.

It has been noted by many observers of sea ice that some common population statistics follow well defined distributions. Perhaps the most well-known is the tendency of the thicknesses of a population to follow an exponential distribution above approximately 2 meters.

Additionally, as described in the work of Rothrock *et. al.* [45], the distance between ridges is approximately log-normally distributed. Aerial measurements have revealed that the area of individual floes in a sea ice population also follows a log-normal distribution [45]. Sonar measurements of the underside of floes has shown them to have a fractal dimension. Given that all of these statistical properties of the sea ice population are a result of the redistribution process, it is worthwhile to attempt to reproduce them and thereby attempt to gain some further insight into the physical processes at work.

A well documented feature of the thickness distribution of sea-ice is the close fit its tail makes to a truncated exponential distribution, [59]A typical example of a sea ice thickness distribution is seen in Fig. 1, which displays the mean population thickness distribution obtained from multi-year sea ice thickness data taken in the Beaufort Sea. On the semilog axes, the exponential tail is linear. Further examples of observations of exponentially distributed populations may be seen in, the work of Wadhams ([55], [56]). The e-folding scale of the distribution varies depending on time of year and geographical location where the data was gathered. An exponential distribution does not accurately describe the entire population: the thinner ice, typically below 2 meters, deviates sharply from an exponential distribution, where the population dynamics are dominated by the growth towards thermodynamic equilibrium (Fig. 1). The ubiquity of the exponential tail in thicker ice over data with enormous spatial and temporal variation strongly suggests that it arises as the consequence of some generic feature of the physical properties of the system, and is not due to a specific temperature regime, or a region-specific pattern in the atmospheric and oceanic forces acting upon the ice.

Although the exponential form of the thickness distribution is well documented, the exact mechanisms responsible for this feature of sea-ice populations have not been fully explored. Most previous work on sea ice dynamics has focussed on large-scale simulations using force balance models with complex redistribution dynamics ([13],[26]). Early force-balance models were unable to capture the details of the dynamics of the thickness distribution due to having a small number of thickness categories, *e.g.*, the two thickness model of Hibler [20]. Variable thickness models derived from Hibler's basin scale model [15], [21], have produced a more realistic thickness distribution, albeit with some discrepancies relative to observations (*e.g.*, typically overestimating the population of thick ice). Interestingly, aside from a proof-of-concept model by Thorndike [51], in which the merits of a stochastic approach are suggested, the task of identifying the essential features of the

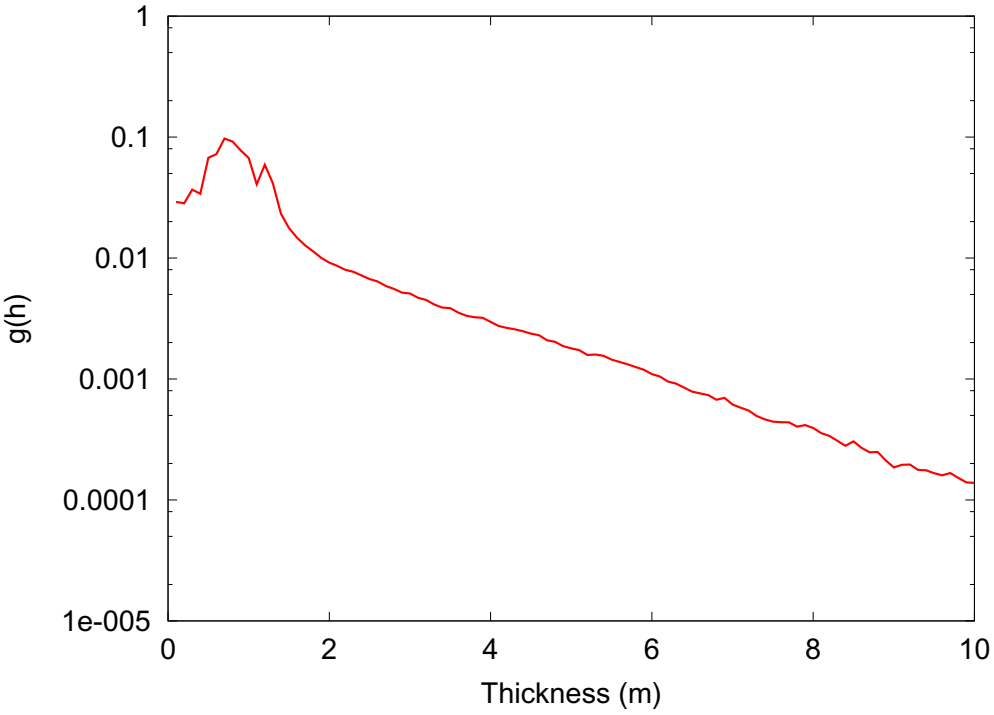

Figure 1.1: Mean thickness distribution g(h) of a January ice population in the Beaufort

dynamics which yield the exponential distribution has not been addressed in detail. Work using a stochastic formulation to examine the statistics of ridge spacing in ice pack has been done [33], but the parameterisation of the ridging processes are highly abstracted, and this earlier work does not provide a direct explanation of the physical causes of the observed thickness distribution statistics.

In this work, we develop a novel method for modelling the effects of the redistribution process on a sea ice population. The dynamic evolution of the population is treated as a stochastic process, which distinguishes this work from the deterministic models of sea ice populations presently in use. The goal of this research was to create a model of the redistribution process that is complex enough to capture the primary statistical features of the evolution of thickness in a population of sea ice, but which is simple enough to serve as a tool to examine the relative importance of the various processes used to describe the population's dynamics. In order to motivate the creation of a model to probe these questions, the nature of the dynamic processes at work in a population of ice must be elucidated. Doing this requires a description of the processes at work, from the formation of ice from the freezing of sea water to redistribution through ridging, shearing, and rafting. The formation of ice is a thermodynamic process and is covered in Section 1.1. A non-technical description of the dynamic redistribution of ice is given in Section 1.2, with an introduction to the technical description of the material properties of sea ice is discussed in Section 1.3. Finally, a brief survey of the history of sea ice modelling is presented in Section 1.5, with the intention of presenting an overview of past techniques used to model the dynamics of sea ice, for the sake of comparison with the present work.

1.1 The Thermodynamic Life-Cycle Of Sea Ice

As stated above, many of the difficulties in modelling the behaviour of sea ice have to do with its complex material properties. Unlike ice formed from fresh water, sea ice has an irregular porous structure due to the circumstances of its formation, and in particular the salinity of ocean water. In order to properly convey the complexity of the material, a brief description of the formation of sea ice is helpful.

The formation of sea ice begins with the nucleation of ice crystals, which may either occur spontaneously if the temperature is low enough, or be catalyzed around nucleation catalysts (undissolved particles) in slightly warmer conditions. At a molecular level, ice crystals are

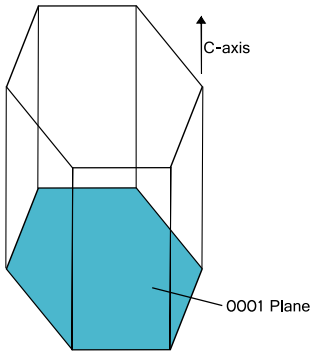

Figure 1.2: Simplified diagram of the crystal structure of ice, showing the 0001 plane and the c-axis

asymmetrical, and this asymmetry results in different rates of heat transfer through their various planes. This property causes the crystals to have a preferred direction of growth along the axis of greatest heat transfer, (Fig. 1.2 - perpendicular to the 0001-plane). Under quiescent conditions, as the ice grows and forms an interface between the water and the air, crystals with their axis of greatest heat conductivity normal to the air-ocean interface will grow faster than those aligned differently, as the conductive transfer rate across the 0001-plane is orders of magnitude larger than for the other planes. This preferential growth results in the relatively homogeneous alignment of the ice crystals being formed, despite their heterogeneous origins. While fresh water has the odd property of reaching a maximum density at 4°C, the presence of dissolved salt in sea water causes this behaviour to be nullified for salt concentrations above 24.7ppt. The difference in the temperature-dependence of density in fresh water and saline water has the consequence that the crystal structure of sea ice is different to that of fresh water ice.

The surface waters in which the ice forms can often be rough. Wind-driven waves disturb the newly-formed ice covering the surface of the water, exposing the ocean to the atmosphere interface and catalysing the formation of more ice. The extant ice is broken into small pieces, known as frazil ice. In areas where the sea surface is largely covered by frazil ice, the ice is described as grease ice. The separate ice shards that comprise grease ice are not frozen together into a homogeneous sheet, and grease ice behaves like a viscous fluid, rather than a solid. Accumulation of grease ice eventually leads to the creation of a thicker type of ice known as ice rind. The ice rind behaves more like a solid than grease ice, although it is still thin, typically less than 0.1m thick. Although the ice rind has a greater structural integrity than frazil or grease ice, it can still be fragmented by the action of waves. Ice rind, frazil, or grease ice can be driven together by winds and waves to form pancake ice. This form of sea ice is typically circular in form, with a raised lip where the surrounding ice is forced against it. Initially, pancakes are comprised of the unconsolidated ice crystals with pockets of liquid brine trapped between them. However, the compression causes the melting point of the ice to drop, and the individual crystals can freeze together. Any brine trapped in the structure will remain liquid, occupying the spaces between crystals. In the event that there is insufficient forcing to convert the grease ice and ice rind to pancake ice, the ice rind can coalesce, forming what is known as *nilas* or black ice, so-called due to its dark appearance. Like ice rind, nilas is does not display great strength, and is still thin enough to be flexible. Following the formation of level sheets of ice, growth continues at the base of the floe. The crystal structure of the ice which forms there is relatively homogeneous, with the majority of the crystals having their axis of preferred thermal

growth aligned parallel to the air-ocean interface. As with the initial formation of ice crystals, incomplete rejection of salt, and the consequent formation of brine pockets is a feature of ice growth at the base of a floe. The growth process of sea ice results in a vertically heterogeneous medium, with liquid brine pockets in a porous network of ice crystals. The vertical heterogeneity stems from the differing processes governing the initial formation of sea ice, and the growth of existing sheets.

The surface temperatures over the winter allow any snow falling on sea ice to remain there for extended periods of time. Snow has a very poor thermal conductivity, and a layer of it on top of a floe increases the insulating abilities of the ice. The snow also increases the albedo of the floe, and the highest measured albedos of sea ice occur on floes covered with fresh snow. Following further precipitation, and during the melt season, the snow is compacted, and, if flooded, may consolidate to add to the ice thickness. Like frazil, the compacted snow layer does not have a coherent structure due to its composition of heterogeneous, randomly distributed and aligned snow flakes. The heterogeneity of the snow layer increases the amount of internal scattering of downwelling radiation which occurs in the surface layers of the floe.

Ice reaches a maximum thickness due to thermodynamic forcing during the spring (approximately March-April). During the summer the ice melts, and the ice thickness reaches a minimum in the fall (September-October). Most of the ice formed during the previous winter is not thick enough to survive a summer and simply melts away. Some ice will survive due to a combination of factors such as its thickness and location: thicker ice in higher latitudes will be more likely to remain intact during the melt season. During the summer, water pools on the surface of the ice floes. This serves to accelerate the melting process, as the pools have a lower albedo than the ice, and thus transfer greater amounts of thermal energy into the floes. Additionally, the hydrostatic pressure can flush some of the remaining brine out of the ice below as the pools drain through it. Through this process, ice which survives a summer has a different structure to ice which is newly formed. There are various descriptors for ice in this stage of melt, as it can range from relatively solid ice with a melt pool on the surface, to rotten or candelling ice which is saturated by water both from the melt and the ocean. Any ice that does survive the summer melt season will have a much lower salinity than it did during the previous winter, due to flushing. During its second winter, it participates in the same processes of freezing, rafting and ridging. Dynamic redistribution of the ice in the form of compressive ridge and keel building (details

Section 1.2), together with the addition of new mass through freezing on the underside of the floe allow the second-year ice to attain greater thicknesses than first year ice, typically approaching 2 to 3 meters during the spring.

Ice which has survived for two or more winters is categorised as multi-year ice. The seasonal processes continue to act upon it in much the same way as they do for first and second year ice. However, the greater thicknesses typical of multi-year ice makes their continued existence less subject to the seasonal cycle. Unlike year-old ice, the repeat flushing of multi-year ice every summer results in ice which has a detectably lower salinity than younger ice. Wind and ocean-current forcing on sea ice is strong enough to allow continued ridging, and through this process, multi-year ice can get much thicker than first or second year ice, averaging between 2 and 6 meters thick. The ridges and keels formed through compressive redistribution melt during the summer, becoming lower, but more cohesive. Ice that survives for several years is transported around the arctic by the Beaufort Gyre and Transpolar Drift. The clockwise motion eventually takes the ice into the Fram Strait, where it enters the North Atlantic and eventually melts. In the Arctic, the typical residence time of multi-year ice is around 10 years.

1.2 The Redistribution Process

When sheets of level ice have formed in a region, velocity gradients across the ice induced by external forcing can lead to the deformation and mechanical redistribution of the ice. Mechanical redistribution encompasses ridging, which has the capacity to create ice features which are thicker than thermodynamic action can produce, and shearing, which can create regions of open water through divergent motion, as well as piling ice on interacting floes. In addition, thinner ice, particularly nilas and ice rind, is sufficiently flexible to be driven atop adjacent ice sheets by winds and current in a process known as rafting.

Compressive forcing produces the largest and most visually apparent feature in the ice pack, the pressure ridge. The portion of a pressure ridge on the upper surface of the ice is referred to as a sail, where the portion below the surface of the water is known as the keel. Pressure ridging in ice is usually initiated by the flexure and buckling of one of the floes undergoing compression, causing fragmentation of the sheet into blocks. These blocks are forced both above and below the surface of the water, forming the keel and sail. The majority of the ice is forced to the underside of the interacting floes, typically producing a keel

of greater depth and width than the sail on the upper surface of the ice. So much ice may be consumed in this manner that the resultant ridge-keel structure may be ten times as thick from ridge peak to keel tip as the source floes. Due to the dependence of the resistance to deformation of ice on its thickness, when a heterogeneous population of ice is subjected to compressive forcing, it is typically the thinnest ice which fails first. In an established sea ice population, the thin ice is found in quantity in leads between thicker floes. As the floes move together, the thin ice in the lead fractures and forms a ridge as the lead closes.

Shearing deformation has a different effect on the ice, typically producing a linear feature along the interface of shearing. This is called a shear ridge, and is comprised of ice blocks from the interacting floes which is forced both upwards and downwards as two floes are dragged along each other. Shearing is unable to produce ridges with keels as large as those produced by compression, but they can often be much larger features in terms of horizontal extent. Shearing also creates leads, open areas of water, resulting from the dilation which occurs when the interface between the shearing floes is not precisely parallel to the direction of shear forcing. Leads are significantly less long-lived than ridges as they quickly freeze over during the winter, due to the extreme temperature gradient between the open water and the atmosphere. Leads are a common feature of multi-year ice and may extend for kilometers.

1.3 Rheological Descriptions Of Sea Ice

Standard models of sea ice behaviour treat the population of ice as a continuum. Under this assumption, Newton's second law of motion can be expressed by an equation of the form

$$m\frac{\mathrm{D}\mathbf{u}}{\mathrm{D}t} = -mf\mathbf{k} + \tau_a + \tau_o + mg\nabla H + F \tag{1.1}$$

where $\mathbf{u}$ is the ice velocity vector, $\mathrm{D}/\mathrm{D}t$ is the material derivative, and the terms on the right hand side are the forces arising from the Coriolis effect, from winds and the relative motion between ice and ocean, gravity when the sea surface is not level, and from the ice interacting with itself. A model developed in this fashion has an additional set of equations describing the thermodynamic growth and ablation of the ice.

The final term in Eqn.1.1 is the representation of the way in which interactions between

ice floes affect the continuum-scale force balance *en masse*. Much work has gone into determining an optimal form for this term. The typical approach is to model the bulk material properties of a substance as regards to its response to deformation. For the purposes of modelling ice, a rheological description, which is a function giving the resistance (stress) to deformation (strain) of the object, is used. The study of rheology defines three fundamental types of material behaviour: elastic, viscous, and plastic. Elastic materials produce a stress proportional to the deformation, while the stress in viscous materials is proportional to the rate of deformation. Plastic behaviour is easier to describe by the material's response to forcing: materials are said to be plastic when they do not deform when the stress is below some threshold level, and 'fail' when the stress is above this threshold, undergoing permanent deformation and not returning to their original dimensions when the forcing is removed. More complex material behaviours can be produced by combining these three elemental rheologies in a variety of ways, or by using non-linear relationships between stress and strain in purely elastic, viscous, and plastic materials.

In specifying the rheological behaviour of a material, the spatial structure of the deformation must be taken into account. The stress and strain at any point in a material may be represented with the tensor

$$\sigma = \begin{pmatrix} \sigma_{xx} & \sigma_{xy} & \sigma_{xz} \\ \sigma_{yx} & \sigma_{yy} & \sigma_{yz} \\ \sigma_{zx} & \sigma_{zy} & \sigma_{zz} \end{pmatrix}. \tag{1.2}$$

Tensor equations are invariant under non-singular coordinate transformations, and we may treat the stress-strain relationship of a material in principal stress space, defined by σ_1, σ_2, and σ_3. Principal stress space is the coordinate system under which the stress tensor has no off-diagonal elements, and in this coordinate system we define the stress tensor elements by $\sigma_{xx} = \sigma_1$,$\sigma_{yy} = \sigma_2$, and $\sigma_{zz} = \sigma_3$, with all off-diagonal elements equal to zero. Sea ice is usually treated as a two-dimensional medium, owing to its large aspect ratio, and we may simplify the rheological equations by integrating over the ice thickness and defining principal stress space in terms of σ_1 and σ_2, yielding equations for the thickness-averaged behaviour.

As will be detailed in Section 1.5, typical rheological descriptions of sea ice incorporate

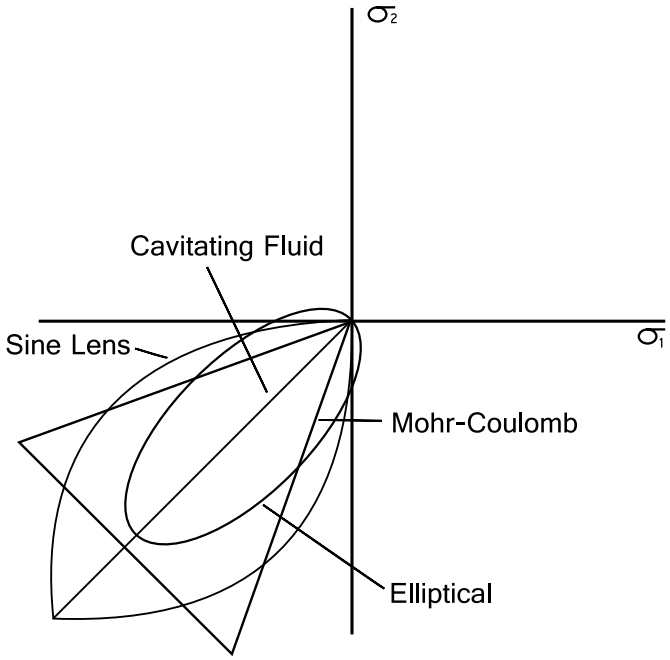

Figure 1.3: Commonly used yield curves in sea ice rheology, plotted in principal stress space

some form of plastic behaviour. In the study of plastic materials, one must define a yield curve, which is a surface in principal stress space that bounds the region of integrity. Stress states on the boundary of the surface cause failure of the material. In one dimension it is specified by an interval in principal stress space. In two dimensions, a closed curve is decribed, *viz.*, $f(\sigma_1, \sigma_2) = C$. The function defining this curve depends on the nature of the material, and it is an essential component of the work done with any sea ice model which uses plastic, or hybrid-plastic, rheology. Typical yield curves used in sea ice modelling are shown in primary stress-space in Figure 1.3, and are discussed in detail in Section 1.5.

1.4 The Thickness Distribution

The sea ice thickness distribution, $g(h)$, is an important measure of the state of a sea ice population. It can be thought of as the probability density function describing the fraction of ice of thickness h in an area. It is an empirical fact that the thickness distribution has a characteristic exponential tail [44], a form which is ubiquitous in observations from a wide variety of locations, *e.g.*, ([55], [56] , [60]). The evolution of sea ice is governed by the competing processes of thermodynamic growth and dynamic redistribution. Under perfectly static conditions, a region of sea ice would grow to a uniform equilibrium thickness of approximately 2.5-3 meters. However, the ice is continually forced by winds and currents, resulting in compressive and shear deformation and the opening of leads. The effect of these dynamical processes is to move the population away from the thermodynamic equilibrium thickness, both by creating thicker ice during compressive piling, and by creating open water in the form of leads opened by sliding action of floes. The most active elements of the population of ice in redistribution are the thinnest, as the energy required to deform ice increases with thickness. In addition to ridging caused by compression, ice less than approximately 1 meter thick is flexible enough to be rafted over adjacent thin ice without being broken into fragments prior to redistribution. The thermodynamic forcing on the sea ice follows a very strong annual cycle, and the tail of the thickness distribution retreats in the summer through ablation. Although the seasonal cycle prevents the ice population from reaching a long-term equilibrium state, the ice can still reach a local equilibrium relative to the seasonal thermodynamic forcing. Although the exponential tail of $g(h)$ is generic, its slope varies regionally, over the course of the season, and between individual time-series gathered from a single area.

The sea ice thickness distribution, $g(h)$, was introduced initially by Thorndike *et. al.*, [53]. Following the standard definition, the thickness distribution is defined for the population of ice occupying an area A, and $g(h)\mathrm{d}h$ is the fraction of the area A occupied by ice with thickness between h and $h + \mathrm{d}h$, *i.e.*,

$$P(h_0, h_1) = \int_{h_0}^{h_1} g(h')\mathrm{d}h' \tag{1.3}$$

where $P(h_0, h_1)$ is the proportion of the populaion ice between h_0 and h_1 meters thick in the population. This definition ensures that the function $g(h)$ has the properties of a probability distribution, *i.e.*,

$$\begin{aligned} g(h) &\geq 0 \quad \forall h \\ \int_0^{\infty} g(h)\mathrm{d}h &= 1. \end{aligned} \tag{1.4}$$

Use of the sea ice thickness distribution introduces the issue of representing the dynamic evolution of $g(h)$ in a force-balance model. The rheological description of the ice included in the force-balance models describes the effect that the ice interactions have on the motion of the pack, but it does not include any description of what the relationship was between the rheology of the ice and changes in its thickness. Translating stresses and strains described by the rheology into changes in the thickness distribution requires the formulation of a redistribution function. The redistribution function takes as input the stress and strain states of the ice, as well as the present state of the thickness distribution, and calculates the resultant change in $g(h)$. There are a number of constraints which can be used to aid in determining a viable form for the redistribution function, including basic physical principles such as conservation of mass or energy. Ensuring that the basic conservation considerations are met does not provide a complete description of redistribution, and the definition of redistribution function requires assumptions to be made regarding the ice strength and the way in which ice is redistributed. The approach taken in [10], [21] was to include a 'participation' function which weights the selection of ice which is available for redistribution, appealing to a 'weakest-link' argument that the thinnest ice will preferentially ridge.

In this approach, the thickness distribution evolves according to

$$\frac{\partial g}{\partial t} = -\nabla \cdot (\mathbf{u}g) - \frac{\partial (fg)}{\partial h} + \psi, \tag{1.5}$$

where the terms on the right account for transport, thermodynamic action on the ice, and the redistribution of the ice due to ridging. The final term can be constrained by conservation laws, *viz.*,

$$\int_0^\infty \psi \mathrm{d}h = \nabla \cdot \mathbf{u}, \tag{1.6}$$

which is a statement of area conservation (and follows from the normalisation of $g(h)$), and

$$\int_0^\infty h\psi \mathrm{d}h = 0, \tag{1.7}$$

which ensures that the redistributor does not create or destroy ice, based on the assumption that ice mass is directly related to thickness. Finally, it is required that the deformational work is equal to the work required to build ridges:

$$C \int_0^\infty h^2 \psi(h) \mathrm{d}h = \Sigma_{ij} \sigma_{ij} \dot{\epsilon}_{ij}, \tag{1.8}$$

where C is a constant which depends on gravitational and buoyancy forces, σ_{ij} is the stress tensor, and $\dot{\epsilon}_{ij}$ is the strain-rate tensor.

A redistribution function $\psi(h)$ which satisfies Eqns.1.6-1.8 is

$$\psi(h) = \delta(h) \left[(P^*)^{-1} \sigma_{ij} \dot{\epsilon}_{ij} + \dot{\epsilon}_{kk} \right] + (P^*)^{-1} \sigma_{ij} \dot{\epsilon}_{ij} W_r(h, g), \tag{1.9}$$

where P^* is the ice strength, the term $W_r(h, g)$ is defined by

$$W_r(h, g) = \frac{-P(h)g(h) + \int_0^\infty \gamma(h', h) P(h') g(h) \mathrm{d}h'}{\int_0^\infty \left[P(h)g(h) - \int_0^\infty \gamma(h', h) P(h') g(h) \mathrm{d}h' \right]}, \tag{1.10}$$

where $P(h)$ is the probability that ice of thickness h will participate in redistribution, and $\gamma(h', h)$ is a function which details how ice is transfered between thickness categories. In order for Eqn.1.9 to satisfy Eqn.1.6,1.7, constraints are placed on $W_r(h, g)$ and $\gamma(h', h)$:

$$\int_0^\infty \gamma(h', h) h \mathrm{d}h = h', \tag{1.11}$$

and

$$C \int_0^\infty h^2 W_r(h, g) \mathrm{d}h = P^*. \tag{1.12}$$

Beyond the conditions imposted by Eqn.1.11,1.12, the choice of $P(h)$ and $\gamma(h', h)$ are open, and determining the best way to represent the redistribution processes through these functions is one of the key problems in designing continuum-scale sea ice models.

It was proposed that the ice available for redistribution could be drawn from a weighted subpopulation of $g(h)$ [53]. A weighting function was chosen to favour the thinnest ice and has the form

$$P(h) = \max \left[\left(1 - \int_0^h g(h) \mathrm{d}h / c_1 \right), 0 \right]. \tag{1.13}$$

where c_1 was the fraction of the population available for redistribution. This form of $P(h)$ allows the thinnest c_1-percent of the population to participate in redistribution.

The approach taken in [21] for the specification of $\gamma(h, h')$, was based upon empirical observations of ridge structure, and the thickness of the ice rubble forming ridges. It assumed a constant value for thicknesses below a constant times the square root of the thickness of the ice undergoing redistribution, and was zero above that, *i.e.*,

$$\gamma(h, h') = \begin{cases} 1/2(H^* - h') & 2h \leq h' \leq 2\sqrt{H^* h} \\ 0 & \text{otherwise} \end{cases} \tag{1.14}$$

where H^* is a constant.

1.5 A Brief History Of Sea Ice Modelling

Most aspects of modern sea ice modelling have their genesis in the AIDJEX program, which ran during the 1970s. AIDJEX involved a combination of field work and data gathering programs, and a parallel effort to improve and refine sea ice modelling techniques with the help of the newly gathered observational data. The sea ice models developed by the AIDJEX program introduced sophisticated hybrid rheologies to describe the physics of ice-ice interactions. Prior to the AIDJEX work, early force-balance sea ice models which included an interaction term (F in Eqn. 1.1) represented the bulk material properties of ice

using a viscous rheology. The first such model used a Newtonian (linear) viscous rheology, and was introduced in 1958 [30]. The linear viscous rheological model was subsequently developed by a number of researchers [46]. These models were simple to implement and had the appeal of a similar mathematical form to extant models of ocean and atmospheric dynamics. In particular, analogies could be drawn between the viscous parameteriation in the sea ice model and eddy viscosities and turbulent behaviour in the atmosphere and ocean [19]. Ultimately, it was discovered that a viscous rheology led to unrealistic ice motion, and that a different representation of the stress-strain relationship was needed. Field observations had suggested that the process of fracture and ridging could be described as being analogous to a plastic material reaching its failure point under stress before fragmenting and deforming. The visual similarity between fields of ice and granular materials such as soil, provided further motivation to use a plastic rheology. Early plastic models provided the starting point for the hybrid rheologies developed in the AIDJEX program. Although the purely viscous rheologies were abandoned in favour of the mixed plastic rheologies, it was demonstrated [19] that a viscous rheology could arise as the ensemble behaviour of a plastic material under a forcing that follows a normal ditribution about some mean value. To a first order approximation, the stress-strain relationship yields a viscous behaviour if the variations in strain rate are large enough, and a plastic behaviour as the variations vanish.

Implementation of purely plastic models of sea ice rheology proved problematic, as the mathematical description of a pure plastic rheology gives no way of determining a unique stress state of ice under forcing that is below the failure threshold. The solution to this problem is to use a hybrid rheology, which treats the ice as having different material properties when it is subjected to sub-critical forcing. An elastic-plastic rheology was one of the first such hybrids proposed in the modelling of sea ice. Elastic-plastic rheologies have the ice behaving as an elastic solid for sub-critical forcings, and have a yield curve that specifies the maximum forcing that the ice can be subjected to before it fails and deforms without resistance. Although introducing this hybrid rheology solves the problem of determining a unique stress for sub-critical states, the elastic-plastic rheology has two serious drawbacks. Due to the direct dependence of the stress on the strain in elastic materials, an elastic-plastic rheology requires any numerical simulations to keep track of the strain state of all ice as an additional state variable. Furthermore, numerical integration of the equations for the elastic-plastic model generally requires a Lagrangian formulation [20], which results in an extremely computationally intensive algorithm that makes model simulations

conducted with large spatial or temporal scales effectively impossible.

The solution to the problems associated with implementing elastic-plastic rheologies was to instead use a viscous-plastic rheology for the ice [20]. This mixed rheology addresses the short-comings of both the plastic and elastic-plastic approaches by presenting a mixed rheology which yields a unique solution for sub-critical states, and which does not require a Lagrangian formulation. The viscous component of this mixed rheology is markedly different from the viscous rheologies experimented with in the 1970s. Although the viscosity of subcritical states is derived from the work done on viscous rheologies arising as a bulk average behaviour of an ensemble of plastic materials with small, random variations in the stress rate [19], the model developed in [20] represented a significant development on that research. The viscous aspect of the model's rheology is not intended to reflect viscous flow in the ice, but is rather a means by which to keep track of the stress state under sub-critical forcing. The value of the viscosity varies spatially, and depends on the local state of the system. For regions with no forcing, the viscosity should become infinite, in order to prevent unrealistic motion of the ice. When integrating the model numerically, the maximum time step which may be used is a function of the viscosity, and so a maximum viscosity is prescribed to allow numerial simulations to be performed. For the viscous-plastic model, an elliptical Von Misces yield curve (Fig. 1.3) was used to determine the yield curve; all states within the curve exhibit viscous behaviour, and states on the curve represent plastic failure points. The curve preserves the physics which require the ice to have greater compressive than shear strength, and little-to-no tensile strength. A primary factor which motivated the choice of an elliptical yield curve, is that the mathematics describing the rheology are simplified and more computationally efficent than the teardrop or sine-lens yield curves, (Fig. 1.3) which had been proposed in earlier work [10]. In the event of failure, a rule is required to determine the direction of the resultant flow of material. Both models [10], [20] make use of the normal flow rule, which specifies that in the event of failure, the strain rate vector is normal to the yield curve. The convex shape of the yield curve and the normal flow rule arise as consequences of Drucker's postulate, which states that for any plastic material under stress, if additional stress is put on the material such that it fails, the work done must be positive. As noted in [10], a plastic model of sea ice does not completely adhere to this rule, but it may be approximated by a model.

The first iteration of this model used two thickness classes, so that a region was either open (water covered), had thin ice, or thick ice. The following year the model was modified [21]

by incorporating the work done on the dynamics of the sea ice thickness distribution [43]. The incorporation of a dynamic, multi-category, thickness distribution improved the accuracy of the model's simulation of ice coverage and extent. By making the sea ice thickness distribution a prognostic variable, model performance in prediction of ice thickness and extent is improved. This model has proved tremendously successful, and most models in use in modern climate models are drawn from its template. In the remainder of this work we shall refer to models with this construction as Hibler-style models. In 1992 a version of the 1980 model which made the assumption that ice had no shear resistance was introduced [14]. Under this assumption, the elliptical yield curve collapses to a line in the negative quadrant of primary stress space ($\sigma_1 = \sigma_2$, Fig. 1.3), and the resulting model has improved computational efficiency without compromising the performance beyond what was considered an acceptable amount for certain climate applications. Materials with this rheology are described as cavitating fluids. Subsequently, the most prominent improvement upon the 1980 model was the introduction of an elastic term into the viscous-plastic rheology [24]. The introduction of an elastic component was not to improve the physical realism of the rheology. Instead, introducing elasticity makes the model more amenable to multi-processor methods, and the problem of viscosity ranging over several orders of magnitude is avoided. Additionally, by including an elastic term, the model becomes more able to deal with transient behaviour.

The decision to model a population of sea ice using a continuum description also invokes the problem of how best to represent the effect of redistribution events. Redistribution events are caused by compressive and shear action resulting from velocity gradients across the ice, and by changing the thickness of the ice, they in turn affect the ice response to velocity gradients. Redistribution events are inherently localised, and resolving them in a model would require a spatial scale well beyond the available computational resources of most (if not all) research groups. To circumvent this issue, much work has gone into finding a rheological description of sea ice which is accurate for large-scale continuum models. The problem of finding a parameterisation to describe the large-scale effect of a large number of small, localised events is conceptually akin to the problems of eddy parameterisation in atmospheric and oceanic dynamics.

The Mohr-Coulomb rheological model (the wedge-shaped yield curve in Fig.1.3) provides another possible characterisation of the yield-curve for sea ice. The Mohr-Coulomb model was developed in the 18^{th} century as a representation of the behaviour of soil under com-

pression and shear. Since that time, it has been recognised as a general description of the behaviour of granular materials which display cohesive-frictional behaviour. Such materials manifest a high resistance to compression, but a relatively low resistance to shear forcing. These materials display very low resistance to dilation. The consensus in the sea ice modelling community is that ice displays a greater compressive strength than shear strength, and has little resistance to dilation and the similarity to the Mohr-Coulomb description is clear. A major advantage in using the Mohr-Columbic formulation is that lead formation arises naturally from the description of the response of the ice to forcing. In the granular model that Mohr-Coulomb rheology describes, the motion of the individual granules against each other may either compact the material or dilate it, depending on the angle of the forcing. These dilations and contractions are interpreted as the formation and closing of leads. Given that shearing processes result in the opening of leads in the ice, a rheology that naturally includes dilation of the pack is certainly desireable. A sea ice model which makes use of the Mohr-Coulomb rheology is the cavitating fluid model introduced by Flato *et. al.* [14], which uses Mohr-Coulomb corrections in shear stresses to aid in the representation of the lead formation process.

Another model which has received significant attention revisits the idea of treating ice as a granular medium, and uses a Mohr-Coulomb rheology (Fig. 1.3) [54]. Although granular flow treatments are often considered to be two phase flows (the motion of a solid component through a liquid medium), as the ice pack is considered a dense granular material, the motion is that of a dispersed single-phase flow. Modelling the motion of pack ice as that of a granular medium places emphasis on the interaction surfaces of the individual ice floes, which are represented as discs of uniform radius. Using the idea that motion occurs with floes sliding against each other on a line of fracture, one may use a Mohr-Coulomb formulation to specify the forces involved. Construction of this formulation produces a yield curve, which takes the form specified for Mohr-Coulomb rheologies.

In the last two decades a variety of alternative approaches to sea ice modelling have been proposed. These models range from Hibler-type models with different rheologies, to discrete element models which are formulated in a completely different manner to the standard approach. The issue that many of these alternative formulations seek to address is representation of the anisotropy of the redistribution process in a continuum model. The rheology of most force balance models makes the assumption that the ice contained within each model grid cell is a representative sample of the population. By making this assumption, a stress-

strain relationship may be proposed as a large scale average of the unresolved redistributions occuring at sub-grid scales. As model resolutions increase with greater computational resources, the assumption that each grid cell contains a heterogeneous sub-population of ice can no longer necessarily be made. One of the key assumptions that is made in Hibler-type models is that the rheology is isotropic, and there are no preferred directions of failure. Alternative approachs do not assume isotropy, and models which take this approach are referred to as anisotropic models. Observations have shown that there is some structure to the fracture patterns in ice pack, with the majority of fracture lines occuring in two directions, which intersect at an angle of approximately 40 degrees. It has been suggested [63] that the primary directions of fracture are aligned with the characteristics of the partial differential equations that describe the stress state in ice. Due to a shortage of observational evidence, this idea has yet to be validated. Although there has been increasing interest in anisotropic approaches, work done using a modified version of the Hibler-style model has demonstrated that it is possible for an isotropic model to produce linear features similar to observation [25]. The modification primarily consists of seeding a Hibler-style model with random variations in ice strength, and allowing the ice strength to evolve dynamically, with a dependence on the divergence of the velocity field. With these modifications a high resolution model was capable of producing oriented fracture patterns.

Despite the advances made in the last 20 years, there remains a lack of consensus on the most appropriate representation of the rheological properties of sea ice, both in models which treat ice as a continuum, and those which treat it as comprised of discrete floes or blocks.

1.6 The Structure Of The Thesis

We approach the problem of modelling the dynamic evolution of the thickness distribution first by examining the statistics of sea ice populations. This is done in Chapter 2, and allows us to identify the features of the populations which are particluarly relevant to this work. The data analysis is followed by Chapter 3 which introduces a well-known family of equations that our model is based on. These equations have been studied in other fields of research and have a number of properties which make them very useful in the construction of a model of the redistribution process. In Chapter 4, we introduce the model which we have developed, detailing its structure, and performing a sensitivity analysis. We conclude with a brief chapter in which we recapitulate the main findings of our work, and propose

the ways in which this research could be used in a wider context.

Chapter 2

Observed sea ice thickness distributions and their variability

2.1 Global observations of sea ice thickness distributions

The thickness distribution of sea ice may be estimated from a variety of different data sets, including those gathered by IPS, draft measurements from submarine cruises, ice cores drilled by surface teams, and electromagnetic induction sounding [58]. Draft and thickness measurements have been used to estimate thickness distributions in many areas of the Arctic and Antarctic.

It has been noted by many sea ice researchers that the distribution of the thicknesses (or drafts) of sea ice is approximately negative exponential. This characteristic form has been observed in sea ice located in both the Arctic and Antarctic. In the Arctic, measurements of the thickness distributions of sea ice have been made at a wide variety of locations. Due to the Transpolar drift, there is a clockwise motion of ice around the Arctic basin, which eventually deposits ice in the Fram Strait, where it enters the North Atlantic. Due to the Transpolar drift transport, the ice populations which are observed at the Fram Strait [57] have a different history than those observed in *e.g.*, the Beaufort sea. They are typically older, and contain ice which has been in the Arctic basin for several years. Despite differences in population makeup, the thickness distribution in sites ranging from the Bering Sea to the Beaufort [59], to the ice exiting the Arctic basin through Fram strait [57], all display exponential thickness distributions, as is clearly seen in the distributions reproduced in Fig.2.1.

The Antarctic presents a different theatre for the creation and evolution of sea ice; unlike the Arctic basin, which is ringed by land, the Antarctic is surrounded by open ocean. Despite the geographical differences, the thickness distributions of Antarctic sea ice also display an exponential form [31],[62]. Comparison of thickness distributions between sites in the Arctic and in the Antarctic has shown that, while there are quantitative differences between the thickness distributions, they both display a clear exponential decrease [64].

The data used in this study were collected by H. Melling at sites along the continental shelf in the Beaufort Sea (Fig. 2.2) along a line which stretches from approximately 70 °N 134 °W to 74 °N 126 °W [37]. These data were gathered between 1990 and 2004 as part of an ongoing effort to gather information about sea ice on the continental shelf in the Beaufort sea. The data were gathered by moorings, which utilize upward-facing sonar to acquire a continuous record of the draft and velocity of the ice passing above [6], [36]. This measurement process creates a continuous record which is divided into tracks of approximately 40km length, each of which contains approximately 40000 draft measurements. The divisions between tracks are made manually, chosen to take into account factors such as notable events in the ice motion. As the intention was to create tracks of length close to $40km$, the time over which a single track was recorded varies from a few days to approximately 3 weeks, depending on the amount of ice transported over the site. The total number of tracks at each site ranges from 48 to 195 (Table A.2). Specific details on the data treatment may be found in [38], [39]. Estimates of the sea-ice draft distribution are computed as histograms with 0.1m bins.

The observational data we make use of in this study were taken by ice profiling sonar (IPS) which measures and records the draft (which, for our purposes, can be used as a proxy for thickness) of the ice passing above it at a fixed interval. Details on instrumentation are given in Appendix A.1. When processing and analysing observational data, a discrete form of $g(h)$ is used (in this and previous studies) due to the finite resolution of the data set. In the data we use, a pseudo-spatial transect of the ice drafts may be reconstructed from the IPS readings, and a thickness distribution may be defined in terms of the length of the reconstructed transect occupied by ice in each thickness category:

$$g_L(h)\mathrm{d}h = \frac{1}{L}\mathrm{d}l(h, h + \mathrm{d}h), \tag{2.1}$$

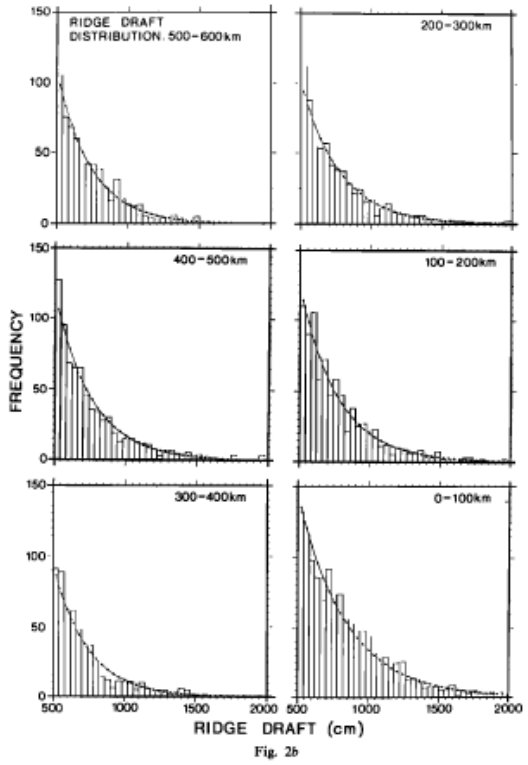

Fig. 2b

(a) Beaufort

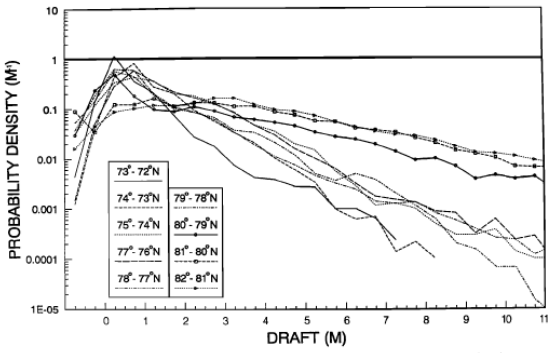

Fig. 7. PDFs of ice draft in 1° latitude bins in the Greenland Sea, from 82°N to 72°N, drawn on semilogarithmic scale.

(b) Greenland

Figure 2.1: Sea ice thickness thickness distributions estimated from observations in the Beaufort Sea and the Greenland Sea, both of which display the characteristic exponential tail (reproduced from [59], [56])

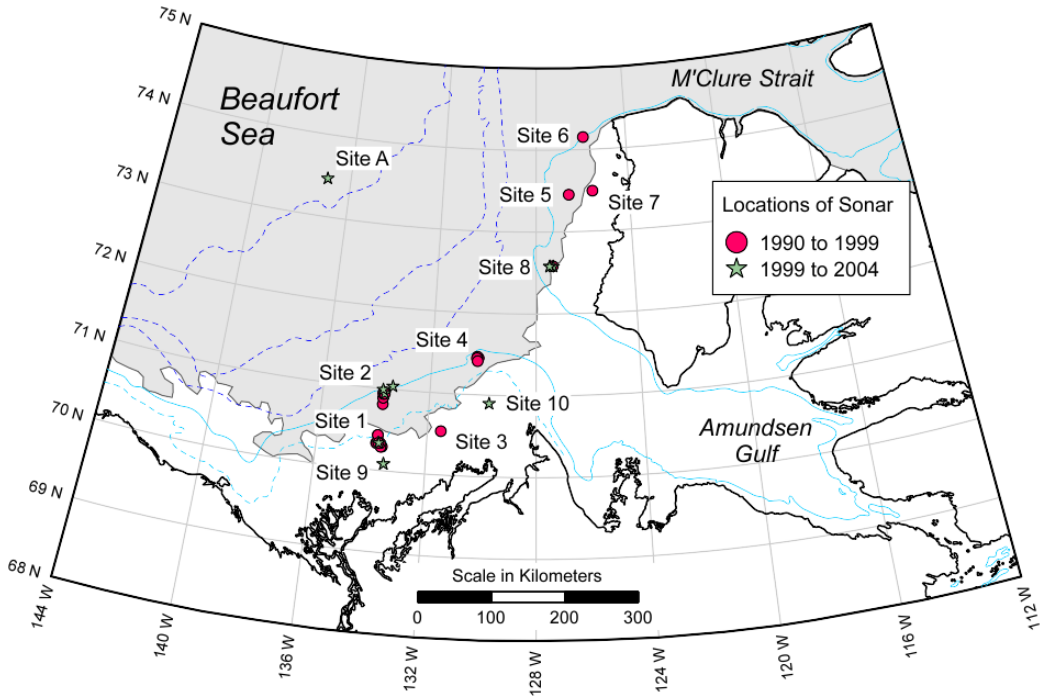

Figure 2.2: Locations of the IPS mooring sites considered in this study. This study uses data from Sites 1 and 8.

where L is the total length of the transect. This work will use the empirical estimate (Eqn. 2.1) when discussing features of the observational data, and the more abstract definition (Eqn. 1.3) in model construction and discussion.

We examine data from Sites 1 and 8. These particular sites have been chosen for two reasons: they have the most extensive records available, and they are located in areas with different annual ice population regimes. Site 1 is in a seasonal ice zone, typically free of sea ice in August and September, whereas Site 8 typically has a year-round ice presence. The data from the perennial ice region are more sparse due to the difficulties the environment presents to the regular maintainence of and access to the moorings. Our primary focus in this study is on the Site 1 observations, because they form the longest continuous record, with the largest number of tracks per month. Site 1 was in continuous operation from 1990 to 2002 and 543 separate tracks were recorded in this interval. Of the 13 annual data records, all but 3 have over 10 entries, and 7 of them have more than 40. Some previous analysis of the track data for Site 1 has been performed in [2], in which draft distributions were generated from the data for the purposes of model evaluation. Data were gathered at Site 8 from 1997 to 2001. The site was located in regions of permanent ice cover in order

to gather data on a more persistant ice population. While there are fewer observations compared with Site 1, Site 8 has the largest dataset of all sites with year-round ice.

2.2 Analysis of annual population statistics in the Beaufort

Although the seasonal cycle of thermodynamic and mechanical forcing prevents an ice population from reaching an long-term equilibrium state, the ice can still reach a cyclostationary state. Furthermore, while the exponential tail of $g(h)$ is generic, its slope and truncation point varies with location and time of year, and between individual time-series gathered from a single area. On short time spans (days to weeks) the change in the population of ridged ice that makes up the exponential tail is influenced less by the thermodynamic process than by the dynamic redistribution of ice. The thicker the ice is, the slower the growth will be (compare growth rates of thick ice to those of thin ice in Fig. 2.2). It should be noted that the melt rates of ridged first-year ice are faster than those of unridged ice, as the rubble forming the keel is typically unconsolidated and the incursion of warm water into the spaces between ice blocks can increase the ablation of the ice [3]. However, increased melt rates in are not seen in multi-year ice ridges, which typically have consolidated keels. Given that unconsolidated ridges form a subpopulation of the ice, and much of the data which we examine is from the ice growth season, we will assume that we may use the melt rates as given by [53]. Given this assumption, we may conclude that major changes in the extent of the exponential tail over short time spans are primarily due to redistribution events. Redistribution events consume more energy with the increasing thickness of the ice involved due to the increase of material strength of ice with thickness and the greater change of gravitational potential energy which accompanies the formation of large ridges. Since the amount of energy available to the population of ice is finite, and the work bounded, the exponential tail cannot grow indefinitely.

In order to explore the effect of the progression of the seasonal cycle we will bin the time series by month. We will use ice draft as a proxy for thickness, and write k for draft measurements, *e.g.*, $g(k)$ for the draft distribution. The data in each monthly bin can generate a ensemble of estimates of the draft distribution in that particular month, and we can compute the mean and standard deviation of $g(k)$ over this ensemble (denoted $g_\mu(k)$ and

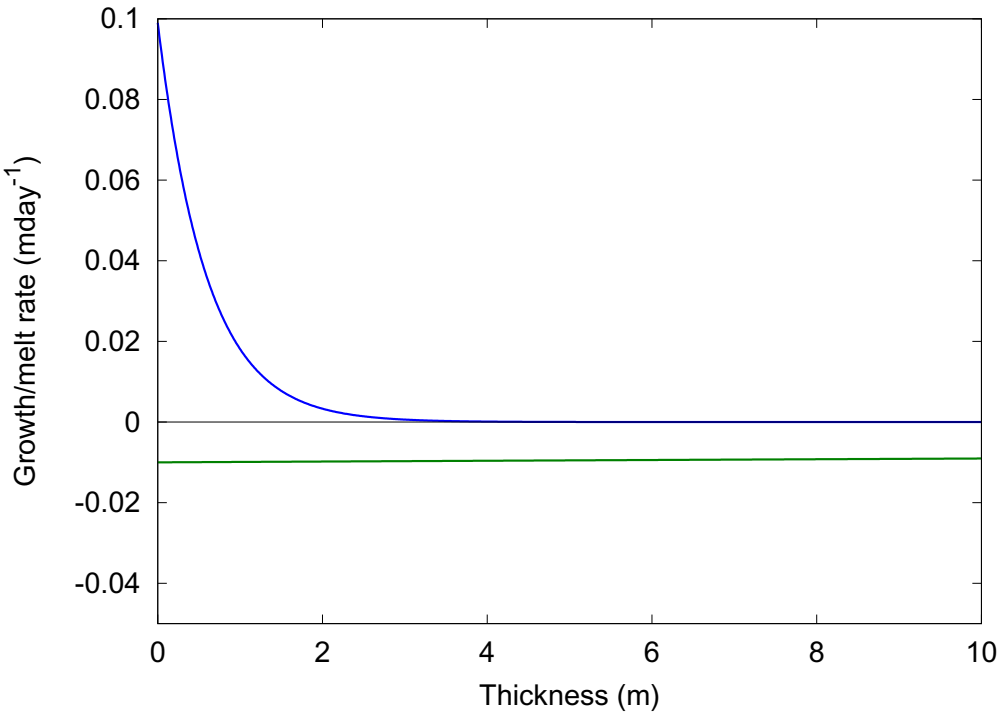

Figure 2.3: Approximate, observationally based, growth and melt rates for sea ice in winter and summer [53]

$g_\sigma(k)$ respectively). Our work does not seek to adjust or compensate for such factors as inter-annual variability, and instead provides a general picture of the statistics of the ice at the two sites we study and its dependence on the seasonal cycle.

In the following sections, we examine the seasonal variation of $g_\mu(k)$ and $g_\sigma(k)$ as estimated from the track data. The variability in the sea ice population is compared to output from a basin-scale sea ice model. In light of these comparisons, conculsions are drawn regarding the ability of a sea-ice model to capture this aspect of the population.

2.3 Observed Thickness Distributions: Mean and Variability

This chapter deals with sets of empirical distributions of sea ice draft estimated from samples of finite size. From these sets of distribution estimates, we may calculate the ensemble-mean draft distribution, $g_\mu(k)$, and the standard deviation of the ensemble of draft distributions around the mean, $g_\sigma(k)$. By examing the variability between samples, we develop a new metric of the state of a population of sea ice. Our rationale in introducing this metric is that it will provide an intuitive means to gauge the degree of variability in the population of ice, and consequently a new test of the performance of sea ice models. We expect some degree of variability as part of the sampling process: if drawn from a population in (local) stastistical equilibrium, an ensemble of empirical distributions $g(k)$ will display the statistics of a binomial distribution in any individual ice draft class[44], [49]. Deviations of the variability from the binomial distribution are due to disequilibrium caused by variability in both thermodynamic forcing and in the dynamic interactions between ice floes.

Our analysis will make use of the ratio of the ensemble standard deviation to the mean as a function of draft, $R(k) = g_\sigma(k)/g_\mu(k)$, as a useful measure of the relative degree of variability in estimates of $g(k)$ between ensemble members. Figure 2.4 shows $R(k)$ for January at Site 1 corresponding to the plots of the mean and standard deviation displayed alongside. For this particular set of tracks, $R(k)$ is within an order of magnitude of unity for drafts greater than the mode, and only varies within one order of magnitude, taking values between 0.5 and 3. Due to the increasing strength of sea-ice with draft, the draft categories most actively involved in redistribution lie below the mode draft of the mean distribution.

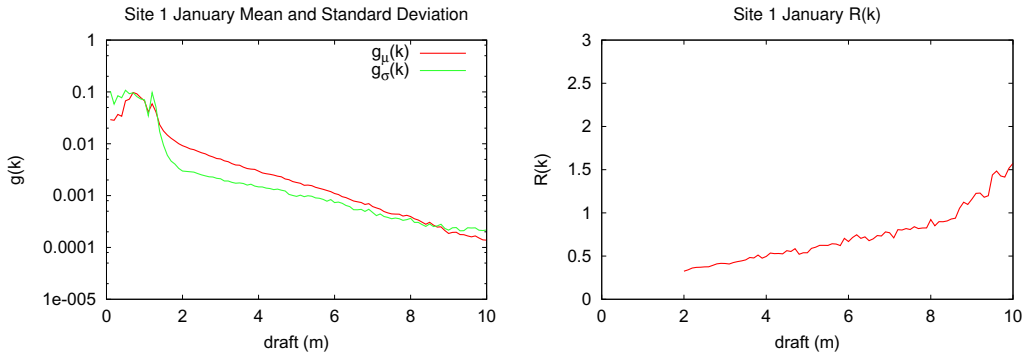

(a) $g_\sigma(k)$ and $g_\mu(k)$ (b) Ratio of $g_\sigma(k)$ to $g_\mu(k)$

Figure 2.4: Mean ($g_\mu(k)$), standard deviation ($g_\sigma(k)$) and their ratio ($R(k)$) for a multi-year composite of Site 1 January Data

The higher values of $R(k)$ for $k < k_{eq}$ are likely due to this feature of sea-ice interactions. The thinner ice is able to raft, which requires less energy than ridging redistributions involving thicker ice do, and so can happen under a greater range of forcings. The ice in thickness bins lower than 2m has growth and melt rates associated with thermodynamic processes which are impossible (using the present data) to disentangle from mechanical causes of changes in thickness. For this reason we will focus on the statistics for the ice above 2m, for which the thermodynamic growth towards a seasonal equilibrium is not as central in the evolution of the ice over the timescales which we consider.

2.4 Observed Sea Ice Draft Distribution Statistics

The ensemble mean and standard deviation ($g_\mu(k)$ and $g_\sigma(k)$) of the draft distributions for each calender month at Site 1 are shown in Fig. 2.5. As is to be expected of an area with seasonal ice cover, there are no data at Site 1 for August and September, when the waters are ice-free. Both October and November statistics show that the region is still in transition between winter and summer ice maximum thicknesses: with a cutoff of $g(k) = 10^{-5}$ or 1 in 100,000 observations, the thickest ice observed is 6m in October and 8m in November.

The ratio $R(k)$ between the $g_\sigma(k)$ and $g_\mu(k)$ of the ice draft distribution takes a minimum value at the 2m cutoff we use (Fig. 2.6). In the months of October and November there are insufficient data to generate reliable frequency statistics on ice thicker than about 6 and 8 meters respectively. Over the period spanning October to June, we see a progressive decrease in the slope of the linear portion of $R(k)$; the slope approaches zero in April. The rate

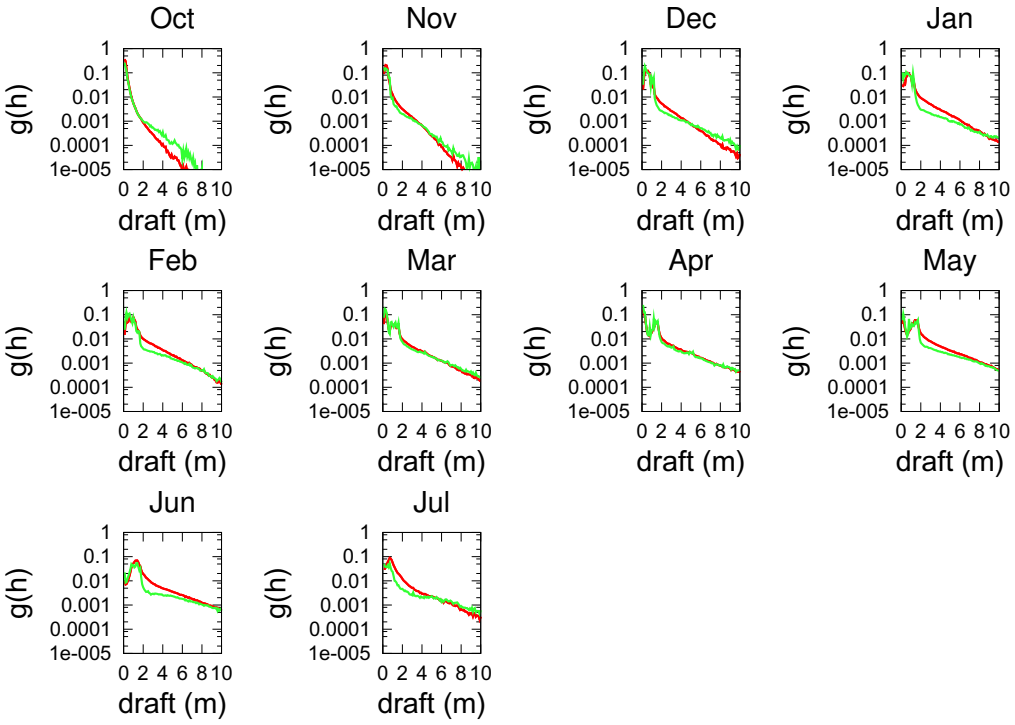

Figure 2.5: Annual procession of mean draft distribution (red) and standard deviation (green) at Site 1

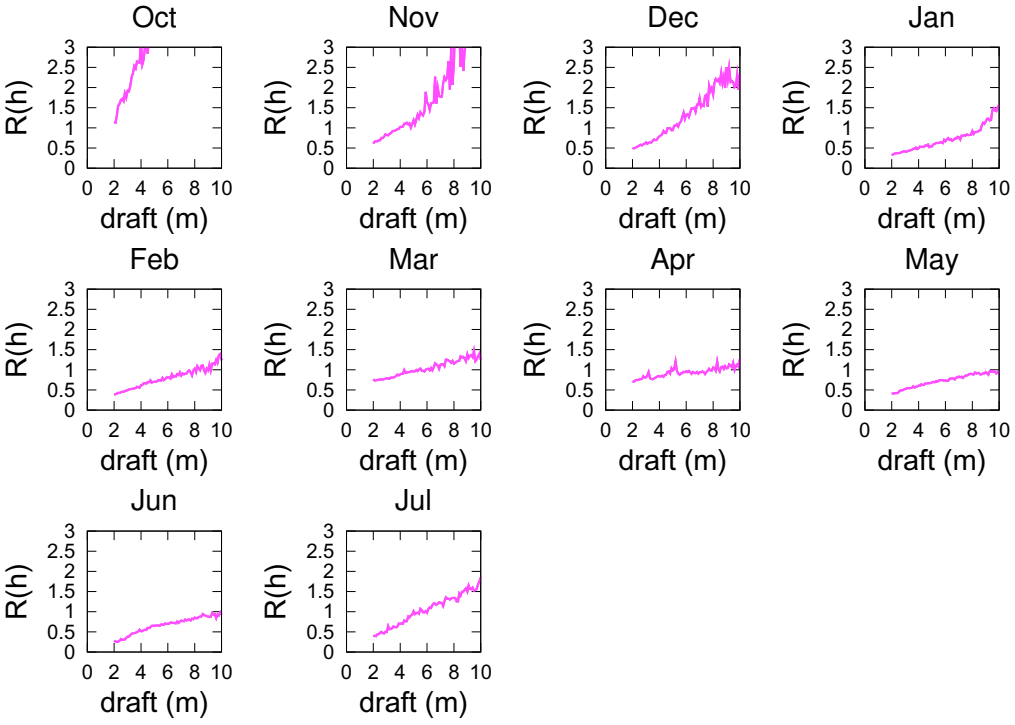

Figure 2.6: Annual procession of the ratio of $g_\sigma(k)$ to $g_\mu(k)$ at Site 1

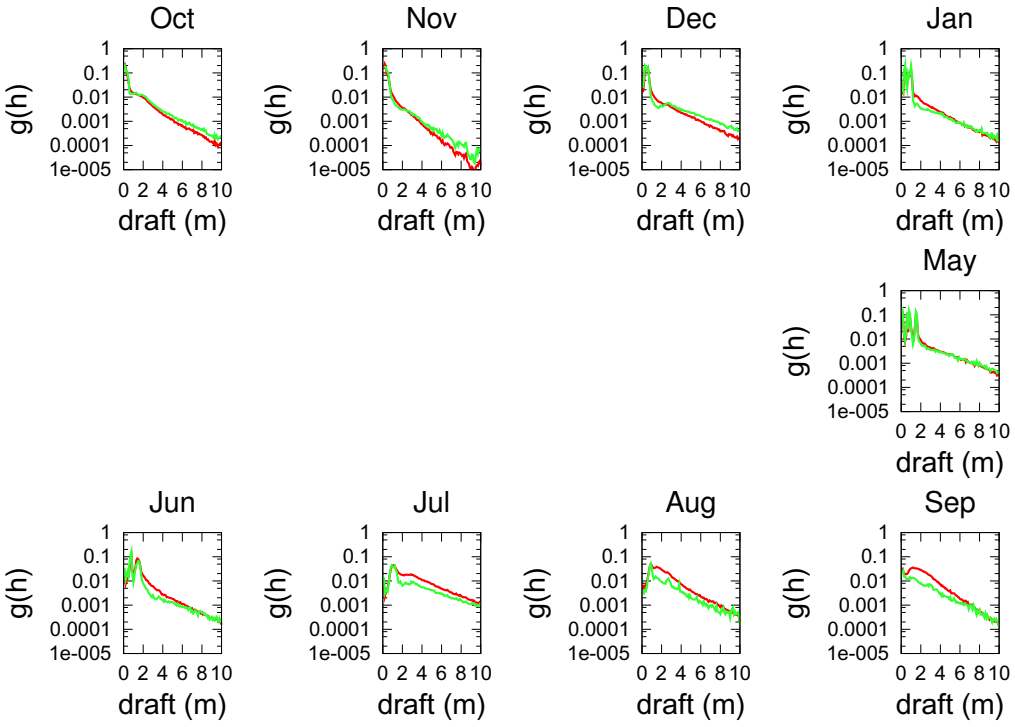

Figure 2.7: Annual procession of mean draft distribution (red) and standard deviation (green) at Site 8

of decrease of the slope from month to month is greatest between October and January.The value of $R(k)$ ranges between approximately 1 and 3 in this segment of the population, and is lowest in October and November, with $R(k < k_{eq}) \approx 1$.

We now contrast the thickness population statistics at Site 8 with those from Site 1. For the months of February, March, and April, there are relatively few track records at Site 8, and we do not compute statistics for these months. Due to the conditions at Site 8 (shorter deployment time and the inaccessability of the site under certain winter conditions), the records of ice from May to January contain the most data points, although it is not as rich a data set as that from Site 1, *c.f.* Table A.2.

Despite the differences in ice conditions at the two locations, the statistics for $g(k)$ and $R(k)$ generated by the Site 8 track data are similar to those from Site 1. The slope of the exponential portion of $g_\mu(k)$ at Site 8 is similar to that of the observations at Site 1 in the winter. The ensemble means $g_\mu(k)$ from Site 8 (Fig. 2.7) show a more pronounced peak around the mode of the population than those from Site 1 (Fig. 2.5), but the same annual

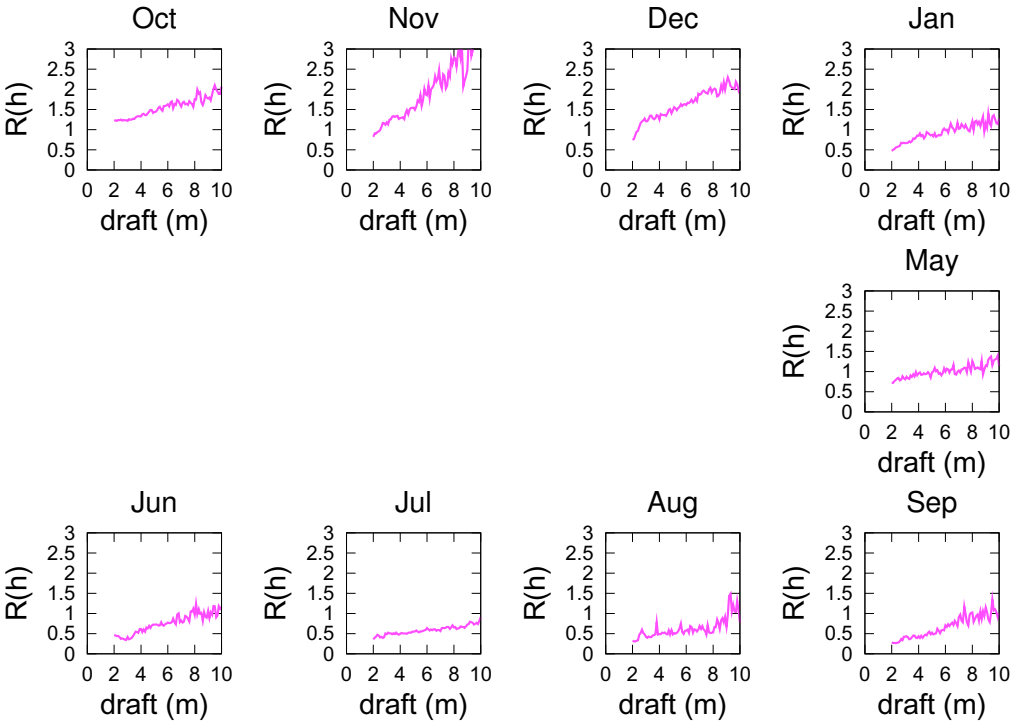

Figure 2.8: Annual procession of the ratio of the standard deviation to the mean draft distribution at Site 8

cycle is present in $R(k)$ and the range of values that $R(k)$ takes is the same (between 0.3 and 3). Comparison of Fig. 2.8 with Fig. 2.6 show that both sites produce a linearly increasing $R(k)$ for ice above 2m. The ratio $R(k)$ takes largest values in the November data. At Site 1, for the period spanning February to June, $R(k)$ for the thicker ice approaches unity, particularly in the period spanning February. At Site 8 we see a similar pattern, although the slope of $R(k)$ smaller, and $R(k)$ is typically less than 1.

At both Site 1 and Site 8 the rate at which the slope of $R(k)$ changes has a seasonal cycle. The slope changes the fastest at the onset of the freezing season (October), and decreases until about January, when the slope is quite shallow relative to the previous months. At both sites, the slope changes very little from January through to June at Site 1 and January through to August at Site 8. The relative consistency of the degree of variability during these periods suggests that the population approaches a static state during the period from October to January. Due to the transition to an ice-free region and back which occurs at Site 1 over the summer, there is a large and rapid increase in variablity, (compare the slope of $R(k)$ for Sites 1 and 8 in October in Fig. 2.6, 2.8), which is not observed to the same degree at Site 8, which has year-round ice cover.

2.5 Comparison with the Hibler model

Given the presence of an annual signal in the variability of the ice populations measured in the Beaufort, it is natural to ask whether this signal is reproduced by a typical sea ice model. As will become clear, the model we use does not produce an accurate representation of the ice population at either site, with large disparities in the thick ice particularly at Site 1. It must be understood that this comparison is not performed in order to test the model's ability to simulate the exact details of $g(k)$ and $R(k)$ at Sites 1 and 8. The aim of our analysis is to gauge the extent to which a typical sea ice model produces cycles in g(k) and R(k) which are qualitatively comparable to the observations. We compare the observations with populations simulated using a Hibler-style model as discussed in Chapter 1. For comparison to the Site 1 and 8 data, model output is taken from a 39 year basin-scale simulation with 28 levels of draft resolution, and 160km^2 grid cells [15]. This grid is sufficiently fine to allow us to identify two separate, non-adjacent, cells corresponding to the locations of Site 1 and Site 8. However, the resolution is much coarser than would be needed to isolate the particular regions in which the physical data was gathered. Furthermore, there is a degree of spatial averaging inherent in the model populations. We also note that the model ice draft

discretisation is not uniform: draft categories are coarser for thicker ice than for thinner ice (Table A.2). As the populations we examine from the field data are concentrated in the 0-10 metre draft range, we use the first 17 draft classes from the model output. As the data from [15] are a single $g(k)$ for each grid cell at one month intervals, we take ten years' worth of data for one calendar month to generate our monthly statistics. Where there are more than 10 tracks available in the observations, we randomly select 10 of them to compare to our ensemble of 10 model distributions.

We plot the annual cycle of the mean and ratio for the model output and observations

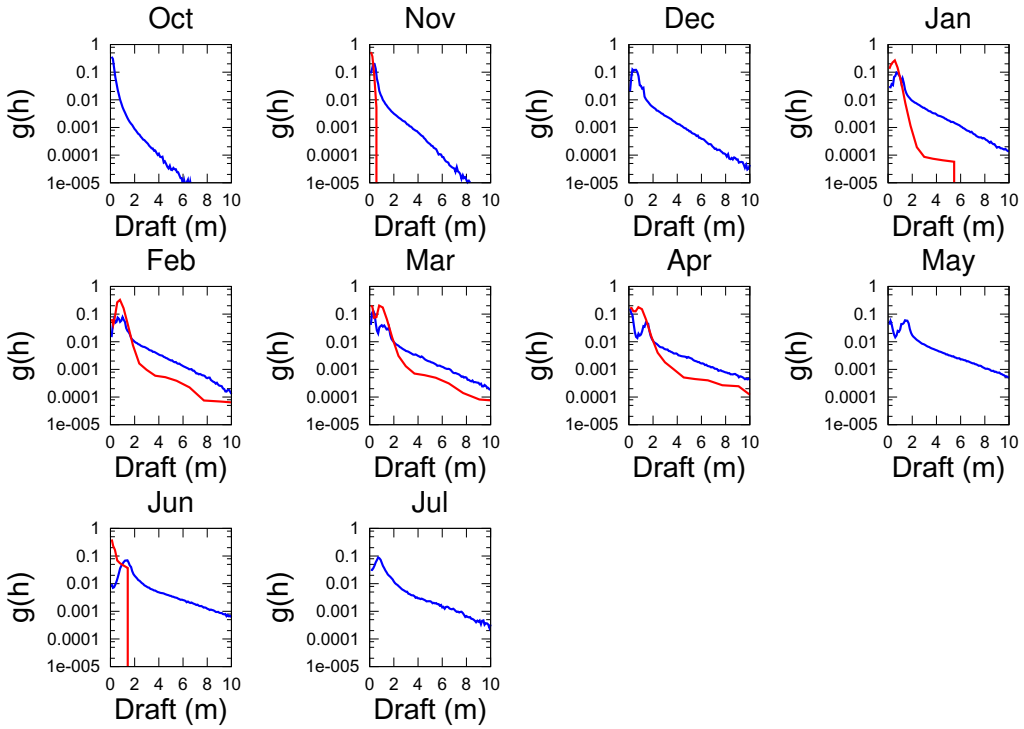

Figure 2.9: Comparison of Site 1 mean draft from observations (blue) and Hibler model output (red)

for both sites in Fig. 2.9-2.12. In comparing $R(k)$ between the model and the observations, it can be seen that the $R(k)$ generated by the Hibler model run is of the same order of magnitude as that generated by the observations. However, the model produces populations with qualitatively distinct kinds of variability at the two sites, which is not seen in the observations. At the grid cell corresponding to Site 1, g_μ may be calculated in the period from January-April, and the region is ice-free otherwise. In months when ice is present, the simulated g_μ has less thick ice than the observations, with the disparity between simulations

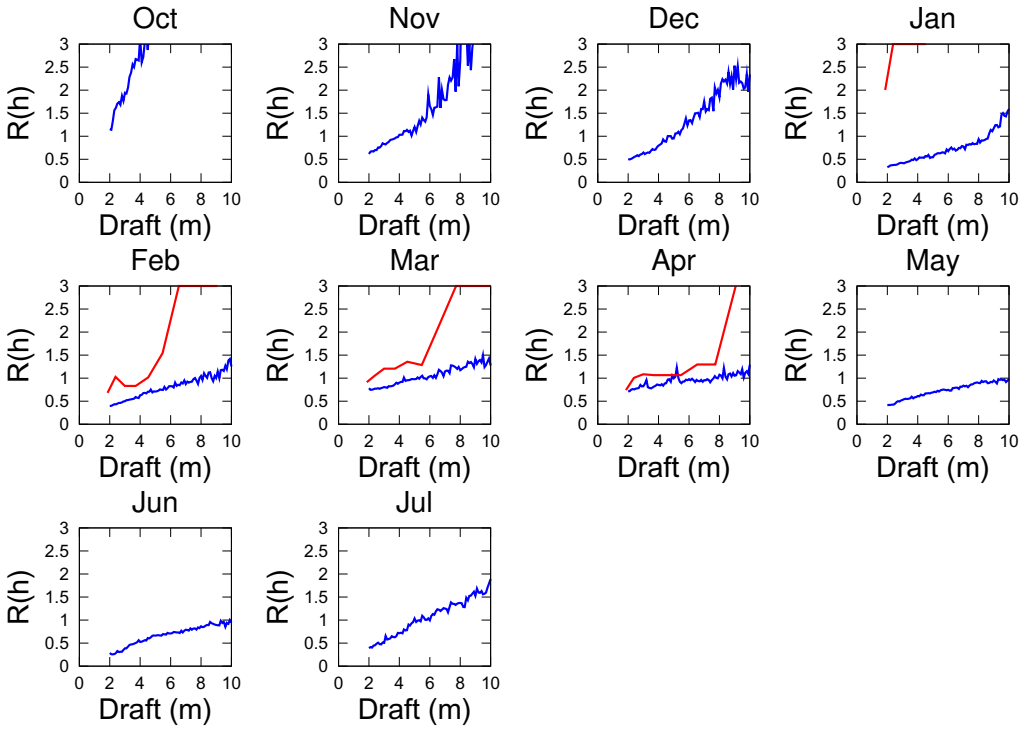

Figure 2.10: Comparison of Site 1 $R(k)$ from observations (blue) and Hibler model output (red)

and observations increasing with thickness. Due to the essentially ice free conditions in the grid cell from July through to November at Site 1, comparison of the model $R(k)$ to observations is impossible. Of the months for which statistics may be calculated, the January population is truncated at approximately 5 meters (the observations show the ice extending to drafts of 10m) and the simulated $R(k)$ rises very rapidly above 2m, terminating at 5m. The form of the simulated $R(k)$ for January is qualiatively similar to observations, however, it is foreshortened by a factor of 2, corresponding to the termination of the population at 5m. While the $g_\mu(k)$ produced by the model for February to April is over an order of magnitude smaller than the obervations for ice above 2m, the $R(h)$ is a good approximation of the observed $R(h)$, featuring the same high values for thin ice, minima at approximately 2m, and increasing values for the thicker ice.

The model has more success in reproducing the population thickness distributions at Site 8, although it performs more poorly than at Site 1 in its representation of $R(k)$. In general, the variability seen in the simulated $R(k)$ at Site 8 is qualitiatively different from the observations. Where the observations have an $R(k)$ which has a minimum at 2m, with a linear

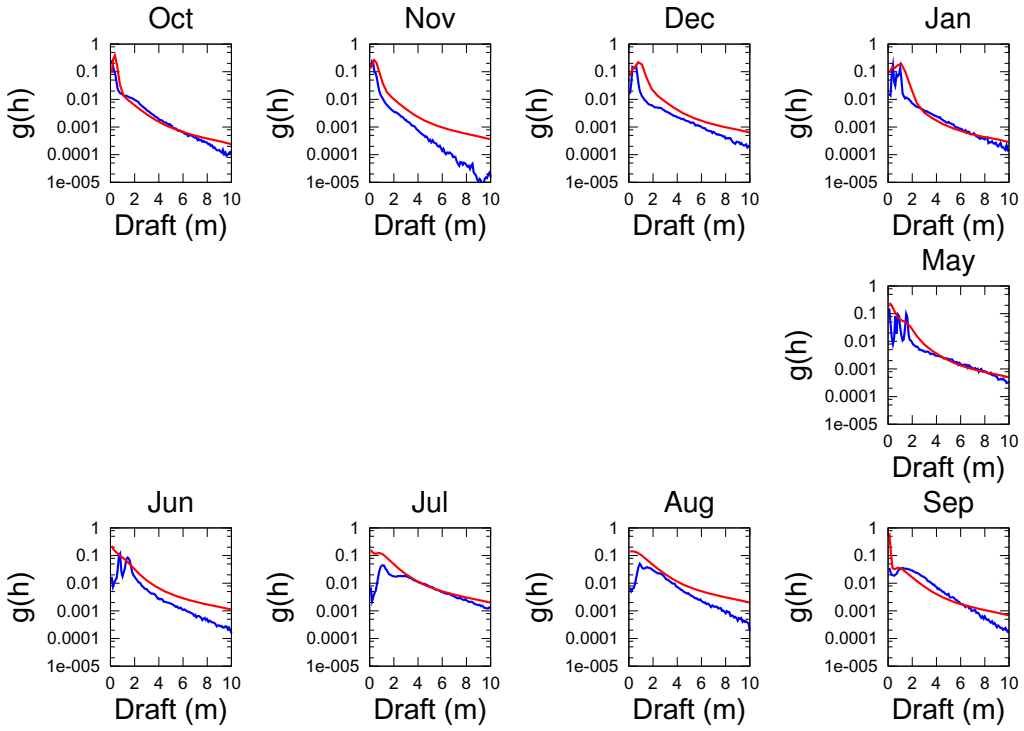

Figure 2.11: Comparison of Site 8 mean draft from observations (blue) and Hibler model output (red)

upward trend for higher k, the populations simulated by the model in the grid cell containing Site 8 have nearly constant $R(k)$. While the slope of the simulated $R(k)$ is similar to the slope of the $R(k)$ from observations, the model underestimates $R(k)$ in the period spanning October to June, and overestimates it from July to September.

The causes behind the almost constant value of $R(k)$ for the simulations in the grid cell corresponding to Site 8 are not readily understood. Where the observed $R(k)$ is larger than the simulated $R(k)$, we posit that the simulated population has a slightly more persistant presence of thick ice, both annually and interannually. It is not clear from the plots of observed and simulated g_μ this situation is the case, however. Where the simulated populations overestimate $R(k)$, we infer that the model treats the relevant range of thicknesses as more active than is actually the case. Ultimately, the apparent cycle in the simulated $R(k)$, progressing from overestimating $R(k)$ for most drafts in October to primarily underestimating it in the period from July to September does not admit a simple explanation, moreso when the disparity between the statistics are compared with those from Site 1, where the model's performance is markedly better, despite producing populations with thickness dis-

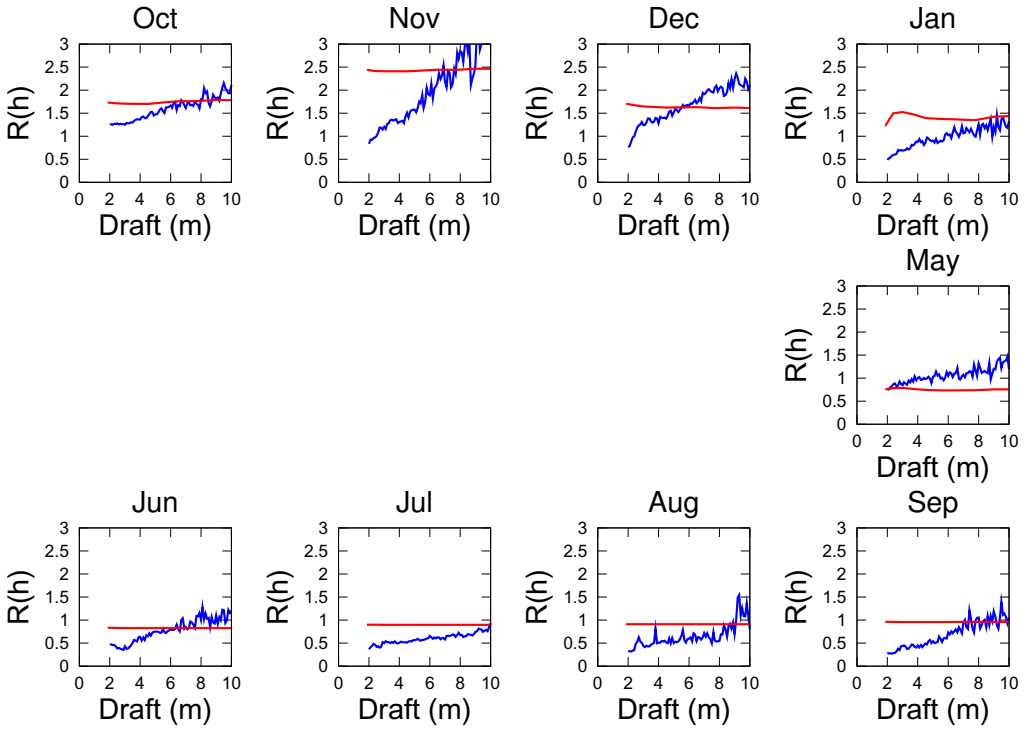

Figure 2.12: Comparison of Site 8 $R(k)$ from observations (blue) and Hibler model output (red)

tributions which differ from the observed thickness distributions to a much larger extent.

2.6 Conclusions

We have analysed the population statistics of sea-ice time-series data from IPS located in the Beaufort. Track data was stratified by calender month and the mean draft distributions and variability between tracks was calculated. When the variability was compared across months, an annual cycle in the variability becomes apparent. The $R(k)$ from the output of a standard basin-scale ice model is compared with the observations and is found to differ qualitatively, suggesting a failure of the model to accurately represent the sensitivity of the ice population to variations in forcing and thermodynamic conditions.

The analysis of the variability between the individual tracks in an ice population could prove useful for data collection and analysis, as it provides a tool to gauge the likelihood that a set of observations are an accurate representation of the population. Furthermore, knowledge of the variability to be expected of a population could improve the confidence

intervals accompanying operational ice forecasts made from observations. For the sea-ice modelling community, the analysis of population statistics provides a new metric by which to judge model performance: not only should a model produce the observed draft distribution, and its seasonal cycle, but the statistical features of the output distributions should match those of the observed ice populations.

This work represents a first step in considering this metric. In order to make it a useful tool for the sea-ice, analysis of the population statistics from a wider set of observations is needed. By doing analysis of a broad range of populations, a classification system can be developed to relate the makeup of a population to the variability it will display. For the modelling community, an analysis of the ability of different sea-ice models to capture the variability of the population as represented by $R(k)$ will yield useful, and previously unutilised, feedback on the performance of model ice thickness redistribution schemes.

Chapter 3

Representation of Ice Thickness Distribution Dynamics with Smoluchowski Coagulation Models

Having examined the statistics of populations of sea ice gathered using IPS in Chapter 2, we turn our attention to the mathematical characterisation of the redistribution process. Smoluchowski Coagulation Models (SCM) have the potential to be excellent tools for studying the relationship between the physical processes that drive the evolution of populations of ice and their statistical features. In its simplest form, the SCM is a system of ordinary differential equations describing the dynamics of a population of individual elements (usually referred to as 'particles') defined by their 'mass' which can interact with each other by combining to form more massive particles. The SCM paradigm may be extended to include fragmentation processes, wherein an particle dissociates into two smaller particles, and the field of fragmentation models examines the behaviour of such systems. Having demonstrated their utility as a tool in statistical mechanics, SCMs are a well-studied family of equations which admit analytical solutions in some instances. Such models are potentially of great use for the study of sea ice populations, in particular providing insight regarding the details of the parameterisations of thickness redistribution processes in sea ice components of GCMs.

In this chapter we will first provide a brief overview of the behaviour of SCMs. We will then examine an example of an existing sea ice model [51] which has some elements in common with SCMs. To provide an illustration of the potential that the SCM formulation

shows in sea-ice modelling, we demonstrate how a simple SCM model of sea ice thickness distribution dynamics can capture many of its essential features, without being dependent on the parameterisation of the various processes involved, or the fine tuning of any constants in the model.

3.1 Smoluchowski Coagulation Models

The Smoluchowski Coagulation Model (SCM) was derived in the early 20th century and describes the dynamics of a population of particles of varying mass which may combine with each other. The coagulation model has been extensively studied due to its utility in a variety of areas in applied mathematics, ranging from astronomy to population genetics. Formally, a function $u(x,t)$ describes the number of particles of mass x in the system at time t. Particle sizes may be discrete or continuous. The interaction rule states that two particles of masses x and y may interact ('coagulate') to create a single particle of mass $x+y$. The rate at which interactions happen is dependent upon the number of particles of mass x and y, and a kernel which describes the interaction rate as a function of particle mass.

In the case where the particle masses are discrete, they may be enumerated by the natural numbers. We may write a set of functions, $u_k(t)$, the k^{th} element of which gives the number of particles of mass k at time t. We may then write the set of coupled differential equations for the discrete SCM:

$$\frac{\mathrm{d}u_k(t)}{\mathrm{d}t} = \frac{1}{2}\sum_{j=1}^{k-1} K(k-j,j)u_j(t)u_{k-j}(t) - u_k(t)\sum_{j=1}^{\infty} K(j,k)u_j(t). \tag{3.1}$$

The k^{th} equation describes the time rate of change of the number of particles of mass k. The first term on the right hand side is a source term, which accounts for all possible ways to make particles of mass k by combining particles of mass j and $k-j$. The second term on the right is the sink term, covering all of the possible combinations that a particle of mass k may make with other particles. To complete these equations, the rate kernel, K must be specified. The kernel K should be symmetric in its arguments, as it is assumed that the only factor which affects the rate at which particle interactions occur (besides the particle number) is their mass. The symmetry of K requires the insertion of a factor of $1/2$ before the source term in order to avoid double-counting of interactions

The continuous analogue of Eqn. 3.1 uses a single function $u(x,t)$ to describe the number density of the population, with dynamics described by the integro-differential equation:

$$\frac{\partial}{\partial t}u(x,t) = C(u) \tag{3.2}$$

where

$$C(u) = \frac{1}{2}\int_0^x K(x-x',x')u(x',t)u(x-x',t)\mathrm{d}x' - u(x,t)\int_0^\infty K(x',x)u(x',t)\mathrm{d}x'. \tag{3.3}$$

As with the discrete equation, the first term on the right hand side is the source term, the second is the sink term, and $K(x,x')$ is a symmetric rate kernel.

3.1.1 Analytic Solutions

Some of the appeal of developing a model of sea ice thickness dynamics based on the SCM formulation is its simplicity and universality. It is a generic representation of a system in which smaller elements combine to form larger ones. A variety of physical systems may be modelled by choosing the appropriate kernel. Although the system is inherently nonlinear, there are some kernels for which it admits a simple analytic solution given the initial conditions of $u_{k^*}(0) = M$ for a particular k^*, and zero otherwise in the discrete case; and $u(x,0) = \delta(x_0)$ for some x_0 in the continuous case ([1]).

For a range of analytic forms of $K(x,y)$ for which analytic solutions can be determined, these solutions (discussed in detail in Appendix A.3) are approximately exponential in form (*e.g.* the plot of the solution to Eqn. A.1 in Fig. A.3). That these near-exponential populations arise from SCMs with a variety of rate kernels makes it tempting to suggest that the robustness of the exponential tail of sea ice thickness is a consequence of the redistribution dynamics naturally being expressed as such a model.

It is important to note that the SCMs in standard form do not conserve the population size, and the total number of particles decreases with time as particles coalesce. The SCM framework may be suitable to describe the way in which ice is redistributed to form ridge structures, but it does not include the relevant process of the formation of open water through shear or thermodynamic ice thickness evolution. The nature of the dynamics described by SCMs precludes the possibility of the creation of particles in the lowest mass category and the decrease in the total number of particles results from the lack of any source terms for

particles of the smallest mass in either Eqn. 3.1 or Eqn. 3.2. For this reason, the SCM cannot provide a complete description of the dynamics of sea ice, and we must consider additional terms, as will be discussed in Section 3.2.

To further illustrate the connection between the solutions of SCMs and exponential distributions, we can consider the features of the population dynamics described by SCMs. It was already noted that as a result of the steady decrease in the number of particles in the population, we cannot interpret u_k as a probability distribution. However, we may look at the distribution at a particular time by normalising each $u_k(t)$ by the total number of particles at that time. With a constant coagulation kernel, differential equations for the moments of the distribution of particle sizes at time $t = t_*$ may be derived, and their asymptotic behaviour analysed [17]. The moments about zero of the probability distribution arising as a solution may be written as

$$\mu_n'(t) = \frac{\sum_k k^n u_k(t)}{\sum_k u_k(t)}. \tag{3.4}$$

Writing $m_r(t) = \sum_k k^r u_k(t)$, the moments about zero are given by

$$\mu_n(t) = \frac{m_n(t)}{m_0(t)}. \tag{3.5}$$

When $K = 1$ in Eqn.3.1 (which corresponds to coagulation rates having no dependence on particle mass) the time evolution of the $m_k(t)$ is given by:

$$\frac{\mathrm{d}}{\mathrm{d}t} m_0(t) = -\frac{1}{2} m_0^2 \tag{3.6}$$

$$\frac{\mathrm{d}}{\mathrm{d}t} m_1(t) = 0 \tag{3.7}$$

$$\frac{\mathrm{d}}{\mathrm{d}t} m_k(t) = \frac{1}{2} \sum_{j=1}^{k-1} \binom{k}{j} m_j(t) m_{k-j}(t) \quad k > 1. \tag{3.8}$$

These equations may be solved given a set of initial conditions $\{m_{i,0}\}$. One may write expressions for the $m_k(t)$ in terms of these initial conditions,

$$\begin{aligned} m_0(t) &= (1 + t/2)^{-1} \\ m_1(t) &= m_{1,0} \\ m_2(t) &= m_{2,0} + m_{1,0}^2 t \\ m_3 &= m_{3,0} + 3m_{2,0}t + 3/2t^2 \\ &\dots \end{aligned}$$

The moments about zero, μ'_k may be then be calculated from the $m_k(t)$. From these terms, the moments of the the mass distribution at a particular time may be calculated: the mean is given by $\mu = \mu'_1$, the variance by $\sigma^2 = \mu'_2 - (\mu'_1)^2$, and so on. With the initial condition that the entire population is comprised of particles of the smallest size, $m_{i,0} = 1$, we may obtain expressions for the moments of the distribution which tend asymptotically towards those of the exponential distribution [17]. Furthermore, it is possible to estimate the rates of convergence of the system's moments. These exact results require the initial conditions to have all particles concentrated in the lowest thickness category, which makes the description of convergence to an exponential distribution analogous to descriptions of the growth by redistribution processes of a population of ice in a region that is ice-free in the summer, and consequently populated by level ice of a single thickness at the start of the growth season.

3.2 A Case Study: Thorndike's Pseudo-SCM

An idealised model exploring the dynamics of the sea ice thickness distribution $g(h)$ under the combined action of ridging and thermodynamic forcing was introduced by Thorndike [51]. This model demonstrates that the exponential tail of $g(h)$ arises in a simple system that assumes a fixed population of ice 'particles', each of a certain thickness. An ice particle of thickness x 'ridges' with a particle of thickness y to create a particle of thickness $x + y$ and one of of thickness 0 (open water). Mathematically, the system may be written

$$\frac{\partial g}{\partial t} = -\frac{\partial (fg)}{\partial h} + r\left[\delta(h) - 2g(h) + \int_0^h g(h')g(h - h')\mathrm{d}h'\right]. \tag{3.9}$$

The first term on the right hand is the annual average thermodynamic growth and ablation rate, given by

$$\frac{\mathrm{d}(fg)}{\mathrm{d}h} = F\frac{\mathrm{d}(H-h)g}{\mathrm{d}h}, \tag{3.10}$$

where H is the thermodynamic equilibrium thickness and F is a coefficient which determines the rate at which ice approaches the thermodynamic equilibrium thickness. The terms arising from ice-ice interactions are all within the square brackets. These interactions occur at some fixed rate, scaled by r, which is independent of the thickness of the ice involved. The delta function represents the creation of open water when two members of the population combine. This open water subsequently freezes over and thus acts as a source for thin ice. The integral is the source term for ice of thickness h, associated with ridging. The term $-2g(h)$ is a sink term, representing the transfer of ice of thickness h to higher thicknesses through the ridging process. This is formally identical to the sink term in the SCM with a uniform kernel, as $g(h)$ is a probability distribution and so

$$g(h)\int_0^\infty g(h')\mathrm{d}h' = g(h). \tag{3.11}$$

A factor of 2 is introduced in front of the sink term, rather than a factor of $1/2$ in front of the source term. Both approximate analytic calculations and numerical simulation demonstrate that in steady state this model predicts an exponential tail for $g(h)$. This formulation is extremely similar to an SCM, although this connection was not made in [51]. The redistribution component of Thorndike's model differs from an SCM only in the addition of the δ function term to create ice of thickness zero (open water). By including this term, the integral over thickness of the redistribution terms, (*i.e.*, the net effect on $g(h)$ of the redistribution process), is formally zero, *viz.*,

$$\int_0^\infty \left[\delta(h) - 2g(h) + \int_0^h g(h')g(h-h')\mathrm{d}h'\right]\mathrm{d}h = 0.$$

The thermodynamic term in Eqn. 3.9 also integrates to zero over h, and we may interpret $g(h)$ as a probability distribution, given that it is positive, and the integral of $g(h)$ over h is constant. As we have remarked, the pure SCM will not normally serve as a model of the dynamic behaviour of a probability distribution (in this case the thickness distribution of

sea ice), as it does not conserve the integral

$$N(t) = \int_0^\infty u(x,t)\mathrm{d}t. \tag{3.12}$$

As noted above, the delta function term in Thorndike's model represents the creation of open water at the same rate as redistributions are occurring, thus conserving total particle number. Consider the populations of ice as a set of floes of constant thickness, each completely occupying a cell on a fixed grid. Redistribution is the process of removing a floe from one grid cell and adding its thickness to a floe in another cell. The difference between the populations described by the SCM and Thorndike's model may be understood as the difference between generating a thickness 'distribution' by examining only the cells occupied by ice (SCM); and generating the population by counting all grid cells, including the ones which are occupied by open water (Thorndike). Given the success of Thorndike's model at capturing the essential features of the equilibrium thickness distribution, it is worthwhile to extend this earlier analysis using perspectives provided by the SCM. The behaviour of the SCM is well understood for the constant kernel, and by comparing a model with a pure SCM redistribution component to Thorndike's model, the degree to which the behaviour of Thorndike's model may be attributed to its similarity to an SCM.

For numerical purposes, we will be using a discrete version of Eqn. 3.9, which takes the form of a coupled set of N differential equations describing the dynamics of each of N thickness categories. The equation for the population of ice in the k^{th} thickness category is

$$\frac{\mathrm{d}g_k(t)}{\mathrm{d}t} = -\frac{\partial T g_k(t)}{\partial h} + r\left[\delta_{k,1} - 2g_k(t) + \sum_{j=1}^{k} g(j)g(k-j)\right]. \tag{3.13}$$

3.3 The Generalised Thorndike Model

A general model of sea ice ridging containing an SCM component can be built using similar assumptions to those Thorndike adopted. The common aspect of the SCM and Thorndike's model is the description of ridging as the combination of ice of thickness k and ice of thickness j to form ice of thickness $k + j$ at a rate dependent on k, j, and the quantity of ice

of those thicknesses. The generalisation of Eqn.3.9 is

$$\frac{\partial g(h,t)}{\partial t} = \frac{\partial T(g)}{\partial h} + C(K,t)\delta(h) + \frac{1}{2}\int_0^x K(h', h-h')g(h',t)g(h-h',t)\mathrm{d}h' - \int_0^\infty K(h,h')g(h,t)g(h',t)\mathrm{d}h', \quad (3.14)$$

where $T(g)$ is a seasonally-dependent thermodynamics function that drives ice towards a cyclo-stationary equilibrium (limit cycle), at a rate dependent on the thickness (k). The model described by Eqn. 3.14 differs from the Thorndike model in the generalisation of the rate term, $K(x,y)$, and consequent change of the coefficient of the source term ($\delta(h)$ in Eqn. 3.9). We generalise the source term for the creation of ice of thickness 0 by calculating the rate at which all redistributions are occurring. With a general kernel, $K(x,y)$, the coefficient of the δ term takes the form

$$C(K,t) = \int_0^\infty \left[\int_0^\infty K(h,h')g(h,t)g(h',t)\mathrm{d}h'\right]\mathrm{d}h. \quad (3.15)$$

Note that when $K(x,y) = 1$, the coefficient of $\delta(h)$ in Eqn. 3.14 is equal to 1 (as in Eqn. 3.13); this follows from the normalisation of $g(h,t)$.

By generalising Thorndike's model in Eqn.3.14, we introduce the choice of rate kernel $K(h,h')$. This kernel is the thickness dependence of the redistribution rate. The choice of the thickness-dependence of the rate at which events occur is a representation of our conception of how the material properties of the ice affect the frequency of redistribution events. When $K = 1$, redistribution occurs at a fixed rate, independent of the thickness of the ice involved. If the kernel is chosen so that it decreases with increasing h, h', redistribution events become less frequent in thicker ice, and if the kernel increases with increasing h, h', events become more frequent in thicker ice. A kernel which decreases with increasing h,$'h$ is the most physically realistic, based on observations, however we will perform simulations with a wide variety of kernels in order to fully explore the behaviour of our model.

The discrete form of Eqn.3.14 is the system of equations

$$\frac{\partial g_k(t)}{\partial t} = U(T(g_k)) + C(K,t)\delta_{k,1} + \frac{1}{2}\sum_{j=1}^{k-1} K(k,k-j)g_j(t)g_{k-j}(t) - \sum_{j=1}^{\infty} K(k,j)g_k(t)g_j(t) \quad (3.16)$$

where $g_k(t)$ is the fraction of the population of thickness k. The function $C(K,t)$ is the discretised analogue of Eqn.3.15, and the thermodynamic term $U(T(g_k))$ is an upwind gradient operator acting on $T(g_k)$. If we were to remove the thermodynamic term in Eqn. 3.16, and the generalised delta function, the system would be of the form of Eqn. 3.1, and the formal results obtained for SCMs would apply to it.

As we have already discussed, distributions with exponential tails (at least approximately) occur naturally in coagulation models over a broad range of kernel forms. For numerical implementation we will truncate the equations at some maximum thickness category, which we may choose to be sufficiently large that ice of that thickness is never created. Based on observations of maximum ice drafts, the physics of the problem will allow us to truncate the population above 20m without encountering problems.

We will numerically integrate this model using a forward finite difference scheme (Eqn. 3.17). Our model uses 200 thickness categories, each representing a 0.1m thickness increment, so:

$$g_k^{t+1} = g_k^t + \Delta t \left(U(T(g_k(t),t)) + \left(\sum_{k=2}^{\infty} \left[\sum_{j=1}^{k-1} K(k,k-j) g_j(t) g_{k-j}(t) \right] \right) \delta_{k,1} + \frac{1}{2} \sum_{j=1}^{i-1} K(k,k-j) g_j^t g_{k-j}^t - g_k^t \sum_{j=1}^{200-k} K(k,j) g_j^t \right) \tag{3.17}$$

Thermodynamic forcing is represented as a simple cyclical function based on observations of sea ice growth and ablation rates [35], transferring a portion of ice in each thickness category to one or other of its neighbouring bins, depending on the thickness of the ice and the season. The amount of ice lost from each thickness category in a single time step is given by

$$T(g_k) = \left[S(t) W_1(k) + \{1 - S(t)\} W_2(k) \right] g_k, \tag{3.18}$$

where

$$W_1(k) = 0.1 \exp(-1.7 k \Delta h) - 0.01 \;\; m\, day^{-1}$$
$$W_2(k) = 0.01 \exp(-0.01 k \Delta h) \;\; m\, day^{-1}$$

where Δh is the width of each thickness category and

$$S(t) = \begin{cases} 1 - t/180 & 0 \leq t < 180 \\ t/180 - 1 & 180 \leq t < 360 \end{cases} .$$

with time t in days. The functions W_1 and W_2 are approximations of the winter and summer growth curves given in [35], as illustrated in Fig. 2.2. As noted Chapter 2, the rates of ablation of first year unconsolidated ridged ice are typically higher than those shown in Fig. 2.2, however we will make the assumption that, as these unconsolidated keels are a subpopulation, and as their growth rates are not different, that the seasonal growth rates given in [35] are sufficient for our modelling efforts. Mass lost from each thickness category due to thermodynamic processes is accounted for in its neighbouring categories (higher thicknesses when $T(k)$ is positive and lower when it is negative). This form of the thermodynamic forcing is idealised, in line with the rest of the formulation of the model. By varying the strength of the thermodynamic term, the interplay between dynamic and thermodynamic forcing may be explored. For most of the model runs which we perform, the strength of the thermodynamic term relative to the redistribution terms is small, and the advance and retreat of the tail of the distribution is not large.

Our analysis of the behaviour of the model within the context of the SCM formulation relies upon the assumption that the coagulation terms are dominant. Evidence to support this assumption can be seen by comparing the magnitudes of the coagulation and thermodynamic terms in Figures 3.1 and 3.2. These plots were produces using the final timestep of a numerical simulation of Eqn. 3.16 with a linear kernel. Because the model includes a a seasonal thermodynamic component, it will never reach equilibrium, and so the thermodynamic and SCM terms will not sum to zero. The first plot in Fig. 3.1 displays the magnitudes of the SCM and thermodynamic terms at the final time step of the simulation displayed in Fig.3.4 over the entire thickness range. The second (lower) plot is a semilog plot, showing the absolute values of the two components for ice thicknesses greater than 3m. In Figure 3.2, we present a semi-log plot shows the absolute value of the two components by displaying the absolute value of the SCM term divided by the absolute value of the thermodynamic term. For ice thicknesses above 3m, the SCM component of the model is a minimum of two orders of magnitude larger than the thermodynamic component, rising to over 4 orders of magnitude at 20m. The large differences in the magnitude of the two components, particularly in the thicker ice, where the tail forms, leads us to conclude that the

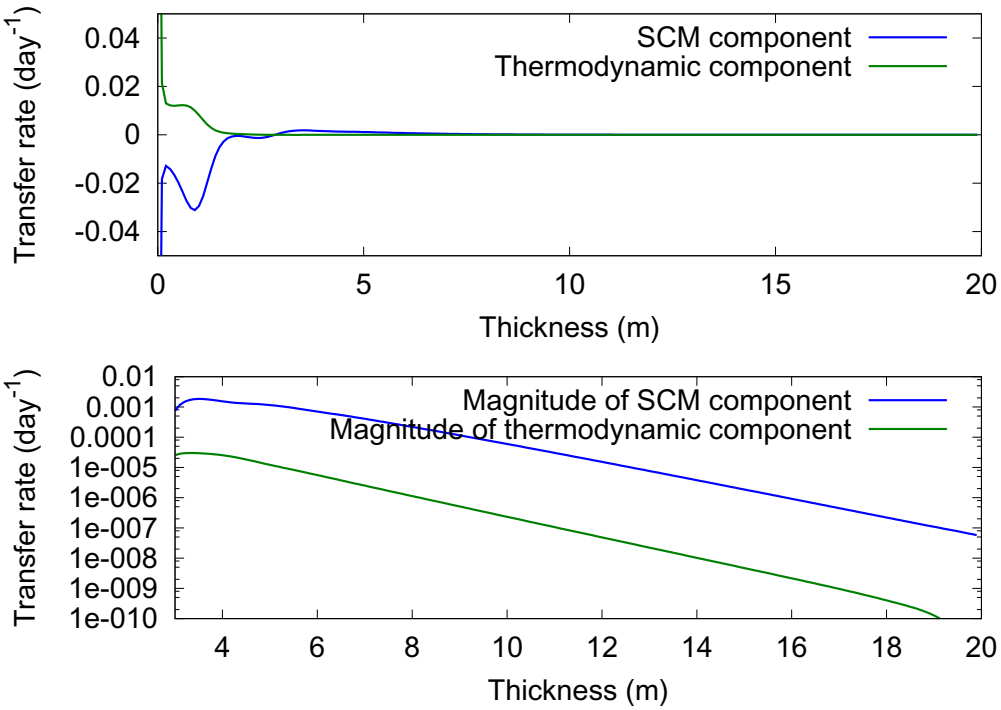

Figure 3.1: Magnitudes of the SCM terms and thermodynamic term in Eqn. 3.16 with an exponential kernel at the final timestep of the simulation displayed in Fig. 3.4

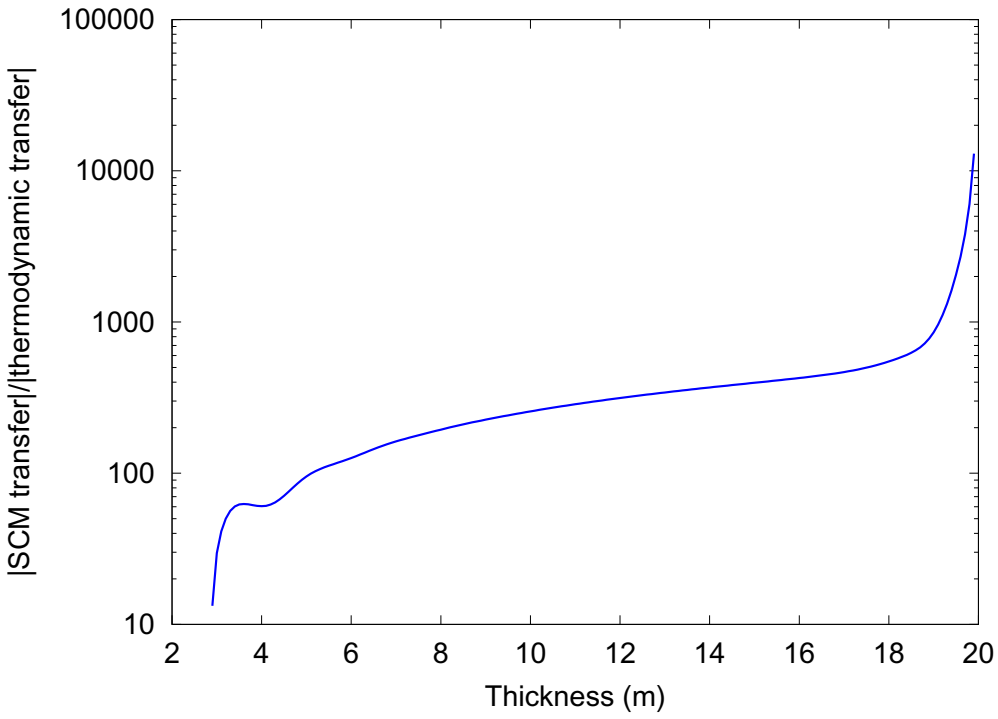

Figure 3.2: Ratio of the magnitude of the SCM term (exponential kernel) to the magnitude of the thermodynamic term in Eqn. 3.16 at the final timestep of the simulation displayed in Fig. 3.4

behaviour of the model in forming a quasi-exponential tail may be reasonably compared with (and attributed to) the behaviour of an SCM model.

Because the model is computationally efficient, we may perform a relatively large number of numerical simulations. This allows us to thoroughly compare the predictions of this model to Thorndike's, and also to examine how altering various parameters affects the model output. There are two major sensitivities to be explored: the functional form of the transfer kernel $K(k, j)$, and the strength of the thermodynamic forcing relative to that of mechanical redistribution. A variety of kernels may be tested, in order to assess the sensitivity of model predictions to this choice. From the discussion in Section 3.1, we do not expect that this sensitivity will be strong (for reasonable choices of kernel form). As part of our experimentation with the kernel, we investigate the inclusion of a representation of the rafting process. In the process of rafting, the ice is transferred laterally onto adjacent ice without having first to be fragmented. This phenomenon occurs in thin ice, which is flexible enough for rafting to be possible. In our model, we may represent rafting by specifying larger values of the kernel $K(k, j)$ for the dynamics of ice below a certain thickness.

We may use the same thermodynamic routine in both the Thorndike model and our model. In contrast with the focus on equilibrium solutions in Thorndike [51], the time-dependence of the thermodynamic forcing in the present study allows us to consider evolution of the thickness distribution across the seasonal cycles. In the runs which we perform, using $T(h)$ as defined by Eqn.3.18, the strength of the thermodynamic growth and melt relative to the redistribution is small, and the advance and retreat of the tail of the population is not large, following its initial formation.

Model simulations of 2000 days are sufficient to allow the population to reach its maximum extent (corresponding to late winter conditions). Model simulations are shown in Figures 3.3 and 3.4. Both Thorndike's model and that given by Eqn. 3.16 with an exponential kernel produce exponential, or near-exponential tails (appearing as straight line segments on the semi-log plots). The ripples observed in these simulated populations near the mode thickness are the result of the presence of the thermodynamic forcing term, and are transients created by the implementation of seasonality in the model. Such ripples are not observed in sea ice populations, and it is expected that they arise in these simulations due to the simplicity of the thermodynamic component of the model.

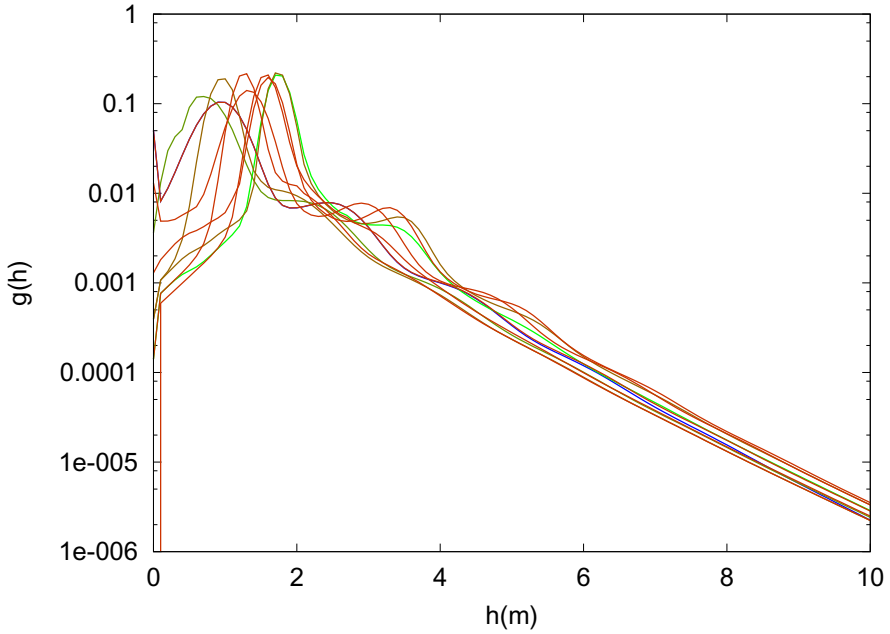

Figure 3.3: Simulations run with Thorndike model (Eqn.3.9). Population is plotted every 200 days from runs of 2000 days, with color changing from green to red with increasing t.

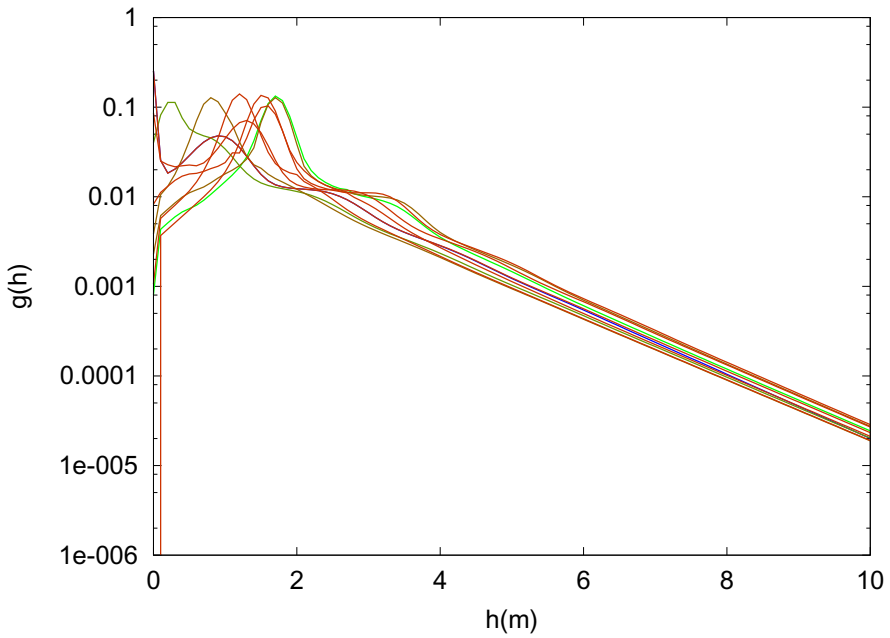

Figure 3.4: Simulations run with the Coagulation model (Eqn.3.16) with exponential kernel. Timing and colouring as in Fig. 3.3

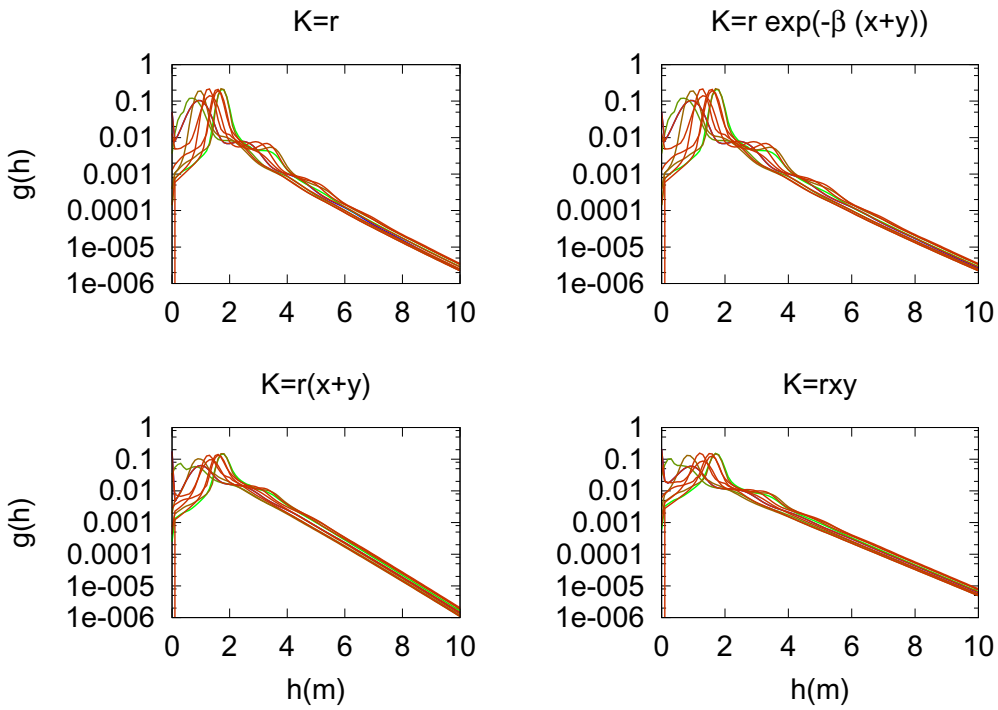

Figure 3.5: Coagulation model with kernels from Table 3.1. Timing and colouring as in Fig. 3.3

Simulations suggest that the choice of coagulation kernel has little qualitative effect on the population (Fig. 3.5). The set of kernels considered is presented in Table 3.1; note that for pure SCMs the constant, additive, or multiplicative kernels admit analytic solutions. By including the additive and multiplicative case, which describe population dynamics unlike those seen in sea ice populations we provide further evidence that the addition of the thermodynamic and source terms does not alter the qualitative nature of the simulated populations, and demonstrates the robustness of the quasi-exponential distribution under a variety of qualitatively different representations of the redistribution process. The additive and multiplicative kernels were used in the original application of SCMs, in the modelling

Run Number	Kernel $K(x,y)$
1	r
2	$r\exp^{-\beta(x+y)}$
3	$r(xy)$
4	$r(x+y)$

Table 3.1: Rate kernels for coagulation model, with scaling constant r (note that r takes different values for each kernel)

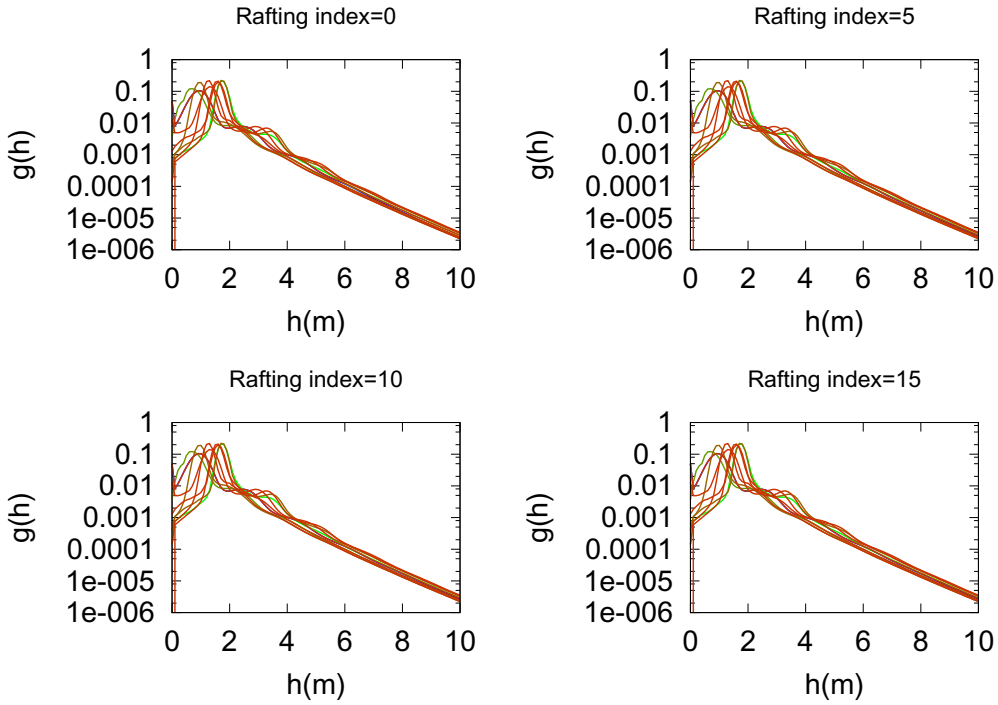

Figure 3.6: Coagulation model runs using a piecewise constant coagulation kernel with varying rafting cutoff indices as indicated. Rafting ice has kernel $K = 4$, ice above the rafting cutoff has $K = 1$. Timing and colouring as in Fig. 3.3

of particle coagulation in gases. In each instance the rate scaling coefficient r is adjusted so that the results of the simulation resemble those of Thorndike's model in the extent and slope of the exponential tail produced during the simulation. The transient evolution of $g(h)$ is qualitatively similar for all of the kernels as the model evolves from the initial condition that $g(h, 0) = \delta(0)$. This is unsurprising in light of past studies made of the properties of the SCM family, which have focused on kernels which increase with their arguments.

We may also implement a crude representation of rafting by constructing $K(x, y)$ to take larger values for thin ice, to represent the lower energy required to cause thin ice to override neighbouring floes. Using the constant coagulation kernel, we double the value of the constant for all ice thickness categories below a set thickness h_R,

$$K(x, y) = \begin{cases} 2r & h < h_R \\ r & h \geq h_R. \end{cases} \tag{3.19}$$

Although transfer rates of thin ice are enhanced, the quasi-exponential form of the solution

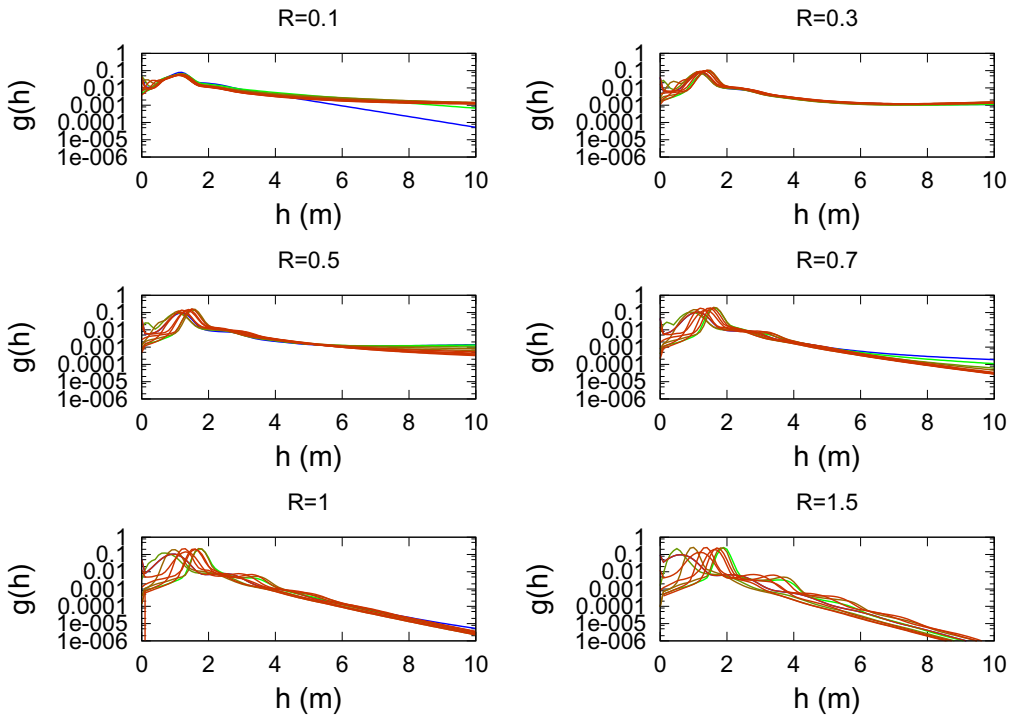

Figure 3.7: Coagulation model runs with varying relative strengths of thermodynamic and dynamic components. Snapshots of population taken every 2000 timesteps for 20000 timesteps, with the initial curve pure blue, and the final curve pure red.

is not affected (Fig. 3.6). The increased transfer rates of thin ice speed up the formation of the extended quasi-exponential tail, to a degree dependent upon the number of thickness categories with a higher transfer rate. Small values of the rafting index have a smaller effect on the simulation because the population of thin ice is naturally evacuated by the thermodynamic process in the model. As the population of raftable ice is depleted, the effect of the rafting terms will become less important to the evolution of the system.

The relative strengths of the thermodynamic and dynamic (SCM) terms are central in determining the simulation behaviour. We compare simulations with differing relative strengths of these components in Fig.3.7. Using the constant coagulation kernel, $K = R_T^{-1}$, we may examine the effect on simulations of varying the relative strength of the two components (as R_T corresponds to the relative strength of the terms). The value of R_T determines the slope of the tail of the population. When the thermodynamic term is weaker ($R_T < 1$), the coagulation component of the model dominates, and the slope of the tail becomes nearly flat. Conversely, when $R(T) > 1$, we see the slope of the tail decreasing, and at large values

of R_T ($R_T > 5$), the thermodynamics dominate the simulation, producing cyclical behaviour (attributable to the seasonal thermodynamic forcing).

3.4 Fragmentation And Self Similarity

In the previous section, we discussed the relationship between the SCM and Thorndike's sea ice model [51], and examined the utility of the SCM as a component of a model describing the evolution of the thickness distribution of a population of sea ice. While this is the main focus of our work, it is worthwhile to bring to attention another aspect of sea ice modelling in which an SCM perspective may prove useful.

Measurements show that the distribution of floe sizes typically follows a log-normal distribution [45]. It is known that log-normal distributions have the property of self-similarity. It has also long been known that the fractile behaviour of brittle solids typically produces a population of fragments whose size follows a power law. Systems of equations that produce self-similar solutions are of particular interest in modelling brittle fracture. Through the examination of observations of sea ice failure behaviour over a broad range of scales, it has been noted that the pressure threshold for ice failure followed a power law over 10 orders of magnitude in scale [47] (Eqn. 3.20), suggesting that the processes at work in sea ice fragmentation display self-similarity.

$$P_{fail} = C(\text{contact area})^{-s}, \tag{3.20}$$

where s is a constant between $1/4$ and $1/2$ [47].

A simple renormalised group (RNG) method of modelling brittle failure in ice was developed in [40]. From this simple model it is possible to produce an estimate of the dependence on area of the failure pressure of ice, with the prediction that $s = 1/2$. More recently a model of fragmentation processes in ice which can lead to log-normal distributions of floe size was developed by Lensu [32]. A population of ice occupying an area $N(t)$, with $N(t)f(x)$ floes of area x at time t evolves according to

$$\frac{\partial}{\partial t}N(t)f(x) = 2N(t)\int_x^1 \alpha(z)\beta(z \to x)f(z)\mathrm{d}z - N(t)\alpha(x)f(x), \tag{3.21}$$

where $\beta(z \to x)\mathrm{d}x$ is the probability that a floe of area z produces a floe of area x through fragmentation, and α is the rate at which floes of area x themselves fragment. Lensu assumed that $\alpha = 1$, and that fragmentation behaviour is area independent. We may then write

$$\beta(z \to x) = (1/z)\beta(x/z) \tag{3.22}$$

so that $\beta(x)\mathrm{d}x$ is a probability distribution defined for $x \in [0,\ 1]$.

The SCM may be expanded to include the process of spontaneous fragmentation of members of the population into smaller particles. In the continuous case, the equations describing a coagulation-fragmentation system take the form

$$\frac{\partial}{\partial t}g(x,t) = C(g) + \int_x^\infty L(x,x')g(x',t)\mathrm{d}x' - g(x,t)\int_0^x L(x,x')\frac{x'}{x}\mathrm{d}x'. \tag{3.23}$$

The second term on the right hand side of Eqn. 3.23 represents the formation of particles of mass x from larger particles breaking down, and the third term represents the fragmentation loss from the population of members of mass x. The presence of the term $\frac{x'}{x}$ in the final integral ensures that the system conserves mass. The function $L(x,x')$ is the fragmentation kernel, and is analogous to the coagulation kernel, although it is not symmetric in its arguments (*i.e.*, with $x' < x$, particles of size x' cannot form particles of size x through fragmentation). For convenience, we write the full equation of a fragmentation-coagulation system in short as

$$\frac{\mathrm{d}}{\mathrm{d}t}g(x,t) = C(g) + F(g). \tag{3.24}$$

The structure of Lensu's model (Eqns. 3.21, 3.22) corresponds to a pure fragmentation model with constant kernel $L(q,y) = 1$. It is shown in [32] that this system admits the solution

$$G(p) = \exp\left(2\int_0^1 q^p\beta(z)\mathrm{d}zt - 1\right), \tag{3.25}$$

$$N(t) = N_0\exp(t) \tag{3.26}$$

where $G(p)$ is an integral transform:

$$G(p) = \int_0^1 x^p f(q)\mathrm{d}q.$$

Analysis of the solution as $t \to \infty$ reveals that the distribution of fragment sizes, f approaches a log-normal form [32]. When either $F(g)$ or $C(g)$ is zero in Eqn. 3.24, the system does not display a stationary solution except in the trivial case when both are zero. It has been proved ([12], [16]) that a broad class of kernels admit self-similar solutions for both pure coagulation ($F(g) = 0$) and pure fragmentation ($C(g) = 0$) models, where a self-similar solution $g(x, t)$ can be written in terms of a scaling function $s(t)$:

$$g(x, t) = s^{-2}(t)v(xs^{-1}(t)). \tag{3.27}$$

Fragmentation functions of the form

$$b(y, y') = b_0(y)B(y'/y) \tag{3.28}$$

with

$$b_0(y) = y^\beta \tag{3.29}$$

$$\gamma \geq -1 \tag{3.30}$$

and $B(\cdot)$ is (effectively) a probability distribution defined on the interval $[0,\ 1]$ (as $y' < y$) were considered in [12]. The model considered by Lensu in [32] belongs to the class of models considered in [12] with $\beta = -1$ in Eqn. 3.29, and the results in [12] apply to Lensu's work.

Given that the fragmentation SCMs are well studied, and there are general results about their behaviour which apply to existing sea ice models, there is further value in developing the use of SCMs in modelling sea ice fracture processes, both as tools for modelling, and as conceptual objects used to further our understanding of the processes at work, and the distributions they generate.

3.5 Discussion

The SCM provides a powerful framework to address many open questions in sea ice modelling. The simplicity of the SCM allows the study of a wide variety of parameterisations of coagulation and fragmentation processes without creating strong demands on processor time, and the conceptual clarity of the SCM makes it a useful tool in studying sea ice redistribution. The robust presence of exponential and quasi-exponential populations produced by models with a wide variety of rate kernels, suggests that the description of the redistribution process given by the SCM is sufficient for the production of populations which are qualitatively similar to observations. Clearly, the implementation of a SCM formulation in sea ice thickness distribution modelling in anything other than an idealised context must be adjusted to best represent the physical realities of the system under study. In the types of models we have considered, the ridging events are viewed as analogous to the interaction of two particles in the SCM. The 'block-stacking' representation of ridging is an oversimplification, but the coagulation model formalism provides a useful idealised framework for the study of the interplay between mechanical and thermodynamic process in sea ice.

As can be inferred from the analytic solutions of the SCM, exponential and quasi-exponential distributions arise naturally as a feature of the equations over a broad range of kernel specifications. That said, the rate kernels for which analytic solutions exist are not suited for sea ice modelling, particularly as the additive and multiplicative kernels model systems in which larger particles interact *more* frequently than smaller ones. While the constant kernel, $K = 1$, considered by Thorndike, is too simple to be a representation of the physical reality of ridging, it is at least not manifestly unphysical. Numerical simulations with a variety of rate kernels demonstrate that the quasi-exponential tails arise even in the case where these kernels do not admit analytic solutions.

While the thermodynamic term in our model is orders of magnitude smaller than the coagulation term for thick ice (as shown in Fig. 3.1, Fig. 3.2) , our work nevertheless demonstrates the need for a balance between the thermodynamic forcing and the tendency of the ridging process to increase ice thickness in an unchecked fashion [51]. A similar conclusion regarding the relationship between dynamics and thermodynamics is obtained in much more detail in [8], using a viscous-plastic basin-scale model. Use of simple coagulation models to further explore this aspect of sea ice models, would be a valuable avenue of research, as SCMs have been studied extensively and there is an extensive body of literature

on their behaviour. With a firm understanding of the behaviour of both the thermodynamic and dynamic components of such a model, efforts could focus on the effect of their interaction on the population statistics.

In addition to our examination of the coagulation model, we have compared the related fragmentation model with work on sea ice floe size distribution, and shown that work done by Lensu [32] is a form of fragmentation model for which the mathematical properties are understood, and which display many of the features we seek in a model of the floe size distribution. The derivation of a model which we have shown to be mathematically equivalent to a fragmentation model in the literature, coupled with the known mathematical properties of this type of system suggest that further investigation of fragmentation models could be valuable.

The persistent presence in sea ice populations of clear statistical features, such as the exponential tail of the thickness distribution and the log-normality of floe size distribution, begs the question of the processes leading to these properties. It is known that the detailed dynamic interactions which drive the evolution of the population are complex due to the nature of the material. As we have shown, the SCM presents an appealingly simple and robust tool which may provide a deeper understanding of the processes which drive the statistics of sea ice populations. In the next chapter we develop a model of sea ice thickness distribution dynamics which treats redistribution in a similar fashion to the models explored in this chapter, but which features redistribution processes directly informed by our understanding of the physical properties of sea ice, and its observed redistribution behaviour.

Chapter 4

An Idealised Monte Carlo Model of Sea Ice Thickness Dynamics

4.1 Overview

In this chapter, we will build on the ideas introduced in Chapter 3 in order to develop a new idealised model of the dynamics of the thickness distribution of a population of ice. The model is intended to be a conceptual tool, with a simplified construction which will allow us to examine the relative importance of the different processes at work on a population of sea ice. We will use the model to explore the sensitivity of the population dynamics to changes in parameterisations of relevant physical properties such as ice strength, the gross material properties of the ice, and the relative contributions of thermodynamic growth and dynamic redistribution. This model will expand on the results of the previous chapter, adding a greater degree of physical realism to the representation of the dynamic processes involved in redistribution.

Section 4.2 provides a brief recapitulation of the modelling approaches used to represent the dynamic interactions in standard sea ice models. This section also discusses the primary processes comprising the dynamic interactions of sea ice, with particular attention paid to the effects of these on the thickness distribution. The following section discusses the use of stochastic processes as an alternative approach to the description of ice-ice interactions and their effect on the thickness distribution. Model ridging in an ice population is described, and two model variants are introduced based on different parameterisations of the ridging process. The specifics of model construction are detailed in Section 4.4. Simulation results

from the models are then compared for a range of parameter values and parameterisations of the physical properties of the ice in section 4.5, followed by a discussion and concluding remarks.

4.2 Characterisation Of Redistribution Dynamics

The evolution of the thickness distribution of a sea ice population is driven by thermodynamic processes (growth and melt) and dynamic interactions between ice floes (forced by winds and currents). The thermodynamic forcing of the ice is marked by a strong seasonality, with ice growth in the winter (generally Oct-Apr) and melt in the summer (generally May-Sept). This study is primarily concerned with the exponential tail of the population, which is created through the ridging process, and will focus on capturing the effect on $g(h)$ of the redistribution caused by dynamic ice-ice interactions. Thermodynamic processes (freezing and ablation) will be represented in a highly simplified form.

The major dynamical processes driving the evolution of sea ice populations are the deformation, fragmentation, and piling of floes caused by ice-ice interactions. Due to velocity gradients induced across a region of ice by winds and currents, floes are driven together, and the pressure can result in buckling and fragmentation. On the large scale (*i.e.*, spanning many floes) the ice pack resists the deformation because of its internal strength. The strength is a function of the large-scale mean ice thickness and its small-scale geometry. The characterisation of the connection between strength and deformation (stress and strain) - the rheology - is a basic aspect of any force balance sea ice model. Characterisations of the rheology of sea ice ([9],[10],[14],[20]) remain approximate because of its complex material properties. In this current work, we will avoid dealing directly with sea ice rheology and instead assess whether the thickness distribution dynamics can be simulated using a direct, simplified, simulation of individual redistribution events.

4.3 A description of redistribution

Rather than attempt to refine the rheological component of a continuum force-balance model, ice thickness redistribution is modelled in the present study as a Markov processes consisting of a sequence of discrete redistribution events occurring with probabilities that

depend on the amount of ice involved and the energy available from external forcing. This idea has antecedents in earlier models developed to treat the thickness redistribution process as a series of discrete events, [33], [51], [52]. In comparison with earlier studies, we use a more detailed representation of the redistribution process which allows assessment of the relative importance of the different types of redistribution which may occur. We also present a novel mathematical framing of the redistribution process based on the ideas developed in Chapter 3.

4.3.1 Modelling Redistribution Dynamics

To describe the evolution of the thickness distribution of a population of ice, the model must represent both thermodynamic processes and dynamic ice redistribution processes. We will assume that the two processes may be treated separately, *i.e.*, that dynamic processes do not affect the thermodynamics and vice versa. While this is not strictly true, as the compressive and shear strength of intact ice does vary with temperature, we will be treating the strength of the ice as a function of thickness alone. The representation of the thermodynamic process will be simpler than that of the dynamic processes. The thermodynamic processes simulated are ice growth and melt, and the healing of damaged ice. As the main focus of this study is on the tail of $g(h)$ above the thermodynamic equilibrium thickness which can only be produced by redistribution processes, the characterisation of these constitutes the core of the model. These processes are described by the types of change that can occur to the thickness distribution through a variety of mechanical redistribution processes which occur in sea ice populations, and their rates. We will also consider the dynamical implications of damage to sea ice caused by motion which does not directly alter the thickness distribution. In this model we will simulate the dynamics of the thickness distribution $g(h)$ directly, using a zero-dimensional model which is effectively a mean-field representation of the ice dynamics.

In modelling sea ice dynamics, it is generally assumed that the dissipation of energy in an ice redistribution event is proportional to the amount of ice involved [42]. Furthermore, the consumption of energy does not appear to depend on the rate at which deformation occurs [42]. Taking advantage of these two features of redistribution energetics, our model treats thickness redistribution as a series of discrete events. As the energy used in redistribution events is rate independent, we do not need to track the progression of a single redistribution event, and may instead characterise it solely by the resulting change in the

thickness distribution. The energy difference between two states is taken to be proportional to the difference in gravitational potential energy as measured by the change in the thickness distribution. While the total energy expended in ridging and redistribution is much greater than the change in potential energy, the fact that the total energy dissipation scales well with potential energy change [23] implies that the energetics of redistribution will scale with the change in potential energy.

The redistribution process can be categorised as involving two fundamental types of event, each with a distinct effect on the thickness distribution: compression and dilation. In observations of ice pack dynamic interactions, these two types of behaviour are rarely observed in isolation, and redistribution events are typically a combination of compression and dilation in complex spatial patterns. In this model, we identify compression with the processes of ridging and rafting, and dilation with the process of shearing and we refer to the redistribution events caused by purely compressive motion as ridging, or rafting in thinner ice, and the redistribution events caused by pure dilation as shearing. Observed ice redistributions do not show as clear a distinction as in the model; this specification of the nature of events is made for conceptual clarity. As the model does not include spatial information, the three different types of redistribution (ridging, rafting, and shearing) are distinguished by their different energetic requirements and the different effects that they have on the thickness distribution. Compression of the pack results in ridging, as ice sheets buckle and fragment and the resulting rubble is pushed both above and below the ice. Ridging is the primary agent in the creation of ice above the thermodynamic equilibrium thickness, and leads to the largest changes in the thickness distribution. A process similar to ridging is rafting, which occurs when thin ice (of thickness less than approximately 1 meter) is forced compressively. Such ice has enough flexibility to over-ride neighbouring floes of similar thickness without buckling or breaking into rubble. We model this as a separate process from compressive ridging, assuming that it requires less energy and characteristically transfers ice from thickness h to thickness $2h$. The assumption that rafting requires less energy than ridging is based on the observation that the process does not require the ice to fracture, and the assumption that the frictional dissipation arising between two intact sheets of level ice will be much less than that between a floe and rubble. The maximum thickness at which ice may raft will be denoted h_{ra}. In the event of dilation, the ice will shear along a fault line. Although some piling of the ice occurs, shearing is primarily a sink of energy due to friction. Shearing creates regions of open water along the shear line which repopulate the lowest thickness categories of the population as they freeze. The piling of ice which occurs during shearing

is represented as the transfer of ice from the shearing interface to the upper surfaces of the interacting floes. This has the effect of transferring ice from thickness h to thickness $2h$ during a shearing event, in addition to creating ice of zero thickness (*i.e.*, open water).

The model incorporates a single idealised forcing, f, to represent the combined effect of winds and currents. It is assumed that f is not affected by the state of the ice itself (the influence of the roughness of the ice on wind and current patterns is assumed to be a higher-order effect). The idealised forcing should not be thought of as a measure of the force being applied to the pack, but rather as a representation of the velocity gradient generated over the ice field through the actions of wind and currents, as it is non-zero velocity gradients (deformation) that lead to redistribution. In our modelling we specify the maximum amplitude of f and allow it to vary randomly between 0 and that value each time step.

4.3.2 Modelling Friction and Damage

In the process of compression of the ice pack, a great deal of brittle failure of sea ice occurs prior to redistribution of ice into a ridge. Two versions of this model are considered, one which explicitly includes a representation of the influence of damaged ice on the redistribution process and one which does not. These are referred to respectively as the models with and without memory. As mentioned in Section 1.5 the detailed rheological description of damage and brittle failure in the sea ice is extremely complicated due to the complex material properties of sea ice. We simplify this aspect of redistribution dynamics by introducing a damage function, $\eta(h)$, representing the proportion of ice of each thickness class which has undergone failure of some kind, has fragmented into smaller pieces, and is available for redistribution. In one variant of our model, we will impose the requirement that ice must be damaged before it participates in a redistribution event. This parameterisation, along with another describing the energy needed to damage ice, is intended as an idealised representation of the more complex rheological descriptions in force-balance models. In a model which includes the damage function, the state of the ice population is completely described by $g(h)$ and $\eta(h)$. The damage function is akin to the participation function introduced by Rothrock [43], which was used to define the portion of the sea ice population that could be involved in redistribution. Unlike the participation function of Rothrock, $\eta(h)$ is a state variable which evolves in time in response to both mechanical and thermodynamic forcing.

The evolution equation for the damage function must also represent the mechanism of plastic failure in sea ice. From the analysis of Sanderson [47], the pressure required to cause failure is a function of the area of contact between the interacting floes:

$$\text{pressure} = c(A)^{-\alpha},$$

where α is an empirical constant between $\frac{1}{2}$ and $\frac{1}{4}$. This relationship is observed to hold over nearly ten orders of magnitude. As ice is a brittle solid, it breaks into increasingly small fragments as it is damaged. Further damage to the ice results from forces transferred between these fragments. As the fragments decrease in size, their resistance to compressive forcing increases. Our damage scheme will reflect this observation by requiring that the energy needed to increase η by a fixed amount is an increasing function of η. Comparison of the variant of the model without memory to the one with will allow us to assess the importance of the manner in which the relationship between the fragmentation of ice and its redistribution is represented. The model without memory is built upon the assumption that all ice is equally available for redistribution, regardless of its state of damage, whereas the model with memory assumes that the ice must undergo fragmentation before it is available for redistribution, and that these two processes are typically separated in time.

4.3.3 A stochastic approach to sea-ice dynamics

As mentioned at the beginning of Section 4.3, rather than writing a set of (partial) differential equations expressing conservation of momentum, energy and mass with a detailed parameterisation of ice rheology and solving them numerically, we describe the system dynamics as a Markov process, and simulate these using Monte Carlo techniques. Although implemented using Monte Carlo techniques, this approach bears many similarities to and is informed by the dynamics of a family of mathematical equations known as Smoluchowski Coagulation Models (SCMs), discussed in Chapter 3. In this section, we will provide a brief overview Markov Chain Monte Carlo (MCMC) methods.

Monte Carlo methods are a broad class of numerical techniques based on the approach of using guided random selections to describe the random evolution of a system [27]. Markov Chain Monte Carlo methods are well established in many areas of numerical simulation, including recent application in climate and atmospheric modelling, *e.g.*, [11], [28], [34]. They are suitable for numerical simulations of both equilibrium and dynamic states. In implementing an MCMC method, we must choose a function to define the transition rates of

the system, based on the difference in potential between present and proposed states. Our work is based on the hypothesis that, while it is important to include the effects of individual redistribution events on the thickness distribution, the detailed evolution of these events can be neglected. Monte Carlo methods can be used to model the system dynamics as a series of (guided) random redistributions of the ice, representing the formation of ridges and leads. We consider a system in a particular state $\mathbf{X} = [g(h),\ \eta(h)]$ at time t, subject to external forcing f, and specify a function to assign a probability that the system makes a transition to another state $[g^*(h),\ \eta^*(h)]$ at time $t+1$. This transition rate is a function of the difference in 'potential' between the two states. Specification of the potential function and the transition probability is at the heart of the modelling process. Expressed in this way, the system's dynamics are cast as a Markov process, as the transition rates only depend on the current state of the system.

This implementation advances the ice population from its present state $\mathbf{X}$ to a future state by proposing a trial change, $\mathbf{X}^*$, and then determining the probability that the transition from $\mathbf{X}$ to $\mathbf{X}^*$ will occur, based on the difference in potential between the two states, $E(\mathbf{X}^*) - E(\mathbf{X})$. A random number is then drawn to determine if the transition occurs. If not, the proposed change is discarded without any effect on the thickness distribution. In the variant of the model which includes a damage function, the energy that would have been expended in the proposed redistribution instead acts to increase the population of damaged ice. At each time step a specified number of redistribution attempts, N, is made, and the thickness distribution is updated with each successful trial. The timescale of the model is specified by the thermodynamic routine. For an observed growth rate of x meters per day, the length of the timestep will be determined by the amount of growth which we allow to happen at each new timestep. In section 4.5, we will investigate the sensitivity of model behaviour to the specification of different transition rate functions. Some of our trial transition functions will be used for their mathematical simplicity, while others will be idealised representations of physical processes.

4.4 Idealised Model Of Sea Ice Thickness Redistribution Dynamics

Using the framework laid out in Section 4.3.3, we develop a stochastic model of ice interaction and redistribution dynamics. Two forms of the model will be presented, one with a

sub-population of 'damaged' ice created through past interactions (referred to as the memory model) and one without. The model with memory assumes that ice must be damaged before it can ridge, and uses the damage function $\eta(h)$ described in Section 4.3.2. The thickness distribution and the damage function are discretised for the model and represented by the vectors $\mathbf{g}$ and η:

$$\mathbf{g}_i = \frac{1}{\Delta h} \int_{i\Delta h}^{(i+1)\Delta h} g(h')\mathrm{d}h' \tag{4.1}$$

$$\eta_i = \frac{1}{\Delta h} \int_{i\Delta h}^{(i+1)\Delta h} \eta(h')\mathrm{d}h' \tag{4.2}$$

For this model, the rates of thermodynamic processes are based on estimates of ice growth and ablation detailed in [35]. This model's representation of redistribution processes makes use of the Markov Chain Monte Carlo methods described in Section 4.3.3. A flow chart of the operations performed by the model in a single time step is displayed in Fig. 4.4.

As noted in Section 4.3.2, the energy consumed in building an ice ridge is proportional to the difference in gravitational energy before and after redistribution events. Consequently, we will use the gravitational potential energy as the measure used in the calculation of the probability that the system changes state. In classic Monte Carlo models such as the Monte Carlo Ising Model [29], choosing a potential future state is simple, as the system is a lattice of binary elements, and a new state may be generated by changing the value of a single element. In our model however, we can choose any vector of the same length as $\mathbf{g}$ as a potential future state (as long as the sum of its elements is 1). With this much freedom, it is easy to generate large numbers of physically inaccessible potential states; the physics of the problem are taken into consideration by using energy conservation to constrain the range of potential transitions. From within this range of possible transitions, changes to $\mathbf{g}$ are made according to the characteristic redistributions caused by ridging, shearing and rafting.

In the model which incorporates memory, an amount from a particular thickness class of ice to engage in redistribution is randomly selected from the sub-population consisting of the damaged ice. Recalling that $\eta(h)$ is the fraction of the ice that has undergone failure, the probability distribution of damaged ice of thickness h_i is proportional to $\mathbf{g}_i\eta_i$. In the memoryless model we randomly select ice from the whole population. Following selection of the source ice, a redistribution event is randomly generated, consisting of the proportions

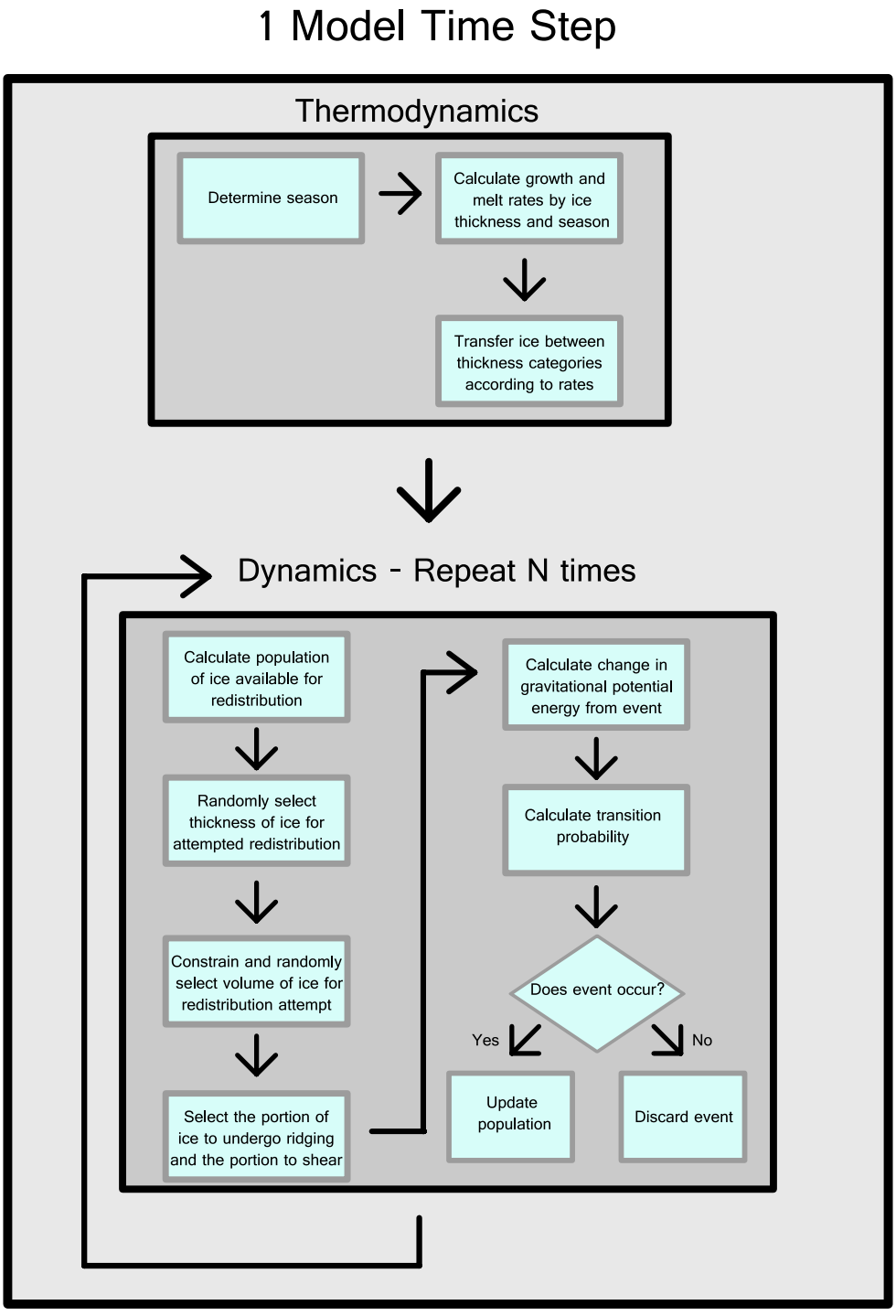

Figure 4.1: Operations performed in 1 time step in the model

of the redistribution which will be undertaken by ridging and shearing, the thickness of the ridge created, and the redistribution caused by shearing.

In the event that the ice selected has thickness above the rafting cutoff, h_r, we select the fraction of ice involved in the redistribution that will compress, ζ, which we obtain by taking a random sample from a uniform distribution on $[0, 1]$. With $\zeta = 0$, the event is purely compressive (ridging/rafting), and with $\zeta = 1$, the event is pure dilation (shearing). The values of ζ and the volume of ice we have available constrains the maximum ridge height that it is possible to create, subject to the further constraint that the difference in gravitational potential energy (GPE) between the final and inital states not exceed the forcing energy f. The change in gravitational potential energy accompanying redistribution is scaled by a coefficient which represents frictional dissipation. Different frictional dissipation scaling coefficients are specified for ridging, shearing, and rafting. The thickness of the redistributed ice is then randomly chosen from the range bounded below by the thickness of the source ice, and the upper bound imposed by our conservation laws. Thin ice is likely to raft instead of ridging and shearing, and the model captures this by using a separate redistribution with a lower energy consumption and different characteristic shape for ice below a specified cutoff thickness. The process of rafting is taken to include shearing process as well, thus providing a mechanism for the creation of open water (ice of thickness zero) during rafting.

In creating ridges, we will be creating triangular features by redistributing ice of thickness h_o equally between all thickness categories from the one immediately above the source thickness (h_{o+1}) to the ridge height h_r. For the purpose of computational efficiency, when calculating GPE to constrain the maximum ridge height, we will be assuming that the ridge is formed entirely of ice of thickness h_r, with a change in GPE $g_b(\zeta v_s)2h_r$, where v_s is the fraction of the population involved in the redistribution, ρ is the linear density of ice (ice mass per unit thickness), and g_b is the net buoyant force. We scale this quantity by a factor of F_r, to include the energy consumed by frictional dissipation. Although this produces an underestimate of the maximum ridge height possible, it dramatically simplifies the calculations. We multiply the GPE of the redistributed features by tunable coefficients F_r and F_s to represent the frictional dissipation from ridging and shearing (respectively). By requiring that the difference between the frictionally scaled GPE from ridging and shearing and the source ice is less than the energy available, we obtain the inequality

$$g_b \left[F_s(1-\zeta)h_{sh} + F_r\zeta h_r - h_o\right] v_s \rho h_o \leq f.$$

From this we may solve for the maximum height of the ridge, h_r

$$h_r \leq \frac{1}{F_r \zeta}\left[\frac{f}{v_s \rho g_b} + h_o - F_{sh}(1-\zeta)h_{sh}\right]. \tag{4.3}$$

To constrain h_r, we must specify the shear ridge height, h_{sh}, and we will make the assumption that the shearing can lift the ice on the shearing interface onto the upper surface of the interacting floes. This is represented in the model by shear ridges with a height of twice the source thickness, $h_{sh} = 2h_o$.

Once a redistribution event has been generated, and the difference in energy between the current and proposed state has been calculated, we must assign the rate at which the event occurs, $T([\mathbf{g}, \eta] \rightarrow [\mathbf{g}^*, \eta^*])$ (abbreviated to $T(x \rightarrow y)$ below). The rate may also be thought of as the probability that an event will occur in a single time step. An important element of the present study is the assessment of the robustness of the model simulation of the thickness distribution evolution to changes in the specifics of the model formulation. Accordingly, the transition rate and components of the model describing the dynamics of the damage function will be treated as adjustable parameters in the model runs.

We will use a number of different transition rate functions in our sensitivity analysis. The simplest form of transition rate is a constant value. If we set $T(x \rightarrow y) = 1$, we allow all proposed events that do not require more energy than is available to the system to occur. We will also use the uniform probability distribution on [0 1] in our assessment of the model sensitivity to a variety of transition rates. Under the uniform distribution the probability for a specific event will be different each time it is calculated. This transition rate is deliberately chosen to test the model simulations under a profoundly unphysical configuration, and serves as a 'benchmark test' of the performance of the model under poorly chosen parameterisations. More physically meaningful transition rates depend on the difference between the available energy and the energy required for the redistribution (*i.e.*, the rate at which events occur depends in some way upon their energetic magnitude):

$$T(\mathbf{X} \rightarrow \mathbf{X}') = \phi(f - \Delta\mathbf{E}), \tag{4.4}$$

where $\Delta\mathbf{E}$ is the energy required to move the system from state $\mathbf{X}$ to $\mathbf{X}'$. This formulation assumes that the efficiency of redistribution in converting external forcing into ice movement depends on the thickness of the ice involved and amount only through energetics;

scale dependence can be implemented by including a dimensionless function of thickness (*e.g.* the thickness divided by some characteristic thickness) in the denominator. The function ϕ takes values between 0 and 1, and is zero for $f - \Delta\mathbf{E} < 0$. Under our assumption that the rate at which events occur reflects the efficiency of the system in turning forcing energy (f) into ice redistribution $\mathbf{X}' - \mathbf{X}$, we can additionally stipulate that ϕ must be a monotonically increasing function. In addition to forms of ϕ described by Eqn.4.4, we may construct formulations of ϕ which are energetically scale-independent:

$$T(\mathbf{X} \rightarrow \mathbf{X}') = \phi(\frac{f - \Delta\mathbf{E}}{f}). \tag{4.5}$$

These scale-independent transition rates take input between 0 and 1 (since $f - \Delta\mathbf{E} \geq 0$) and produce output between 0 and 1. We consider them energetically scale-independent because the transition rate does not depend on the absolute magnitude of $\Delta\mathbf{E}$, but rather on its magnitude relative to f.

The simplest form for ϕ is a power law:

$$\phi(x) = x^{\alpha} \tag{4.6}$$

for some power α. This form can be input an argument as in Eqn. 4.4 (for a scale-dependent rate) or 4.5 (for scale independence). We will also consider exponential transition rates, *e.g.*,

$$T(\mathbf{X} \rightarrow \mathbf{X}') = \exp(\beta(\Delta E)). \tag{4.7}$$

as well as an exponential function that features scale-independence:

$$T(\mathbf{X} \rightarrow \mathbf{X}') = \exp(\beta\Delta E/f), \tag{4.8}$$

where $\beta < 0$ in Eqn.4.7,4.8. In Eqn. 4.7, the forcing f is implicity present as it has been used to constrain the maximum value of ΔE.

In the model with memory, external forcing which does not go into redistribution causes the population of damaged ice to increase. This necessitates the introduction of a parameterisation of the energy consumed in damage of the ice. The greater the forcing applied to the ice, the more damage is caused; we will assume that this dependence is linear in the

unused energy. A representation of the dependence of ice strength on its thickness is incorporated by requiring the amount of damage $\Delta\eta(h)$ caused by a forcing f to decrease with increasing h. As discussed in Section 4.3.2, the strength of ice increases as it is broken into smaller pieces, with smaller contact areas. In the model, this is represented by requiring the amount of change in damage to decrease with increasing η. We describe the change in damage $\Delta\eta(h)$ to ice of thickness h, with damage $\eta(h)$ by

$$\Delta\eta(h) = C_d f \left(\frac{\eta(h)}{h}\right)^{\nu}, \tag{4.9}$$

with C_d a scaling coefficent and $\nu < 0$.

The thermodynamic forcing of ice thickness in the model is generated from the growth curves given by [35], using a simple linear interpolation between the summer and winter curves ($W_1(h)$ and $W_2(h)$ respectively; Fig. 2.2 in Chapter 2) to represent seasonal change:

$$\begin{aligned} \Delta g(h) &= \left[S(t)W_1(h) + (1 - S(t))W_2(h)\right] g(h) \\ W_1(h) &= 0.1\exp(-1.7(h)) - 0.01 \;\; m\, day^{-1} \\ W_2(h) &= -0.01\exp(-0.01(h)) \;\; m\, day^{-1} \end{aligned} \tag{4.10}$$

The scaling coefficients in the definition are chosen to fit approximations taking simple exponential form of the observed growth curves. The function $S(t)$ is periodic, taking values between 0 and 1, given by a piecewise linear function, defined for $0 \leq t < 360$,

$$S(t) = \begin{cases} 1 - t/180 & 0 \leq t < 180 \\ t/180 - 1 & 180 \leq t < 360 \end{cases}$$

with time t in days. In implementing the model, we take the model timestep *modulo* 360 as input for $S(t)$. In the model, where $g(h)$ is discretised, thermodynamic processes transfer an ice amount $\Delta g(h_i)$ from the h_i thickness category to one of its two neighbours depending on whether there is net growth or ablation.

In the model with memory, the thermodynamic routine must include a representation of the process of refreezing of damaged ice at a rate dependent on the ice thickness and the thermodynamic growth or ablation. We assume that the ice will 'heal' either through the growth of ice to fill the spaces between the blocks of ice, or through the fusing of the

blocks together as they melt. The 'healing' rate is dependent on the thickness of the ice, with thicker ice healing at a slower rate (assuming that the spaces between the blocks of ice that must refreeze will increase with thickness). The decrease in $\eta(h)$ due to healing is given by

$$\frac{\mathrm{d}\eta}{\mathrm{d}t} = -\psi \left| \left[S(t) W_1(h) + (1 - S(t)) W_2(h) \right] \right| \tag{4.11}$$

where $S(t)$ is defined in Eqn.4.11, $W_1(h)$ and $W_2(h)$ are given in 4.10, and ψ determines the rate of healing relative to the thermodynamic growth and melt.

4.5 Model Tuning and Simulation Results

Setting model parameters is relatively straight-forward, as only a few of these are adjustable. The parameters of the model we focus on are the number of events proposed between each thermodynamic update, N, the strength and nature of the external forcing, f, and the parameter β for model runs using the transition rate (Eqn. 4.7). We also consider model sensitivity to changes in the representation of the redistribution process by varying the maximum thickness at which ice may raft and the proportion of ridging to shearing, ζ. For the version of model with memory we also consider model sensitivity to parameters related to ice damage, specifically the relationship between the thickness of the ice and the energy required to damage it (ν in Eqn. 4.9), and the relative strength of the healing rate of damaged ice (ψ in Eqn. 4.11). As we are using a stochastic technique, in order to obtain meaningful results we run ensembles of 40 simulations using the same parameters and driven by the same forcing. From these, we may compute the ensemble mean and standard deviation of $g(h)$ and compare these with observations.

We will focus on the model simulation of the population in winter (February/March), when the full effects of redistribution processes on the thickness distribution are in statistical balance (*c.f.* Chapter 2). The model is run to (cyclo-stationary) equilibrium to ensure that there is no long-term trend in the ice population under an interannually repeating thermodynamic cycle. The features of the observed thickness distribution which we desire the model to capture are the following:

- In the mean distribution, we desire an approximately exponential tail with approximately two orders of magnitude rolloff between 2m and 10m, as in Fig. 1.

- The mode of the thickness distribution at the thermodynamic equilibrium is also an important feature to capture, which will require an appropriate balance between thermodynamic action and dynamic redistribution.
- The minimum value of the ratio of the ensemble standard deviation to its mean, $R(h)$ should occur at the thermodynamic equilibrium thickness. Above this value, the $R(h)$ should be approximately linear, with a positive slope.

Attempted Moves	40
Number of Thickness Categories	300
Thickness Category Bin	0.1m
Number of Runs	40
Ridging Friction Coefficient	2
Shearing Friction Coefficient	4
Rafting Friction Coefficient	0.5
Max Rafting Thickness Index	10m
Rate coefficient β	$10^{-4}J^{-1}$
η damage exponent ν	-2
η healing exponent ψ	-2
Forcing Strength f	$2 \times 10^3 J$ (Memory model), $4 \times 10^3 J$ (Memoryless)

Table 4.1: Model Base Parameters

In Fig. 4.2 we show the results of model simulation for the two variants of the model. These simulations have been performed using the parameter values listed in Table 4.1, and show the state of the ice population in the model equivalent of March. These parameter values were chosen for their ability to produce thickness distributions similar to the observations described in Chapter 2. Both ice thickness distributions display a pronounced peak at approximately 1.5m and approximately exponential tails. As will be seen in the sensitivity analysis, the model can produce tails which are more truly exponential in form than those of the baseline runs. We have chosen the baseline parameters because they produce thickness distributions which have a large difference in the slope of $g(h)$ between the ice immediately around the mode of the distribution and that forming the tail, which is a clear feature of the thickness data examined in Chapter 2. The ratio $R(h)$ is characterised by largest values in the ice below 1m, and an approximately linear portion with a positive slope above 2m.

To assess the sensitivity of model behaviour to the formulation of the transition rate function, simulations were carried out for a range of functions (holding all other model param-

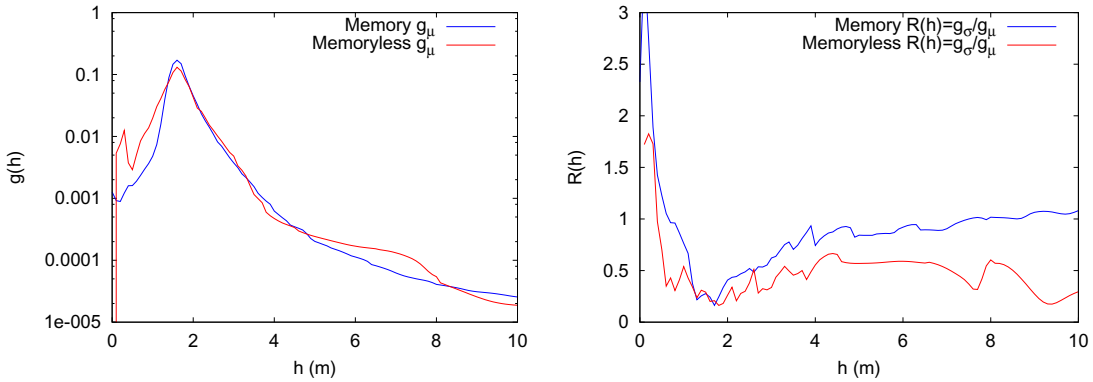

(a) g(h) (b) R(h)

Figure 4.2: Baseline simulated mean thickness distribution $g_\mu(h)$ (left panel) and variability ratio $R(h)$ for both models, using the exponential transition rate (Eqn. 4.7), and parameters given in Table 4.1. Simulations are run for 10 years from an initial condition ice-free waters, terminating in model winter (equivalent of Feb/March)

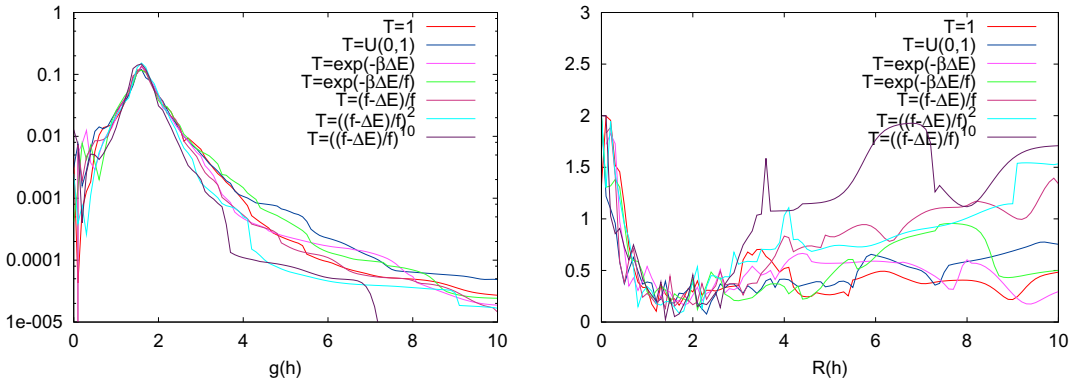

(a) g(h) Jan, 10 year run

(b) R(h) Jan, 10 year run

Figure 4.3: Simulated ensemble mean thickness distribution $g_\mu(h)$ (left panel) and variability ratio $R(h)$ (right panel) for different parameterisations of the transition rates from a 10-year simulation of the model without memory.

eters constant). The transition rates considered were a constant rate $T(\mathbf{X} \rightarrow \mathbf{X}') = C$ (all events that can happen, do so at the same rate), rates drawn randomly from [0, 1], exponential forms based on energy considerations (Eqn. 4.7, 4.8), and the efficiency formulation of Eqn. 4.6 with α= 1, 2 and 10. The qualitative features of the simulation of ensemble mean $g_\mu(h)$ and $R(h)$ are largely insensitive to the choice of transition function (Figs. 4.3, 4.4), with the exception of the extreme case of the rates drawn from [0, 1], and the formulation from Eqn. 4.6 with $\alpha = 10$ (for which large transitions are strongly suppressed). In the simulations shown in Figs. 4.3, 4.4, the values for β and the constant rate were deliberately chosen to give distributions with similar e-folding length to the other simulations, so that meaningful comparison between the ratios $R(h)$ could be made.

We may further test the model's sensitivity to efficiency-based transition rates which allow all events for which $\Delta E/f$ is less than a specified constant value. In the model simulations using the efficiency-based transition rate (Fig. 4.5, 4.6), the model with memory produces populations with sub-exponential tails for all minimum efficiencies, where the model without memory produces populations with abrupt drops in the amount of thick ice which deviate from the sub-exponential tail. In general, the model with memory is better able to form smooth tails in this set of simulations, which is reflected in a greater evacuation of the ice with a thickness below approximately 1 meter. This can also be seen in the greater values of $R(h)$ that the memory model has for the thin ice.

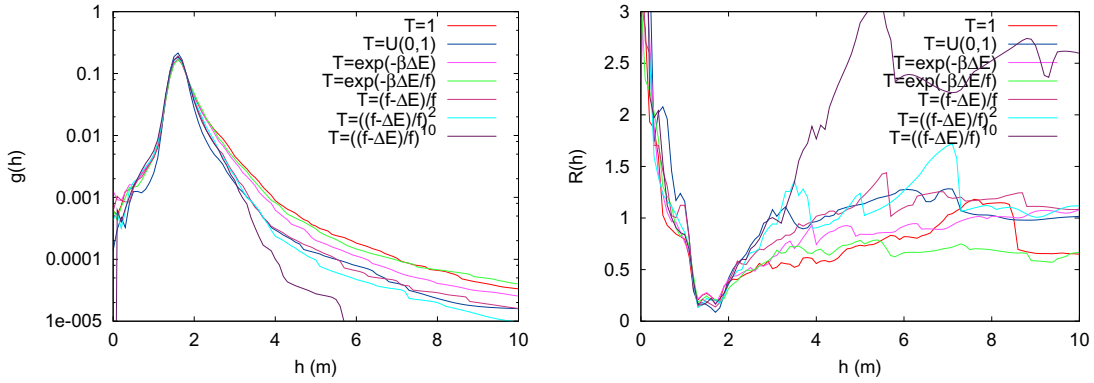

(a) g(h) Jan, 10 year run (b) R(h) Jan, 10 year run

Figure 4.4: Simulated ensemble mean thickness distribution $g_\mu(h)$ (left panel) and variability ratio $R(h)$ (right panel) for different parameterisations of the transition rates from a 10-year simulation of the model with memory.

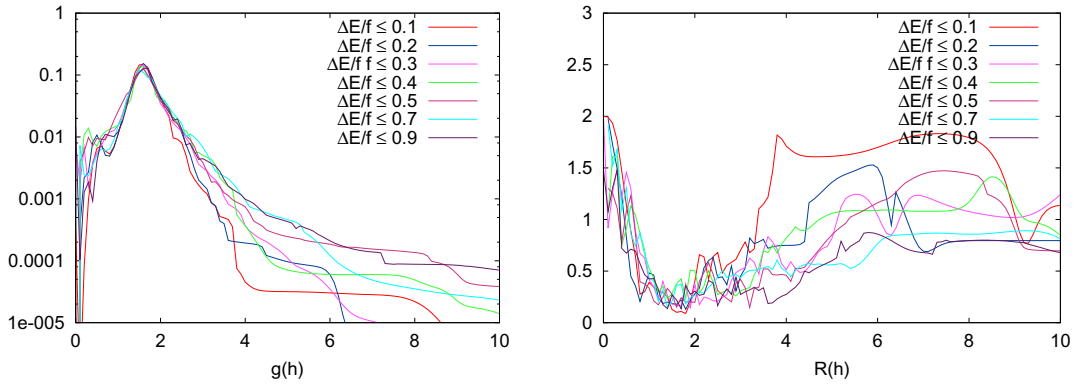

(a) g(h) Jan, 10 year run (b) R(h) Jan, 10 year run

Figure 4.5: Simulated ensemble mean thickness distribution $g_\mu(h)$ (left panel) and variability ratio $R(h)$ (right panel) for different allowed efficiencies of proposed transitions from a 10-year simulation of the model without memory.

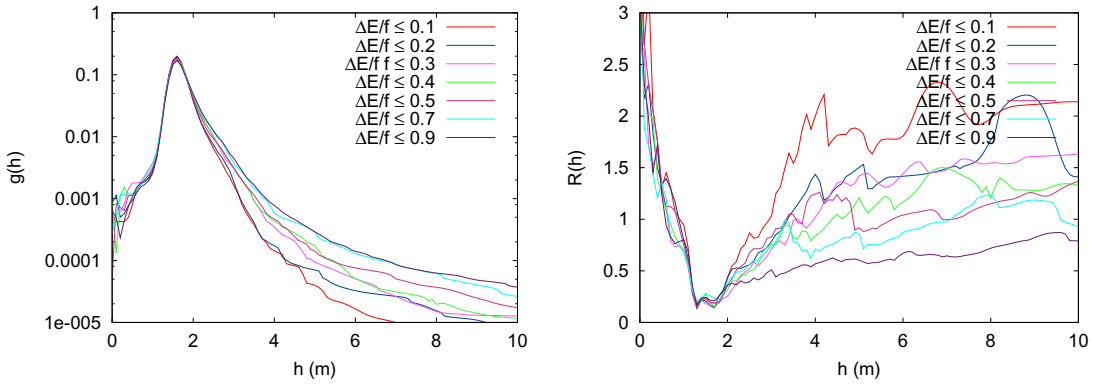

(a) g(h) Jan, 10 year run

(b) R(h) Jan, 10 year run

Figure 4.6: Simulated ensemble mean thickness distribution $g_\mu(h)$ (left panel) and variability ratio $R(h)$ (right panel) for different allowed efficiencies of proposed transitions from a 10-year simulation of the model with memory.

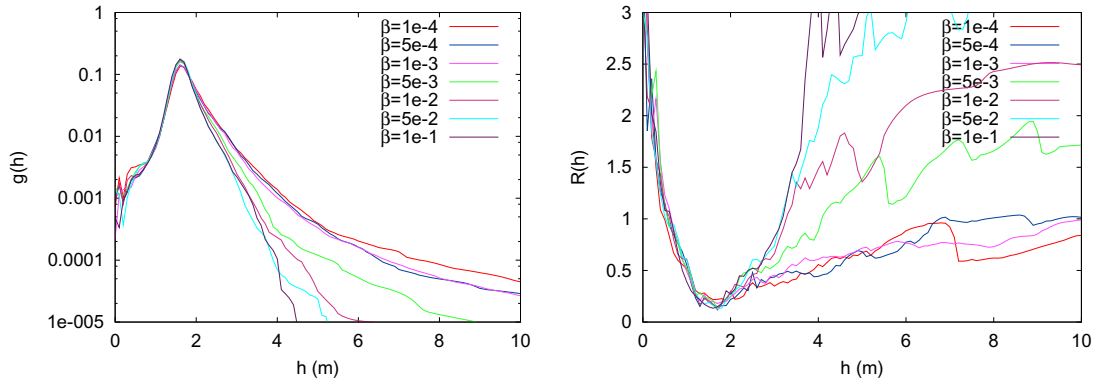

(a) Thickness Dist (b) Ratio

Figure 4.7: Simulated ensemble mean thickness distribution $g_\mu(h)$ (left panel) and variability ratio $R(h)$ (right panel) for varying β from a 10-year simulation of the model without memory.

In the remainder of our simulations, we will use the exponential transition rate (Eqn.4.7) in our exploration of parameter space. This choice allows us to explore the way in which the models react to changes in the transition rate by changing the value of β (as larger values of β reduce the probability of high-energy transition). Figures 4.7 and 4.8 illustrate the model response to changes in the coefficient β (Eqn. 4.7) across five orders of magnitude. As β increases, both models respond in a similar fashion, growing less able to produce an extended tail. It is worthwhile to note that the model sensitivity to changes in β is weak, as it is able to produce tails over several orders of magnitude of β. This weak sensitivity is connected to the weak sensitivity the model displays to the form of the transition rate function (Fig.4.3), and will be discussed in Section 4.6.

For all values of β, both variants of the model have a pronounced peak at approximately 1.5m, which is due to the thermodynamic processes at work on the population. In every simulation, the ratio $R(h)$ is largest in the thinnest ice category, takes a minimum at the mode thickness, and trends upward for ice thicker than approximately 2m. The primary difference between the two models lies in the extent of the tail: the memoryless model shows a more even transition from a population with a very short tail at $\beta = 1 \times 10^{1}$ to one with an extended tail at $\beta = 1 \times 10^{-1}$. In contrast, the model with memory forms approximately similar thickness distributions for $\beta = 1 \times 10^{-1}$ and $\beta = 5 \times 10^{-1}$ and for $\beta = 5 \times 10^{-3}$ and $\beta = 1 \times 10^{-3}$. In addition, the tail of the model without memory is slightly more populated, whereas the population of ice below 1m in thickness is greater in the model with memory. In both models larger values of β produce higher variability in the

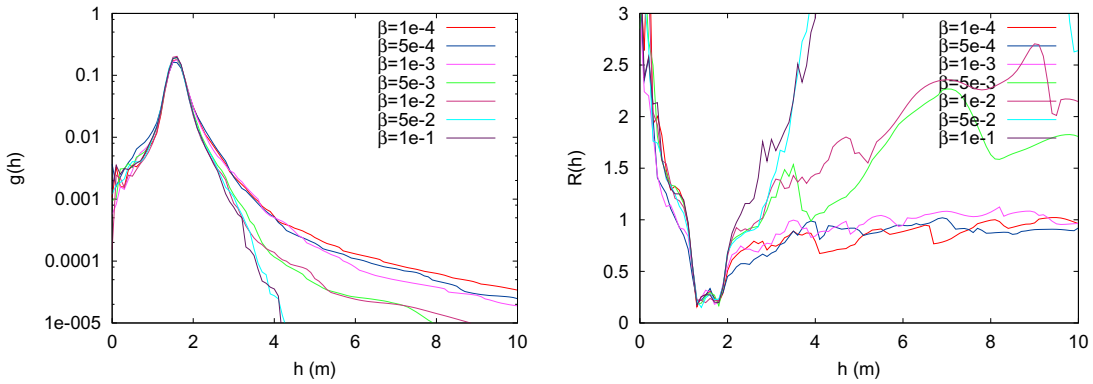

(a) Thickness Dist (b) Ratio

Figure 4.8: Simulated ensemble mean thickness distribution $g_\mu(h)$ (left panel) and variability ratio $R(h)$ (right panel) for varying β from a 10-year simulation of the model with memory.

thick ice, which is shown in the increase of the slope of the upwards trending portion of $R(h)$. This is to be expected, given that larger values of β produce a system with a lower rate of high-energy transitions, which are needed to drive the growth of thick ice.

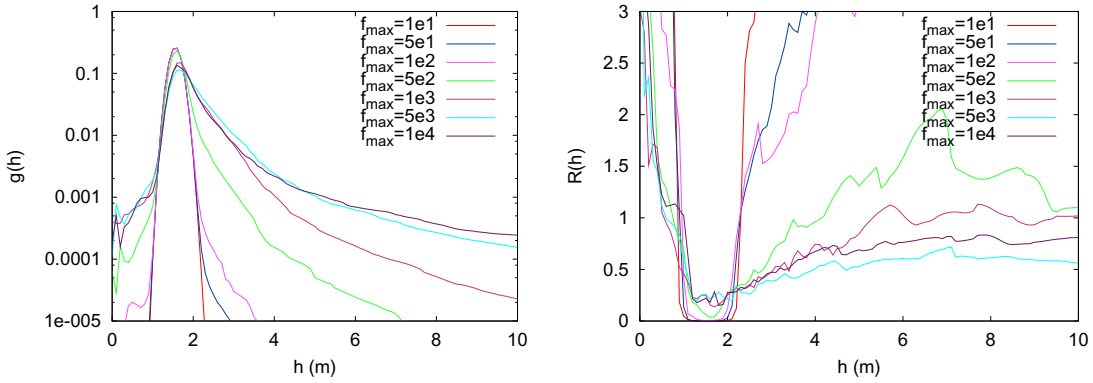

(a) Thickness Dist (b) Ratio

Figure 4.9: Simulated ensemble mean thickness distribution $g_\mu(h)$ (left panel) and variability ratio $R(h)$ (right panel) for varying forcing f from a 10-year simulation of the model without memory.

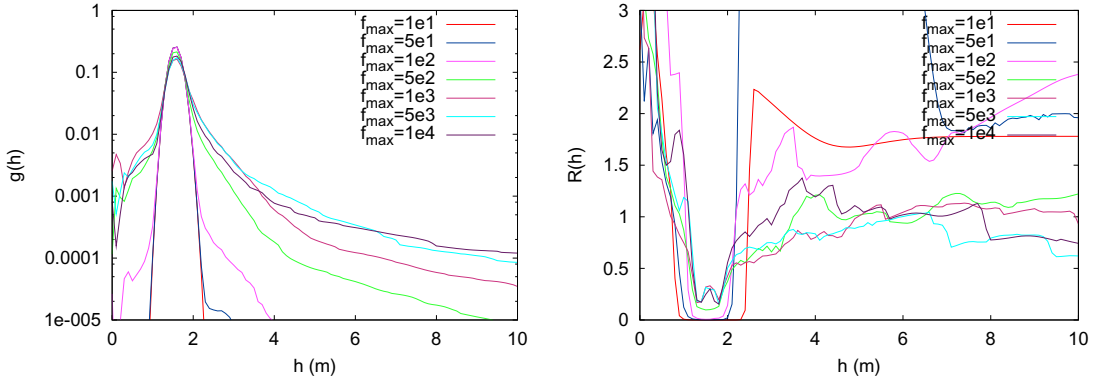

(a) Thickness Dist (b) Ratio

Figure 4.10: Simulated ensemble mean thickness distribution $g_\mu(h)$ (left panel) and variability ratio $R(h)$ (right panel) for varying forcing f from a 10-year simulation of the model with memory.

The sensitivity of the model to changes in F_r, F_s, and F_{ra} is the same as that to changes in the value of f. This is understandable, given the analogous roles they play in the calculations of the energy required for a distribution. As a result, we present model responses to changes in f only, and keep the frictional coefficients fixed.

The strength of the forcing controls the magnitude of redistributions possible. Both models respond in a similar fashion to changes in f, with larger values allowing for the creation of longer exponential tails (Fig. 4.9, 4.10). As the tail extends, the slope of the linear portion of $R(h)$, above the peak, decreases. With larger f, more of the population may be found in the tail, and the peak becomes slightly less pronounced in the model without memory. The primary difference between the two variants of the model is that the memoryless model displays a greater increase in tail extent with increasing f than the model with memory. This result is consistent with the fact that the model with memory requires that ice be damaged to create an exponential tail, and consequently, the population of ice available for redistribution into the tail will be smaller than in the model without memory. The model with memory also produces populations with more ice in the lowest categories, due to the higher frequency of selection of transitions involving the thin ice. As with the form of the transition rate (Fig.4.3), and the value of β (Fig.4.8), the model displays low sensitivity to the value of f, and we may vary f over several orders of magnitude and still produce populations with approximately exponential tails.

The ratio of the number of redistribution attempts (N) made to the number of thermo-

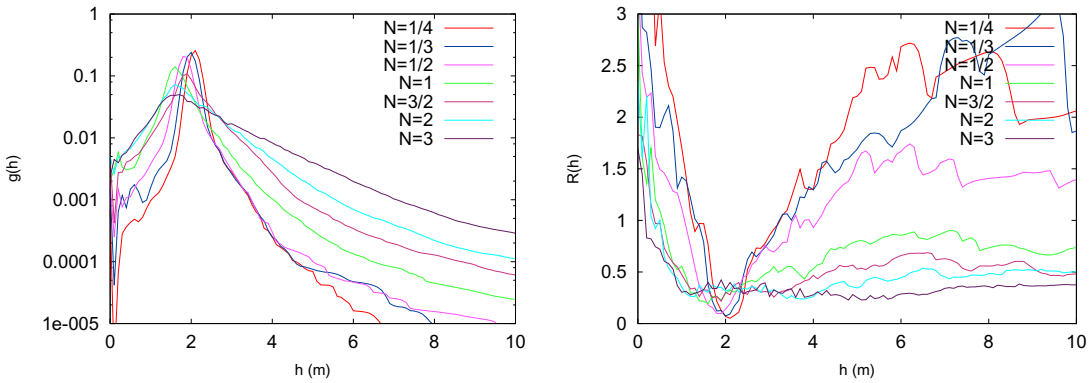

(a) Thickness Dist (b) Ratio

Figure 4.11: Simulated ensemble mean thickness distribution $g_\mu(h)$ (left panel) and variability ratio $R(h)$ (right panel) for varying redistribution attempts per timestep N from a 10-year simulation of the model without memory.

dynamic updates is extremely important in determining model behaviour. This parameter is closely tied to the forcing strength f, and together these two parameters affect the way in which changes to the population take place. With small N and large f, changes in the population occur through small numbers of high-energy events. When N is large and f is small,

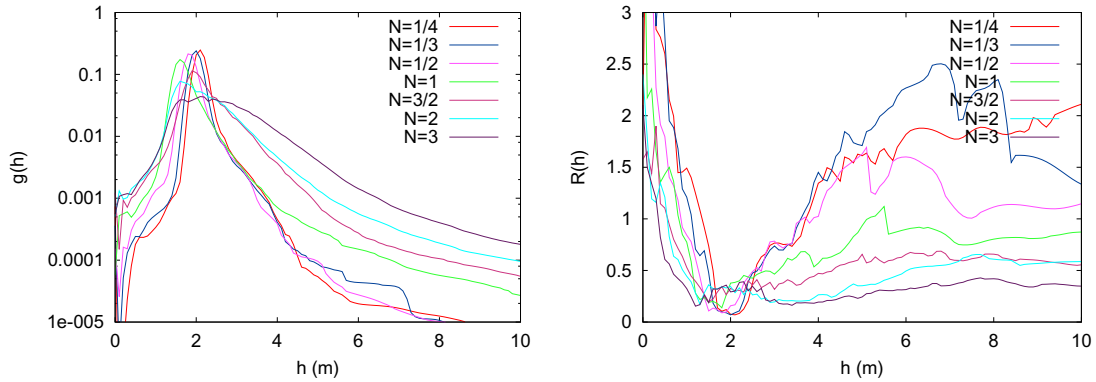

(a) Thickness Dist (b) Ratio

Figure 4.12: Simulated ensemble mean thickness distribution $g_\mu(h)$ (left panel) and variability ratio $R(h)$ (right panel) for varying redistribution attempts per timestep N from a 10-year simulation of the model with memory.

changes in $g(h)$ are brought about through large numbers of low-energy events. Whereas the model responds to changes in the order of magnitude of f, the response to changes in N occurs over a range of less than 10. Both the variant of the model with memory and the one without respond in a similar manner to changes in N. As can be seen in Figures 4.11, 4.12, the exponential tail of the distribution is less populated for lower numbers of redistribution attempts. As this number is increased, the proportion of the population in the exponential tail grows, and as N increases the redistribution process begins to dominate the dynamics of the population, resulting in a population with a smaller peak, which moves below the thermodynamic equilibrium thickness. The decrease in the mode thickness is due to the increased production of thin ice through increased lead formation. With increasing N, the slope of the portion of $R(h)$ above the mode of decreases, as the model provides more opportunities for redistribution events to occur in each simulation, thus increasing the likelihood that thick ridged ice is produced.

In Fig. 4.13, we display several similar population distributions obtained with varying values of f and N in the model with memory. These simulations demonstrate that within a range of values of f and N it is possible to obtain similar populations regardless of whether the dynamics are characterised as having large numbers of low-energy events or vice versa. This result is not true for any value of f, as the model may be unable to produce a substantial tail for any value of N if f is too low. The simulation shown in Fig. 4.13 with $f = 10^2 J$ is at the lower limit of values of f for which similar populations may be simulated by increasing N. Note that the tail of the population is preceded by a plateau, and the tail is more

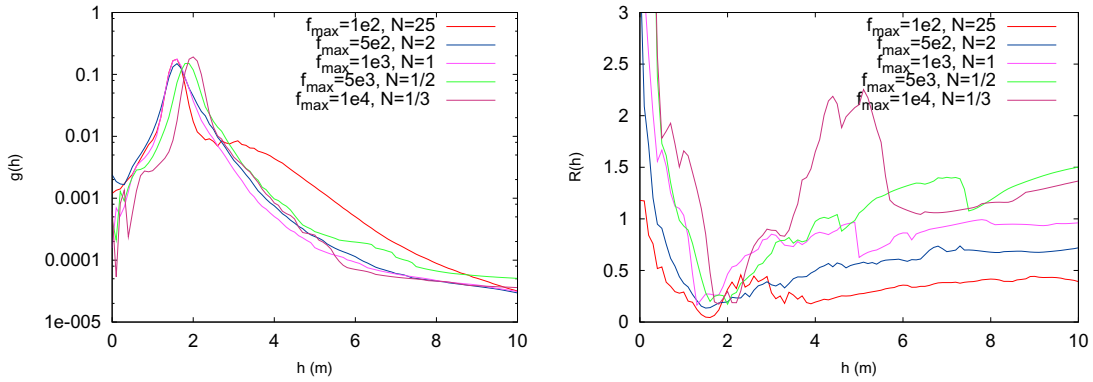

(a) Thickness Dist (b) Ratio

Figure 4.13: Simulated ensemble mean thickness distribution $g_\mu(h)$ (left panel) and variability ratio $R(h)$ (right panel) for varying forcing strengths and redistribution attempt numbers from a 10-year simulation of the model with memory.

purely exponential than for the other two simulations. From a practical perspective, simulations with small N require less computation, and may be completed faster. In addition, the values of $R(h)$ for the population of ice above 2m in the simulations which use large numbers of low-energy events is smaller than observations suggest.

The responses of model simulations to changes in the maximum thickness at which ice

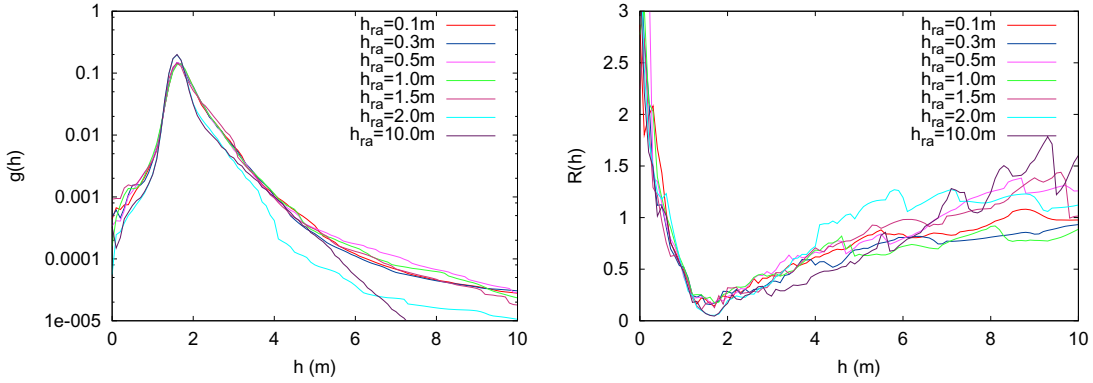

(a) Thickness Dist (b) Ratio

Figure 4.14: Simulated ensemble mean thickness distribution $g_\mu(h)$ (left panel) and variability ratio $R(h)$ (right panel) for varying rafting thickness from a 10-year simulation of the model without memory.

may raft (h_{ra}) are shown in Fig. 4.14, 4.15. The memoryless model's primary response to changes in the rafting thickness is manifest as an increase in the value of $g(h)$ at the mode

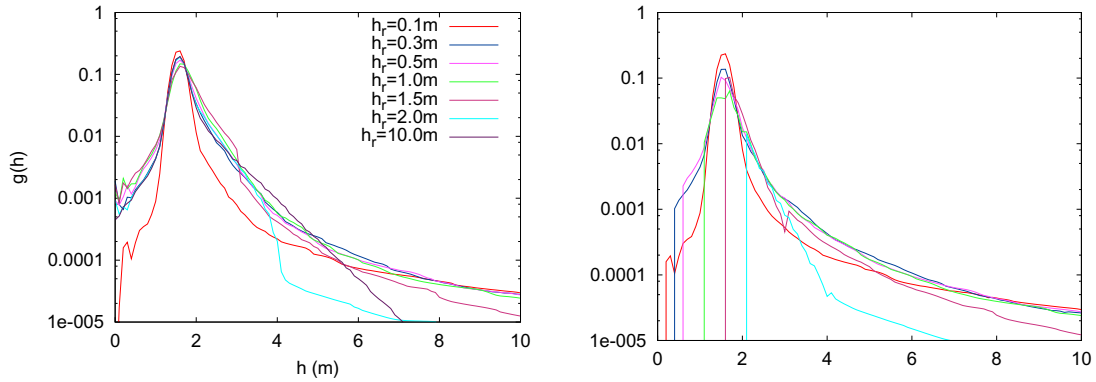

(a) Thickness Dist (b) Ratio

Figure 4.15: Simulated ensemble mean thickness distribution $g_\mu(h)$ (left panel) and variability ratio $R(h)$ (right panel) for varying rafting thickness from a 10-year simulation of the model with memory.

of the distribution when $h_{ra} = 10$m. The ratio $R(h)$ does not show extreme responses to changes in the cutoff thickness, except when it is set high enough to prevent the formation of an extended tail. As the rafting cutoff thickness is increased, $R(h)$ decreases, and the large hump seen in $R(h)$ for $h_{ra} = 0.1m$ is not present for larger values. The response of the model with memory to changes in h_{ra} is more pronounced because the ice which is available for redistribution depends on the maximum rafting thickness. Higher cutoff thicknesses yield a larger portion of the population which does not need to be damaged in order to be available for redistribution. In the model with memory, the population of thin ice decreases with an increase in the maximum rafting thickness and the portions of the population which are formed by rafting (ice thicknesses up to double the maximum rafting thickness) increase accordingly. With increasing h_{ra}, the mode thickness of the distribution increases slightly, moving away from the thermodynamic equilibrium. As h_{ra} increases, the dynamics of the memory model approach those of the memoryless model, with more and more ice not requiring damage in order to participate in redistribution. Very large values of h_{ra} produce two notable results. In both variants of the model, the simulations with large h_{ra} produce a very defined exponential tail. With $h_{ra} = 10m$, the model dynamics simplify to the process of doubling of thickness and the creation of open water. This description of the redistribution process is very similar to the systems described in [51], and was discussed in more detail in Chaper 3. When h_{ra} is large, the bulk of the population of ice is available for redistribution in the model with memory, which accounts for the similarity in population distributions. The second notable response accompanying large h_{ra} appears in the model with memory. In this model, the portion of the population forming the exponential tail

decreases as h_{ra} increases. Only when the rafting thickness is increased to include most of the population ($e.g.\ h_{ra} = 10m$) does the tail repopulate. The model prioritises rafting over other forms of redistribution; by increasing the amount of ice which can raft, the part of the population which can ridge (and thus create ice more than double its own thickness) is reduced. By allowing ice up to 2m to raft, we reduce the amount of ridging to the extent that no exponential tail can be formed.

The maximum rafting thickness may be constrained by observations to 3.3m ([4]), however the rafting of ice 3.3m thick is considered exceptional. Given that the model prioritises rafting over other forms of redistribution, and rafting becomes less common in thicker ice, we expect that a lower thickness than 3.3m for h_{ra} is appropriate . From the simulations displayed in Fig.4.14,4.15, the most realistic model simulations have been made with a rafting cutoff index $h_{ra} < 1$m.

In the standard model runs, we select the proportion of redistribution events that are treated

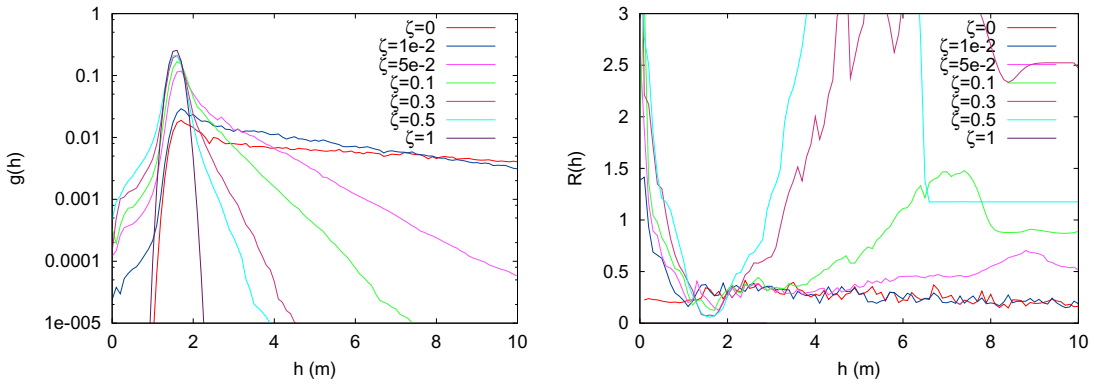

(a) Thickness Dist (b) Ratio

Figure 4.16: Simulated ensemble mean thickness distribution $g_\mu(h)$ (left panel) and variability ratio $R(h)$ (right panel) for varying proportion of redistribution to be purely compressive, ζ, from a 10-year simulation of the model without memory.

as purely compressive (resulting in ridging), ζ, from a uniform distribution $U(0, 1)$, but it is valuable to examine the model output when the value of ζ is held fixed. We perform runs from $\zeta = 0$ (pure ridging) to $\zeta = 1$ (pure dilation). Model simulations illustrate (Fig. 4.16, 4.17) that both the memoryless and memory models respond in a similar fashion to fixed values of ζ. However, the model without memory produces distributions which have almost purely exponential tails, whereas the model with memory produces populations with a dip in the population of ridged ice, due to the limiting of the availability of ice to ridge due

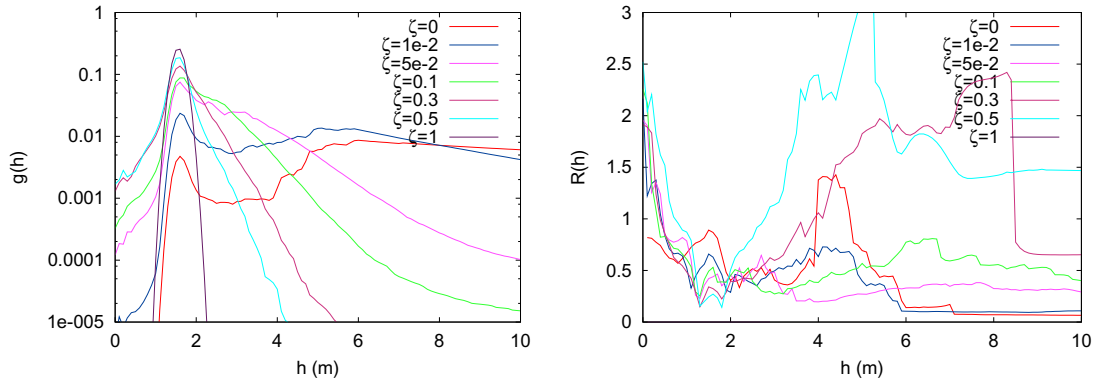

(a) Thickness Dist (b) Ratio

Figure 4.17: Simulated ensemble mean thickness distribution $g_\mu(h)$ (left panel) and variability ratio $R(h)$ (right panel) for varying proportion of redistribution to be purely compressive, ζ, from a 10-year simulation of the model with memory.

to the damage requirement. With $\zeta = 0$, the model produces populations without any thin ice (as it has no mechanism to do so). As well, the model cannot produce thick ice except through shearing and rafting, and these processes do not create enough thick ice to produce a population which is not entrained into a tight band about the equilibrium thickness by the thermodynamic forcing. With $\zeta = 0$, $R(h)$ is small, and does not display the characteristic increase in the thin ice that is seen in the observations. With increasing ζ, $R(h)$ increases for the thin ice, and for the ice above the mode. At $\zeta = 1$, $R(h)$ is effectively zero, as the ice is driven solely by thermodynamics, which are purely deterministic in our model.

The model does not display a high sensitivity to the damage exponent, with both the mean thickness distribution and ratio $R(h)$ showing little response to changes in ν (Fig. 4.18). Model response to varying the healing rate, ψ, (Eqn. 4.11) ranges from a model which is unable to produce a tail when ψ is large, to one which behaves much as the memoryless model when $\psi = 0$. In the case of large ψ, the ice heals rapidly enough that the population of damaged ice is small enough to prevent the formation of ridges. In the latter case, damaged ice does not heal, and under long enough model runs, the entire population of ice will become damaged and thus available for redistribution. Under these circumstances, the memory model acts in an identical fashion to the model without memory.

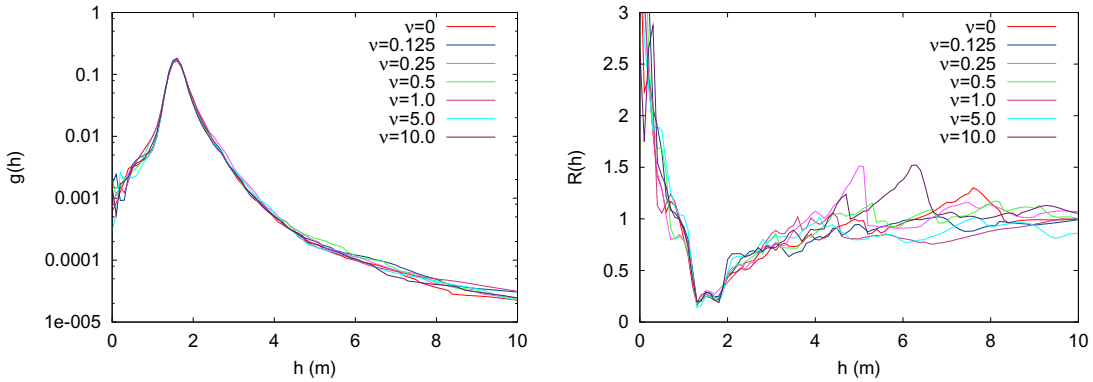

(a) Thickness Dist (b) Ratio

Figure 4.18: Simulated ensemble mean thickness distribution $g_\mu(h)$ (left panel) and variability ratio $R(h)$ (right panel) for varying damage exponent, ν, from a 10-year simulation of the model with memory.

4.6 Discussion

The model simulations produce population distributions with an exponential tail under a wide range of parameterisations and parameter values. The persistence of the exponential tail in the simulations is the result of the similarity that the model formulation has to the systems described by SCMs, as discussed in Chapter 3. A SCM follows the dynamics of a population of 'particles' of various masses where pairs of particles may interact by combining to form a single 'particle' with mass equal to the sum of the two parent particles. If we consider the particle masses to be discrete, with the population of particles of mass i written as $u_i(t)$, the equations describing the population dynamics are

$$\frac{\mathrm{d}}{\mathrm{d}t}u_i(t) = \frac{1}{2}\sum_{j=1}^{k-1} K(k,j)u_j(t)u_{k-j}(t) - u_k(t)\sum_{j=1}^{\infty} K(k,j)u_j(t). \tag{4.12}$$

The first term on the right hand side represents all of the ways of making particles of mass i (a source term for particles of mass i), and the the second term is the ways in which particles of size i can combine with other members of the population to form larger particles (a sink term for particles of mass i). Although SCMs do not conserve the total number of particles, $\sum_{j=1}^{\infty} u_j(t)$, they do conserve the mass of the system $\sum_{j=1}^{\infty} ju_j(t)$. Since the number of particles is not conserved, we may not treat u_j as a probability distribution. What differentiates different members of the family of SCMs is the kernel $K(x,y)$, which describes the rate at which interactions between particles of masses x and y occur.

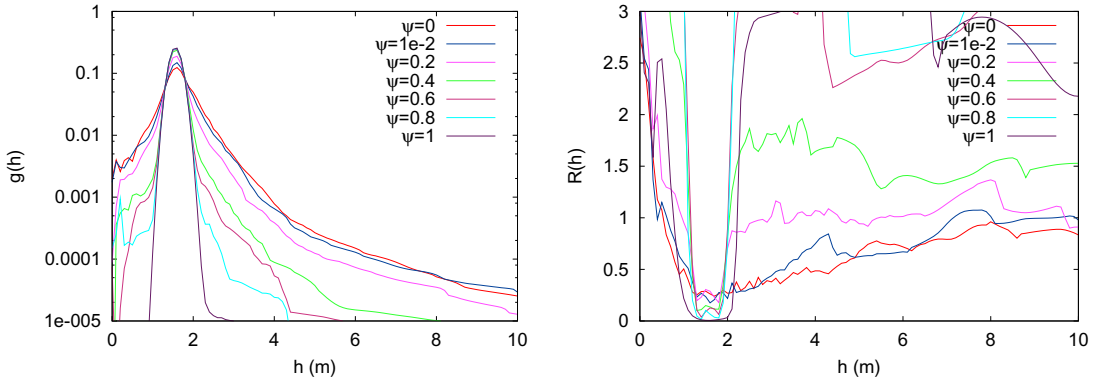

(a) Thickness Dist (b) Ratio

Figure 4.19: Simulated ensemble mean thickness distribution $g_\mu(h)$ (left panel) and variability ratio $R(h)$ (right panel) for varying healing exponent, ψ, from a 10-year simulation of the model with memory.

Many members of the SCM family yield exponential-like distributions of particle masses; in particular, for a constant rate kernel, if the population is normalised and treated as a probability distribution, the moments converge to those of an exponential distribution [17]. The present model includes redistribution processes that extend it beyond the basic SCM formulation, as well as a thermodynamic component, but the fundamental principle is very similar. We have explored simple SCMs in Chapter 3, and compared their output to other conceptual thickness distribution dynamics models of a similar nature [51]. In this chapter, the redistribution events which we generate, and the way that they transfer ice from lower thickness categories is comparable to particle interactions in SCMs. The representation of redistribution in our model is more sophisticated than the particle combinations of SCMs, which allows us to make a greater connection to observed redistribution events (described in Section 4.3.1).

We consider the robust response to changes in the transition rate function to be an important conclusion of this analysis. Although the model does display a strong sensitivity to the values of some parameters, the function describing the rate at which events occur is not of primary importance in determining the model behaviour. There is a strong contrast between the model response to changes in the transition rate and changes in the value of ζ. In this work we have chosen to represent the redistribution events as composites of compressive motion, which moves ice from lower to higher thicknesses, and dilation, which provides a source of new thin ice in the form of open water. When the portion of redistribution events ridging is close to 0 or 1, the populations produced by the model deviate strongly from the more realistic populations the simulation produces with values of ζ centered around 0.5. This dependence suggests that the simulation of the evolution of sea ice thickness distributions requires that the description of the way in which redistribution events transfer ice between thickness categories is of primary importance in model construction. In our model, the representations of the way that ridging and shearing transfer ice between thickness categories have been kept simple, and investigation of the model's response to more detailed redistribution descriptions seems valuable.

Variation in the strength of the term used to represent the forcing of winds and currents yields a range of behaviours. With forcing sufficiently small, the model generates a population dominated by thermodynamic action, with the ice clustered around the equilibrium thickness. When the forcing is large, the model generates an exponential tail with a nearly

flat slope, which extends far beyond typical observations. However, these features only occur with increases in the forcing strength of several orders of magnitude.

The differences in behaviour between the model variations with memory and without are not substantial. In general, the model with memory produces a smaller exponential tail under identical parameter values, which may be attributed to the limiting of the ice available for ridging due to the requirement that ice be damaged before it is redistributed. The other differences between the models are primarily seen in the sensitivity of populations to changes in parameters which effect the relationship between the magnitude and frequency of events (the efficiency tests where $T = 1$ if $\Delta E/f < C$, N), and the parameters which affect the nature of the redistributions (ζ,h_{ra}). In respect to N and the efficiency transition rates, the model without memory shows a stronger sensitivity to changes in these parameters, and is less able to produce exponential tails in the cases where N is small or the maximum allowable value of $\Delta E/f$ is small. This sensitivity is due to the model construction: the model without memory randomly selects ice from the entire population, which can lead to the choice of proposed events with low transition rates. Conversely, the model with memory only selects ice which has either been damaged or is below the rafting cutoff thickness. This favours the selection of events involving thinner ice, and these events typically have a lower energetic magnitude, since the minimum energy required for a redistribution is dependent on the thickness of the ice involved. The more subtle aspects of the model performance lie in its representation of thin ice, and in the variability between the individual runs used to calculate the population mean thickness distribution. The model with memory performed slightly better, capturing more of the variability seen in the low thickness ice, and just above the local thermodynamic equilibrium thickness.

The other major difference between the model with memory and that without is in their sensitivity to changes in the rafting cutoff thickness. The model with memory displays a greater sensitivity to changes in h_{ra}, because the population of ice which may be selected for redistribution events increases with increasing h_{ra}. When the bulk of the ice available for redistribution is in the rafting category, and the thickness of ice which has rafted is still below the rafting cutoff, the model without memory is unable to form an exponential tail. Because the ice which may be redistributed lies almost entirely below the rafting cutoff, ridging is rare, and a large enough body of damaged ice to allow for the formation of a tail cannot be created. Because the model prioritises rafting over other types of redistribution events, we see in both variants a pronounced change in the population distribution when

$h_{ra} = 10.0m$. While this is unrealistically large, this example illustrates the connection between the model which we have developed and the systems described by the SCMs. When the rafting thickness is set this high, nearly all of the redistribution interactions involve the simple doubling of the thickness of ice, and the creation of open water. This kind of dynamic is extremely similar to the model proposed in [51], which is itself closely related to SCMs (as discussed in Chapter 3). Because interactions in rafting ice take the form of ice stacking atop itself, the ice which is below the rafting cutoff thickness behaves in an identical fashion the particles in an SCM with coagulation kernel $K(x, y) = \delta_{x,y}$. For this reason, when we perform simulations with high rafting cutoff thicknesses, the system behaves more directly like an SCM, producing a nearly exact exponential tail.

The model with memory displayed almost no sensitivity to the parameter governing the shape of the damage/energy relationship (ν). The model's parameterisation of the way in which ice is damaged prior to redistribution requires an equal or lesser amount of energy than subsequent redistribution, and consequently parameter values which allow the formation of a tail will do so for a large range of values of ν. While the choice of the value of ν is essentially unimportant, the model shows strong sensitivity to the value of the coefficient which scales the rate at which damaged ice heals (ψ). Changing the rate at which ice heals has a dramatic effect - at one extreme, when no healing occurs, the model dynamics approach those of the model without memory, as all of the ice eventually becomes damaged. When the damaged ice heals quickly, the population is unable to form an extended tail, due to the lack of ice which is available to participate in ridging.

4.7 Conclusions

We have created a conceptual model in order to examine the processes which determine the form and statistics of the thickness distribution of sea ice. By casting the process of deformation-through-interaction in the ice pack as a stochastic process which evolves through a series of discrete steps, qualitatively realistic simulations of the sea ice thickness distribution and populations of sea ice thickness distributions were obtained. In addition to simulating the ensemble-mean thickness distribution, populations of distributions generated by the model display the same low-order statistics (mean and variance) that may be observed in populations of thickness distributions obtained from multiple tracks, as discussed in Chapter 2. The fact that the model is capable of capturing not only the form of

a single realisation but also the statistics of a population of thickness distributions suggests that the simple redistribution dynamics presented in this work capture essential features of the processes responsible for the characteristic observed sea ice thickness distributions. We have also demonstrated that this model formulation is relatively insensitive to some of the quantitative parameterisation of various model mechanisms which we have identified as central in the redistribution process, whereas it displays a high degree of sensitivity to others.

The models which we have constructed in this chapter are closely related to the SCM-derived models studied in Chapter 3. While this chapter's models make use of a Monte Carlo scheme, the manner in which redistribution occurs is very similar to that of the models of Chapter 3. The close kinship between these models is clearly manifested in similar sensitivities to the specification of the rate at which events occur (the kernel K in SCMs, and the rate function in the model of this chapter) and the relative strength of the dynamic and thermodynamic components of the model. These similar sensitivities further strengthen the argument for the use of the SCM paradigm in sea ice thickness distribution dynamic modelling.

The models of this chapter have a more sophisticated representation of redistribution events than SCMs, and changes in the relative amounts of ridging and shearing which occur has a major effect on the shape of the population distribution, primarily in the slope of the exponential tail. The model produced the most realistic distributions when the proportions of ridging and shearing were nearly equal. Observational tests of this feature of the model may be achieved through study of the fracture orientation patterns observed in pack ice, which display regular patterns, [41],[63], and the examination of the typical compression and dilation processes which occur in sea ice.

We tested two variants of the model, one with a memory in the form of a damage function and one without. Although the model with memory had a slight advantage in capturing the variability between distributions in a population, the degree of similarity of behaviour between the two models leads us to conclude that the modelling of sea ice population dynamics does not necessarily benefit from inclusion of ice damage as well as redistribution. Given the model's robustness with regard to the (sensible) choice of rate function suggests that the simple representation of rheology that we have implemented is adequate to a first approximation.

Given the success of the model in producing realistic sea ice populations, the next logical step will be to develop means to incorporate it into an existing force balance model. We conceive of this union as a two-scale construct, where the force-balance model would be used to determine large-scale motion of the ice, and our model would represent the subgrid scale behaviour, and control the local thickness distribution dynamics, using the forcing from the large scale to drive the redistributions. We have also begun work on a spatial model of ice dynamics which embeds our zero-dimensional model in a two-dimensional grid. The intent of this model is to look at ice behaviour on a small spatial scale, such as seen in ice grounding, ice jams, and other interactions between sea ice and the geographical particulars of the area in which is is moving.

The benefit of the construction of a model such as that considered in this study, relative to the more complex force-balance models with detailed rheological descriptions, is that its simplicity makes it extremely easy to explore the parameter and function space of its various components in order to investigate the relative importance of various processes which influence the thickness distribution. In addition, the simplicity of the model makes it more comprehensible than models featuring complex rheological constructs which translate continuum behaviour into the dynamics of $g(h)$. By demonstrating that the model produces qualitatively realistic results, we anticipate that the model will prove useful in assisting in prediction of the changes in $g(h)$ which will occur in different physical environments, or those which will result from different parameterisations in a force-balance model.

Chapter 5

Conclusion

In this research, we have examined the statistics of sea ice thickness distributions, and modelled the processes that lead to the ubiquitous exponential tail. The models we have developed differ radically from most existing models, as they treat redistribution dynamics as a stochastic process. This work can be divided into three separate, but related, sections: analysis of the ensemble statistics of a set of thickness distributions, examination of the properties of the family of Smoluchowski Coagulation Models with attention paid to those features which make them an attractive template for representations of redistribution processes, and the development of a process model of the dynamics of the thickness distribution.

Whereas previous work on sea ice populations has only made use of the mean statistics of ice thickness distributions, we have examined the variability between sea ice thickness track data in Chapter 2, and found an annual cycle. Analysis of simulations performed by a Hibler-style model showed that while it captured some aspects of the variability, it did not produce a qualitatively consistent representation of the population statistics at the two grid cells corresponding to the locations of the observations.

Although the sea ice modelling community has touched upon aspects of a family of equations known as Smoluchowski Coagulation Models, the connection between aspects of redistribution modelling and SCMs had never been made. The SCMs are a natural form to describe the manner in which ice floes combine through ridging to form thicker ice. Connecting the redistribution process to SCMs offers insight into the nature of the population distributions which this system can create. Some simple SCMs offer analytic solutions, and from examination of these solutions, and from numerical simulations of more complex

SCMs, it may be seen that the exponential or quasi-exponential tails arise as solutions for a wide variety of SCMs. That these tails are a generic feature allows us to propose that if one assumes that the effect that redistribution has on a sea ice population's thickness distribution may be represented as a type of coagulation model, the exponential tail of the thickness distribution arises due to the basic fact that thicker ice is made by the interaction of thinner, rather than because of any particular properties of sea ice or the conditions populations of ice exist in.

The primary product of this work was the construction of an idealised process model of the dynamics of a sea ice thickness distribution. The model presents a simplified representation of the ridging, shearing and rafting processes, and treats their occurrence as stochastic in nature. The complex rheologies of present-day sea ice models were replaced with a description somewhat analogous to pure plasticity: the likelihood of redistributions occurring is a function of the difference between the available energy and the amount and thickness of the ice under consideration. Two versions of the model were developed and analysed, one which required that ice first be damaged before it became available for redistribution, thus introducing a form of memory, and one which allowed all ice to be considered for redistribution. Both models were successful at producing qualitatively accurate annual cycles of the thickness distribution, and furthermore, the variability found to exist between the members of a population of thickness distributions.

As can be expected from the study done on SCMs, neither model is particularly sensitive to the parameterisation of the probabilities that events occur. A variety of transition rate functions could be used in simulations to produce approximately exponential tails. Transition rate functions tested included ones which allowed all proposed events (which were constructed as to conserve energy) to occur, to ones which depended on the amount of the energy made available through forcing. In nearly all cases, the models were able to produce approximately exponential tails using the base parameter set. The only transition rates which were not as able to produce the tail were functions of the energy of redistribution such that transition rates diminished rapidly as the energy of events increased.

While the models did not display a strong sensitivity to the form of the transition rate, the simulated populations were strongly affected by the description of the way in which the redistribution process moved ice between thickness categories. This was clearly seen in the model's response to the types of events proposed: when either shearing or ridging was

allowed to dominate the redistribution process, the model simulations deviated markedly from observations, either producing a distribution with a short or non-existent tail, or producing a tail that extended beyond any observed population thickness distribution.

The other aspect of model construction which strongly affected simulations was the description of the strength of the redistribution events relative to the thermodynamic growth and melt process. This relationship was expressed in the model as the ratio of the number of redistribution attempts made between thermodynamic updates, and in the SCM-derived models using the constant kernel $K = 1/R_T$. When this ratio was large ($N > 5$,$R_T < 1$), the maximum thickness of the population increased, and the slope of the tail decreased. When the ratio is small ($N < 1$,$R_T > 5$), the thermodynamic processes dominate, and a tail can be prevented from forming.

The shared sensitivities of the model developed from physical principles in Chapter 4 and the SCM-derived models studied in Chapter 3 suggests that both models capture an essential feature of redistribution processes in sea ice. The similarities in construction and behaviour are strong enough to suggest that the ubiquity of the exponential tail of thickness distributions in sea ice populations can be explained by a description of the redistribution process based on SCMs.

Given the success of the modelling approach that we have developed, the natural question to ask is what applications might the model have in a wider context. Because it is a zero-dimensional, stochastic model, it is not naturally suited to the typical basin-scale modelling tasks that sea ice models are used for. However, a multi-scale model could be constructed that uses a more traditional formulation for the large scale motion of the ice population, and the stochastic model for the redistribution events at the sub-grid scale. The two levels of the model would communicate with each other, the continuum model provides forcing information to the stochastic model, as well as handling the effect of transport on the thickness distribution, and the stochastic model would calculate the changes to the thickness distribution caused by redistribution. In order to use the idealised model in a wider range of applications, work must be done to relate model parameters to measurable quantities. In particular, the rate function T, the parameter N, specifying the number of redistribution attempts to make during each thermodynamic timestep, and the parameters involved in calculating the energetic magnitude of events. The SCM-based model would also require further study in order to link the rate kernel K to measurable quantities.

In addition to the prospect of creating a hybrid model, we have begun work on extending the model to include spatial results by embedding a number of independent zero-dimensional models in a two-dimensional grid. This work will allow the model to be used to study the role that ridge clustering plays in the evolution of the thickness distribution. Furthermore, spatial information will allow for the introduction of bathymetry and land boundaries, which opens the possibility of using the model to study ice grounding and scouring in shallow waters, and ice jams in narrow channels. A number of technical issues regarding parameterisation of transport, and the best means to generate realisations from the grid of thickness distribution remain to be resolved, but early simulation results show great promise, producing linear features and plausible spatially-averaged thickness distributions.

This work has been primarily concerned with the question of the root cause of the ubiquitous exponential tail of the sea ice thickness distribution, and an abstract approach has been taken towards isolating it. The models which we have constructed and studied have demonstrated that the form of the thickness distribution may be largely due to the essential nature of the redistribution process, rather than because of any specific physical properties of sea ice. Both in the highly conceptualised SCMs studied in Chapter 3, and in the physically-based model developed in Chapter 4, it has been possible to produce thickness distributions with exponential and quasi-exponential tails under a wide variety of parameterisations. We have clearly demonstrated a strong connection between the physically-derived model and the SCMs, and shown that the stochastic model of Chapter 4 can reproduce not only first order (mean) but higher order (variability) statistical properties of observed sea ice populations.

Appendix A

Appendix

A.1 Instrumentation

To gather the data set considered in this study, both ice profiling sonar (IPS) and Acoustic Doppler Current Profiler (ADCP) meters were used. The IPS gathered ice draft data while the ADCP obtained ice pack velocities. These instruments were deployed on seabed-mounted moorings, and were designed to operate continuously for a year. The deployment and recovery of the moorings was performed annually, when possible, from the CCGS Sir Wilfrid Laurier. For the moorings deployed in the seasonal ice zone, there were no access problems over the study period. However, for the sites in regions of perennial ice, there were a number of years when the ice cover prevented access to the mooring.

The IPS was developed by the Institute for Ocean Science, and is a sonar device with an emitter/reciever pointing vertically. It was designed for optimal operation at a depth between 30 and 100 meters below the sea surface, which allows it to be deployed in any type of ice-covered water with minimal risk of damage from passing floes. The sonar sends a pulse of sound to the undersurface of the ice and measures the return time. This pulse returns draft measurements for approximately 1m^2 of ice. In addition to the sonar, the pitch and depth of the instrument (which will vary due to currents) are measured). Both sets of observations are used to reconstruct the draft time-series. Further technical details on the IPS and mooring program can be found in [38].

As the IPS is moored, it requires the motion of the ice pack to gather data for a population. The sonar sampling rate is calibrated to log 85 percent of the ice that passes over it

1	0.0
2	0.11
3	0.23
4	0.37
5	0.56
6	0.79
7	1.08
8	1.43
9	1.86
10	2.38
11	2.99
12	3.70
13	4.53
14	5.47
15	6.54
16	7.73
17	9.07
18	10.54

Table A.1: Centre of draft partitions used in [15]

Month	Jan	Feb	Mar	Apr	May	Jun	Jul	Aug	Sep	Oct	Nov	Dec
Site 1	43	29	25	29	53	33	23	0	0	47	65	47
Site 8	13	9	4	8	10	15	18	13	15	20	26	18

Table A.2: Number of tracks observed at Sites 1 and 8 by month

when the ice is moving at a mean speed of about 0.08ms^{-1}. It is important to note that care must be taken when the ice is moving significantly slower or faster than this, as this will result in oversampling or aliasing, which is relevant to the conclusions we draw regarding the statistical stationarity of the population from which the data is gathered.

Month	Jan	Feb	Mar	Apr	May	Jun	Jul	Aug	Sep	Oct	Nov	Dec
Site 1	0.23	0.37	0.23	0	0	0	0	0	0	0	0	0.23
Site 8	0.23	0.79	0.37	0.23	0	0	0	0	0	0	0.37	0.56

Table A.3: Maximum draft of ice available for redistribution in Hibler model runs by month

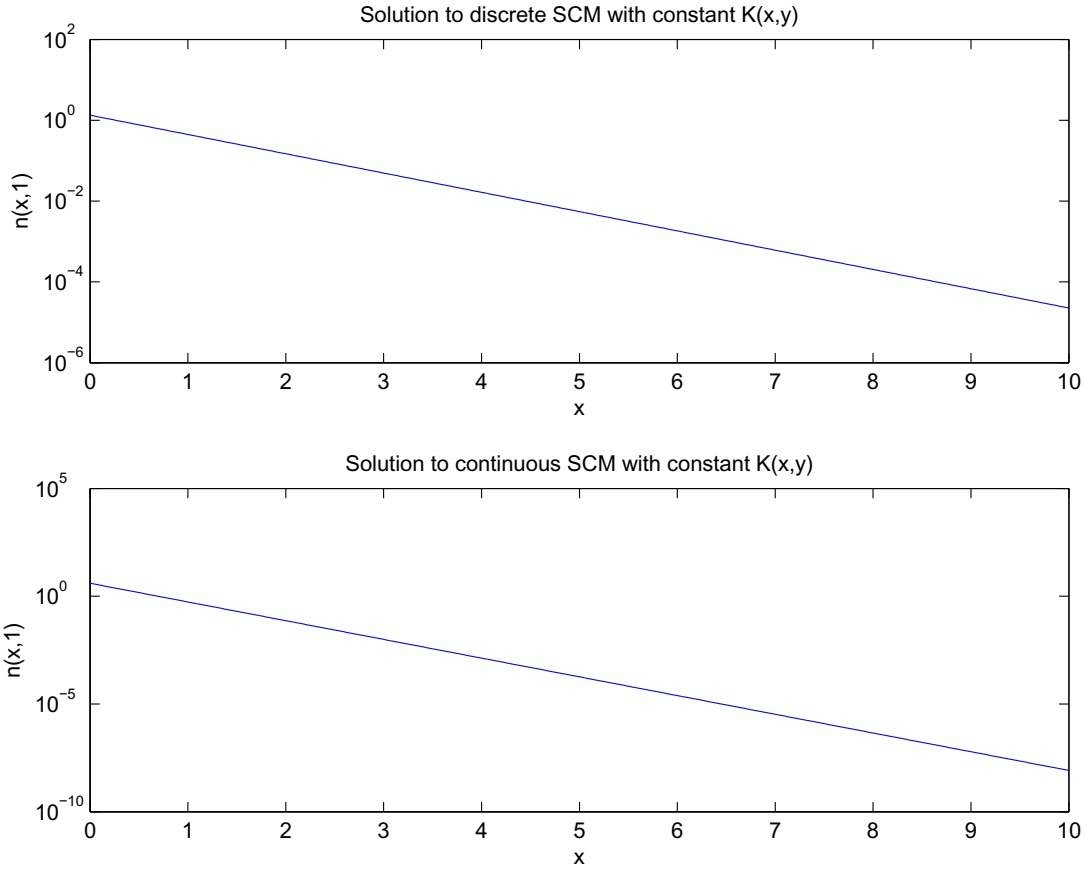

Figure A.1: Solutions to SCM with $K(x, y) = 1$

A.2 Tables

A.3 Examples of SCMs with Exact Solutions

The existence of analytic solutions to some SCMs increases their appeal as a modelling tool. Study of the analytic solutions of SCMs can yield insight into the behaviour which may be produced in a model which includes an SCM component. When $K(x, y) = 1$, the discrete SCM (Eqn. 3.1) has the solution

$$g_k(t) = \left(1 + \frac{t}{2}\right)^{-2} \left(\frac{t}{2+t}\right)^{k-1}. \tag{A.1}$$

For the linear rate kernel, $K(x, y) = x + y$, the solution to the discrete system is of the form

$$g_k(t) = e^{-t} B(1 - e^{-t}, k), \tag{A.2}$$

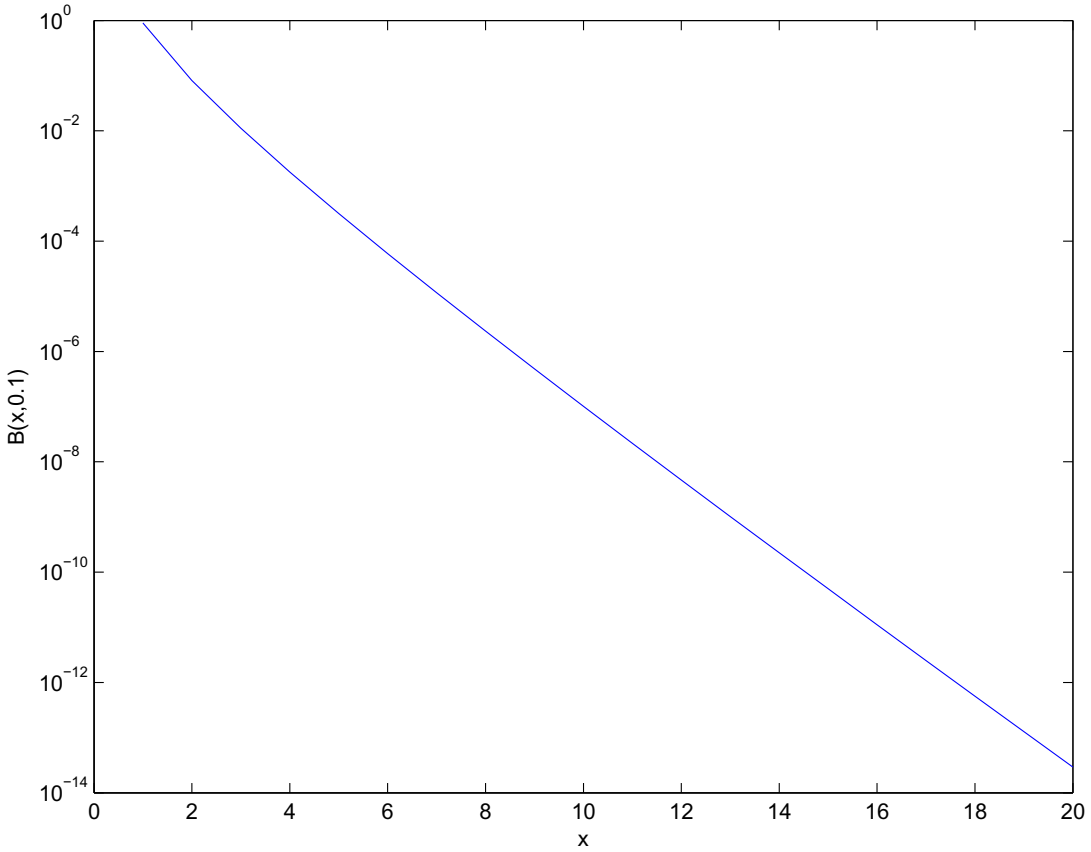

Figure A.2: The Borel distribution with $t = 0.1$

where $B(t, x)$ is the Borel distribution:

$$B(t, x) = \frac{(tx)^{x-1} e^{-tx}}{x!}. \tag{A.3}$$

When $K(k, j) \propto kj$, the solution in the discrete case is given by

$$g_k(t) = i^{-1} B(t, k), \tag{A.4}$$

where $B(t, k)$ is the Borel distribution again.

For the constant kernel, the solution to the continuous equations (Eqn. 3.2) is $g(x, t) = 4t^{-2} e^{-2x/t}$. When the kernel is a linear function, the continuous system has the solution

$$g(x, t) = \frac{1}{\sqrt{2\pi}} e^{-t} x^{-3/2} e^{e^{-2t} x/2}. \tag{A.5}$$

Finally, the continuous system with multiplicative kernel, $K(x, y)$, has the solution

$$g(x, t) = (2\pi)^{-1/2} x^{-5/2} e^{-t^2 x/2} \tag{A.6}$$

The solution to the SCM with multiplicative kernel (Eqn. A.4) can become unbounded in finite time under certain conditions. The solutions to the SCM with constant and additive kernels are bounded for all time, and they conserve the total mass of the system ($\sum_{k=0}^{\infty} k g_k(t)$, $\int_0^{\infty} x g(x, t) \mathrm{d}x$) for all time *viz.*, [48].

Bibliography

[1] D. J Aldous. Deterministic and stochastic models for coalescence (aggregation and coagulation): a review of the mean-field theory for probabilists. *Bernoulli*, 5(1):3–48, 1999.

[2] Trisha L. Amundrud, Humfrey Melling, and R. Grant Ingram. Geometrical constraints on the evolution of ridged sea ice. *Journal of Geophysical Research*, 109(C6), 2004.

[3] Trisha L. Amundrud, Humfrey Melling, R. Grant Ingram, and Susan E. Allen. The effect of structural porosity on the ablation of sea ice ridges. *Journal of Geophysical Research*, 111:C06004, June 2006.

[4] O. Babko, D. A. Rothrock, and G. A. Maykut. Role of rafting in the mechanical redistribution of sea ice thickness. *Journal of Geophysical Research*, 107:14 PP., August 2002.

[5] J. L Bamber and A. J Payne. *Mass balance of the cryosphere: observations and modelling of contemporary and future changes*. Cambridge Univ Pr, 2004.

[6] R. Birch, D. Fissel, H. Melling, K. Vaudrey, W. Lamb, K. Schaudt, and J. Heideman. Ice-profiling sonar. *Sea Technology*, 41(8):48–54, 2000.

[7] C. M. Bitz, M. M. Holland, A. J. Weaver, and M. Eby. Simulating the ice-thickness distribution in a coupled climate model. *Journal of geophysical research*, 106(C2):2441–2463, 2001.

[8] C. M. Bitz and G. H. Roe. A mechanism for the high rate of sea ice thinning in the arctic ocean. *Journal of Climate*, 17(18):3623–3632, 2004.

[9] M. D. Coon. A review of AIDJEX modeling. *Sea Ice Processes and Models*, pages 12–25, 1980.

[10] M. D. Coon, G. A. Maykut, R. S. Pritchard, D. A. Rothrock, and A. S. Thorndike. Modeling the pack ice as an elastic-plastic material. *AIDJEX Bull*, 24:1–105, 1974.

[11] D. Crommelin and E. Vanden-Eijnden. Subgrid-scale parameterization with conditional markov chains. *Journal of the Atmospheric Sciences*, 65(8):2661–2675, 2008.

[12] M. Escobedo, S. Mischler, and M. Rodriguez Ricard. On self-similarity and stationary problem for fragmentation and coagulation models. In *Annales de l'Institut Henri Poincare (C) Non Linear Analysis*, volume 22, pages 99–125, 2005.

[13] D. L Feltham. Sea ice rheology. *Annual Review Of Fluid Mechanics*, 40:91–112, 2008.

[14] G. M Flato and W. D. Hibler. Modeling pack ice as a cavitating fluid. *J. Phys. Oceanogr*, 22(6):626–651, 1992.

[15] G. M Flato and W. D Hibler III. Ridging and strength in modeling the thickness distribution of arctic sea ice. *Journal of Geophysical Research. C. Oceans*, 100:18611–18626, 1995.

[16] N. Fournier and P. Laurenot. Existence of self-similar solutions to smoluchowskis coagulation equation. *Communications in Mathematical Physics*, 256(3):589–609, 2005.

[17] M. Frenklach. Dynamics of discrete distribution for smoluchowski coagulation model. *Journal of colloid and interface science*, 108(1):237–242, 1985.

[18] Christian Haas. Late-summer sea ice thickness variability in the arctic transpolar drift 1991-2001 derived from ground-based electromagnetic sounding. *Geophysical Research Letters*, (31), 2004.

[19] W. D Hibler. A viscous sea ice law as a stochastic average of plasticity. *Journal of Geophysical Research*, 82(27):3932–3938, 1977.

[20] W. D. Hibler. A dynamic thermodynamic sea ice model. *Journal of Physical Oceanography*, 9(4):815–846, 1979.

[21] W. D. Hibler. Modeling a variable thickness sea ice cover. *Monthly weather review*, 108(12):1943–1973, 1980.

[22] M. M Holland, C. M Bitz, E. C Hunke, W. H Lipscomb, and J. L Schramm. Influence of the sea ice thickness distribution on polar climate in CCSM3. *Journal of Climate*, 19(11):2398–2414, 2006.

[23] M. A Hopkins. On the ridging of intact lead ice. *Journal of Geophysical Research. C. Oceans*, 99:16, 1994.

[24] E. C. Hunke and J. K. Dukowicz. An elastic-viscous-plastic model for sea ice dynamics. *Journal of Physical Oceanography*, 27(9):1849–1867, 1997.

[25] Jennifer K. Hutchings, Petra Heil, and William D. Hibler. Modeling linear kinematic features in sea ice. *Monthly Weather Review*, 133(12):3481, 2005.

[26] W. D. Hibler III. Sea ice fracturing on the large scale. *Engineering Fracture Mechanics*, 68(17-18):2013–2043, 2001.

[27] Malvin H. Kalos and Paula A. Whitlock. *Monte Carlo methods*. Wiley-VCH, November 2008.

[28] M. A Katsoulakis and D. G Vlachos. Mathematical strategies for the Coarse-Graining of microscopic models. *Handbook of Materials Modeling*, pages 1477–1490, 2005.

[29] R. Kindermann, J. L Snell, and American Mathematical Society. *Markov random fields and their applications*. American Mathematical Society Providence, Rhode Island, 1980.

[30] D. L. Laikhtman. O dreife ledyanykh polei (Drift of ice fields). *Tr. LGMI*, 7:129–137, 1958.

[31] M. A. Lange and H. Eicken. The sea ice thickness distribution in the northwestern weddell sea. *Journal of Geophysical Research*, 96(C3):PP. 4821–4837.

[32] M. Lensu. Correlations between fragment sizes in sequential fragmentation. *Journal of Physics A: Mathematical and General*, 30:7501, 1997.

[33] Mikko Lensu. *The Evolution of Ridged Ice Fields*. PhD thesis, Helsinki University of Technology, 2003.

[34] A. J Majda and B. Khouider. Stochastic and mesoscopic models for tropical convection. *Proceedings of the National Academy of Sciences of the United States of America*, 99(3):1123, 2002.

[35] G. A Maykut and N. Untersteiner. Some results from a time-dependent thermodynamic model of sea ice. *Journal of Geophysical Research*, 76(6):1550–1575, 1971.

[36] H. Melling. Detection of features in first-year pack ice by synthetic aperture radar (SAR). *International Journal of Remote Sensing*, 19(6):1223, 1998.

[37] H. Melling. Ips records 1990-2004. Raw data records from IPS logs - private communication, 2004.

[38] H. Melling, P. H Johnston, and D. A Riedel. Measurements of the underside topography of sea ice by moored subsea sonar. *Journal of Atmospheric and Oceanic Technology*, 12(3):589–602, 1995.

[39] H. Melling and D. A Riedel. Development of seasonal pack ice in the beaufort sea during the winter of 1991-1992: A view from below. *Journal of Geophysical Research*, 101(C5):11975, 1996.

[40] A. C. Palmer and T. J. O. Sanderson. Fractal crushing of ice and brittle solids. *Proceedings: Mathematical and Physical Sciences*, 433(1889):469–477, June 1991. ArticleType: primary_article / Full publication date: Jun. 8, 1991 / Copyright 1991 The Royal Society.

[41] Robert S. Pritchard. Mathematical characteristics of sea ice dynamics models. *Journal of Geophysical Research*, 93(C12):PP. 15,609–15,618.

[42] D. A. Rothrock. The energetics of the plastic deformation of pack ice by ridging. *Journal of Geophysical Research*, 80(33):4514–4519, 1975.

[43] D. A. Rothrock. The mechanical behavior of pack ice. *Annual Review of Earth and Planetary Sciences*, 3(1):317–342, 1975.

[44] D. A. Rothrock. Ice thickness distribution-measurement and theory. *The geophysics of sea ice*, pages 551–575, 1986.

[45] D. A. Rothrock and A. S. Thorndike. Measuring the sea ice floe size distribution. *Journal of Geophysical Research*, 89(C4):6477–6486, 1984.

[46] M. I. Ruzin. The wind drift of ice in a heterogeneous pressure field. *Tr. Arkt. Antartkt. Inst.*, 226:12335, 1959.

[47] T. J. O. Sanderson. *Ice mechanics: Risks to offshore structures.* Kluwer Academic Publishers, Norwell, MA, 1988.

[48] M. Shirvani and H. Roessel. The mass-conserving solutions of smoluchowski's coagulation equation: The general bilinear kernel. *ZAMP Zeitschrift fr angewandte Mathematik und Physik*, 43(3):526–535, 1992.

[49] H. Von Storch and F. W Zwiers. *Statistical analysis in climate research*. Cambridge Univ Pr, 2002.

[50] David Neville Thomas. *Sea Ice*. John Wiley and Sons, November 2009.

[51] A. Thorndike. Sea ice thickness as a stochastic process. *Journal of geophysical research*, 105(C1):1311–1313, 2000.

[52] A. S. Thorndike. Estimates of sea ice thickness distribution using observations and theory. *Journal of Geophysical Research*, 97(C8):605, 1992.

[53] A. S. Thorndike, D. A. Rothrock, G. A. Maykut, and R. Colony. The thickness distribution of sea ice. *J. Geophys. Res*, 80(33):4501–4513, 1975.

[54] L. B Tremblay and L. A. Mysak. Modeling sea ice as a granular material, including the dilatancy effect. *Journal of Physical Oceanography*, 27(11), 1997.

[55] P. Wadhams. Sea ice thickness distribution in fram strait. 1983.

[56] P. Wadhams. Sea ice thickness distribution in the greenland sea and eurasian basin, may 1987. *Journal of Geophysical Research-Oceans*, 97(C4), 1987.

[57] P. Wadhams. Sea-ice thickness distribution in the trans polar drift stream. 1989.

[58] P. Wadhams. Sea ice morphology. 1994.

[59] P. Wadhams and T. Davy. On the spacing and draft distributions for pressure ridge keels. *J. Geophys. Res*, 91(C9):10697–10708, 1986.

[60] P. Wadhams and M. Wallis. Arctic sea ice extent and thickness [and discussion]. *Philosophical Transactions: Physical Sciences and Engineering*, pages 301–319, 1995.

[61] Peter Wadhams. Sea ice thickness distribution in the greenland sea and eurasian basin, may 1987. *Journal Of Geophysical Research - Oceans*, 97(C4), 1992.

[62] Peter Wadhams, Manfred A. Lange, and Stephen F. Ackley. The ice thickness distribution across the atlantic sector of the antarctic ocean in midwinter. *Journal of Geophysical Research*, 92(C13):552.

[63] K. Wang. Observing the yield curve of compacted pack ice. *Journal of Geophysical Research*, 112(C5):C05015, 2007.

[64] W. F. Weeks, S. F. Ackley, and J. Govoni. Sea ice ridging in the ross sea, antarctica, as compared with sites in the arctic. *Journal of Geophysical Research*, 94(C4):PP. 4984–4988.